DEVELOPMENT OF B-TYPE AND MULTI-ION DOPED CARBONATED HYDROXYAPATITE BIOCERAMICS

MARJAN SAFARZADEH

FACULTY OF ENGINEERING
UNIVERSITY OF MALAYA
KUALA LUMPUR

2020

DEVELOPMENT OF B-TYPE AND MULTI-ION DOPED CARBONATED HYDROXYAPATITE BIOCERAMICS

MARJAN SAFARZADEH

THESIS SUBMITTED IN FULFILMENT OF THE REQUIREMENTS FOR THE DEGREE OF DOCTOR OF PHILOSOPHY

FACULTY OF ENGINEERING
UNIVERSITY OF MALAYA
KUALA LUMPUR

2020

UNIVERSITY OF MALAYA

ORIGINAL LITERARY WORK DECLARATION

Name of Candidate: Marjan Safarzadeh

Matric No: KHA160014

Name of Degree: Doctor of Philosophy

Title of Thesis ("this Work"):

DEVELOPMENT OF B-TYPE AND MULTI-ION DOPED CARBONATED HYDROXYAPATITE BIOCERAMICS

Field of Study: Materials Engineering

I do solemnly and sincerely declare that:

(1) I am the sole author/writer of this Work;
(2) This Work is original;
(3) Any use of any work in which copyright exists was done by way of fair dealing and for permitted purposes and any excerpt or extract from, or reference to or reproduction of any copyright work has been disclosed expressly and sufficiently and the title of the Work and its authorship have been acknowledged in this Work;
(4) I do not have any actual knowledge nor do I ought reasonably to know that the making of this work constitutes an infringement of any copyright work;
(5) I hereby assign all and every rights in the copyright to this Work to the University of Malaya ("UM"), who henceforth shall be owner of the copyright in this Work and that any reproduction or use in any form or by any means whatsoever is prohibited without the written consent of UM having been first had and obtained;
(6) I am fully aware that if in the course of making this Work I have infringed any copyright whether intentionally or otherwise, I may be subject to legal action or any other action as may be determined by UM.

Candidate's Signature Date: 31 March 2020

Subscribed and solemnly declared before,

Witness's Signature Date: 31 March 2020

Name:

Designation:

ABSTRACT

The present research is aimed to investigate the effect of varying the carbonate to phosphate (CO_3^{2-}/ PO_4^{3-}) molar ratios from 0.5 to 5 on the physical and mechanical properties of carbonated hydroxyapatite (CHA) synthesized by a wet chemical method. The sintering was performed under dry carbon dioxide atmosphere at 900 °C to maintain the B-type CHA structure. It was found that increases in CO_3^{2-}/ PO_4^{3-} ratio was accompanied by an increase in the *c/a* lattice ratio. The diffraction peaks of the synthesized 0.5-5 CHA powders exhibited a single phase material except for 5CHA which revealed the some minor calcite or ($CaCO_3$) as a secondary phase. The sintering studies indicated that all CHA was thermally stable and retained the apatite structure after sintering. The relative density of the sintered CHA was found to decrease along with the Vickers hardness and fracture toughness as the CO_3^{2-}/ PO_4^{3-} ratio increased from 0.5 to 4. The improvement in the mechanical properties was associated with improvement in the relative density and the larger grain size of the sintered samples.

The CHA with upper limit of carbonate was chose as the optimum CHA for the next investigations. Subsequently, evaluate the effect of varying sintering temperature (800 °C, 900 °C, 1000 °C and 1100 °C) under the dry CO_2 atmosphere on the compacted CHA sample. The results shown that all samples retained single phase B-type CHA except at 1100 °C which was accompany with the formation of CaO in the apatite structure. Increasing sintering temperature led to a gradual decrease in the carbonate content of the CHA pellets and an increase in mechanical properties up to 1000 °C. In particular, the H_V and K_{Ic} values increased with increasing sintering temperature.

An in vitro bioactivity test was evaluated on the 0.5-4 CHA pellets using simulated body fluid (SBF) solution. It was found that increasing the carbonate content enhanced the solubility of CHA pellets and increased the thickness of the apatite layer on the sample's surface.

Lastly the effect of multi-ions (Mg^{2+}, SiO_4^{4-}, Zn^{2+} and Cu^{2+}) doping on the properties of carbonated hydroxyapatite (CHA) prepared by a wet chemical method was investigated. Different combinations of ions were doped into the CHA and the as-synthesized compacts were sintered at 900 °C and wet CO_2 atmosphere prior to body characterization. It was found that regardless of ions doping, the lattice structure of the CHA was not disrupted. In addition, secondary phases were not detected for all the multi-ions doped samples. The XRD and FTIR results further confirmed the presences of a B-Type CHA in the as-synthesized and sintered samples. The XRD analysis revealed that the lattice parameters (*c/a* ratio) increased with dopant addition and resulted in a smaller crystallite size. The FESEM examination also showed the presences of smaller grain size for the multi-ions doped CHA samples thus indicating that the doping was beneficial in suppressing grain coarsening in carbonated hydroxyapatite.

The main advantageous of this synthesis method is low production costs and relatively time-saving that exhibited higher mechanical properties at lower sintering temperature in CO_2 atmosphere. Additionally, the presence of minor elements in CHA is more promising to enhance biomedical properties.

Keywords: CHA, Carbonated hydroxyapatite, Multi-ions, Doping, CO_3^{2-}/ PO_4^{3-} ratio, Mechanical properties, Bioceramics

ABSTRAK

Penyelidikan ini bertujuan untuk mengkaji kesan nisbah karbonat kepada fosfat (CO_3^{2-}/ PO_4^{3-}) bermula dari nisbah molar 0.5 hingga 5 kepada sifat fizikal dan mekanikal hidroksiapatit berkarbonat (CHA) yang disintesis dengan menggunakan kaedah kimia basah. Pensinteran dilakukan di bawah keadaan karbon dioksida kering pada suhu 900 °C bagi mengekalkan struktur CHA jenis B. Didapati peningkatan nisbah CO_3^{2-}/ PO_4^{3-} telah menyebabkan peningkatan nisbah *c/a* kekisi. Puncak difraksi bagi serbuk 0.5-5 CHA menunjukkan bahan fasa tunggal kecuali 5CHA yang terdiri dari beberapa kalsit kecil atau ($CaCO_3$) sebagai fasa sekunder. Kajian sintering menunjukkan bahawa semua CHA stabil haba dan mengekalkan struktur apatite selepas sintering. Ketumpatan relatif CHA yang telah disinter didapati berkurang bersama dengan kekerasan Vickers dan ketumpatan fraktur ketika nisbah CO_3^{2-}/ PO_4^{3-} meningkat dari 0.5 ke 4. Peningkatan sifat-sifat mekanik dikaitkan dengan peningkatan ketumpatan relatif dan saiz bijian yang lebih besar daripada sampel yang telah sinter.

CHA dengan had karbonat paling tinggi telah dipilih sebagai CHA optimum untuk penyelidikan seterusnya. Selanjutnya, kajian terhadap kesan suhu sintering berbeza (800 °C, 900 °C, 1000 °C dan 1100 °C) di bawah suasana CO_2 kering pada sampel CHA yang dipadatkan telah dijalankan. Keputusan menunjukkan bahawa semua sampel mengekalkan satu fasa CHA - B kecuali pada 1100 °C yang disertai dengan pembentukan CaO dalam struktur apatite. Peningkatan suhu sintering membawa kepada penurunan secara beransur-ansur dalam kandungan karbonat pelet CHA serta peningkatan sifat mekanik sehingga 1000 °C. Khususnya, nilai H_V dan K_{Ic} meningkat dengan peningkatan suhu proses sinter.

Ujian bioaktiviti in vitro dinilai pada pelet 0.5-4 CHA menggunakan larutan cecair badan simulasi (SBF). Didapati bahawa peningkatan kandungan karbonat meningkatkan

keterlarutan pelet CHA dan meningkatkan ketebalan lapisan apatit pada permukaan sampel.

Selain itu, kesan multi-ion (Mg^{2+}, SiO_4^{4-}, Zn^{2+} dan Cu^{2+}) terhadap sifat hidroksiapatit berkarbonat (CHA) yang disediakan oleh kaedah kimia basah juga disiasat. Gabungan ion-ion yang berbeza telah disebatikan ke dalam CHA dan kompak as-sintetik telah disinter pada 900 °C dalam keadaan CO_2 basah sebelum pencirian sampel dijalankan. Keputusan pencirian menunjukkan bahawa tanpa mengira doping ion, struktur kisi CHA tidak terkesan. Di samping itu, fasa kedua tidak dapat dikesan untuk semua sampel dope berbilang ion. Keputusan XRD dan FTIR seterusnya mengesahkan kehadiran CHA Jenis-B dalam sampel yang disintesis dan disinter. Analisis XRD mendedahkan bahawa parameter kekisi (nisbah *c/a*) meningkat dengan tambahan dopan dan menghasilkan saiz kristal yang lebih kecil. Ujian FESEM juga menunjukkan kehadiran saiz bijian yang lebih kecil untuk pelbagai sampel doped CHA sekaligus menunjukkan bahawa doping itu bermanfaat untuk menutup butiran kasar dalam hidroksiapatit berkarbonat.

Kelebihan utama kaedah sintesis ini adalah kos pengeluaran yang rendah dan menjimatkan masa selain mempamerkan sifat mekanik yang lebih tinggi pada suhu sintering yang lebih rendah dalam keadaan bersifat CO_2, tambahan pula kehadiran unsur-unsur kecil dalam CHA menjadikan ianya lebih sesuai untuk ciri- ciri bioperubatan.

Kata kunci: CHA, Hidroksiapatit berkarbonat, Multi-ion, Doping, Nisbah CO_3^{2-}/ PO_4^{3-}, Sifat mekanik, Biokeramik

ACKNOWLEDGEMENTS

I would like to express my sincere gratitude to the following individuals that have constantly guided and supported me throughout my PhD research.

- My supervisor, Prof. Ir. Dr. Ramesh Singh for his motivation, support and immense knowledge in completion of this research and providing me an opportunity to complete my PhD thesis.
- My co-supervisors, Assoc. Prof. Dr. Tan Chou Yong and Assoc. Prof. Dr. Hari Chandran A/L Thambinayagam for their assistance and important suggestions and advice.
- Prof. Dr. Ahmad Fauzi Mohd Noor of USM for the support rendered in this research.
- Dr. Chee Chin Fei for his guidance throughout writing this thesis.
- The Center of Advanced Manufacturing and Material Processing, University of Malaya for providing facilities and instrument.
- My dear friend Sharifah Nazneen for all she has done for me throughout my PhD. I am also indebted towards her for her generosity and selfless support.
- My parents for their unceasing encouragement, support, attention and care throughout my life.

TABLE OF CONTENTS

LIST OF FIGURES

LIST OF TABLES

LIST OF SYMBOLS AND ABBREVIATIONS

BCP	:	Biphasic Calcium Phosphate
BGS	:	Bone Graft Substitute
Ca/P	:	Calcium to phosphate molar ratio
Ca^{2+}	:	Calcium ion
$CaCO_3$	:	Calcium carbonate
CaO	:	Calcium oxide
CHA	:	Carbonated hydroxyapatite
CO_3^{2-}	:	Carbonate ion
EDX	:	Energy Dispersive X-Ray
FESEM	:	Field Emission Scanning Electron Microscopy
FTIR	:	Fourier Transform Infra-Red
GBA	:	Grain Boundary-affect
GOF	:	Goodness of Fittings
HA	:	Hydroxyapatite
Hv	:	Microhardness
I_C	:	Calculated Intensities
ICDD	:	International Centre for Diffraction Data
I_O	:	Observed Intensities
KBr	:	Potassium Bromide
K_{Ic}	:	Indentation Fracture Toughness
MW	:	Molecular Weight
O/W	:	Oil-in-Water
PBS	:	Phosphate Buffer Saline
PO_4^{3-}		Phosphate ion

R_{exp}	:	Expected Profile Residual
R_p	:	Profile Residual
RT	:	Room Temperature
R_{wp}	:	Weighted Profile Residual
S_{BET}	:	Specific Surface Area using BET Method
SBF	:	Simulated Body Fluid
TCP	:	Tricalcium Phosphate
TTCP	:	Tetracalcium Phosphate
W/O	:	Water-in-Oil
XRD	:	X-Ray Diffraction
XRF	:	X-Ray Florescence
θ	:	Theta
β	:	Beta
α	:	Alpha
°	:	Degree
°C	:	Degree Centigrade

LIST OF APPENDICES

CHAPTER 1: INTRODUCTION

Background

Bone is an extremely complex living tissue having elegant structure of distinct levels of hierarchical structural units (Stevens & George, 2005; Roveri & Iafisco, 2010). The major component of bone is a composite of inorganic compound (carbonated hydroxyapatite) and organic compound (collagen) (Siddiqi et al., 2018). Typically, bone assist in locomotion activity, protects the organs, produces blood cells and store mineral ions. In order to fulfill its key functions, bone is exquisitely design to be a couple process where its constantly broken down and rebuilt throughout the lifetime of an individual (Rodan, 1992; Sommerfeldt & Rubin, 2001). Bone also possesses unique intrinsic properties for regeneration process to take places. Unlike in other tissues, bone injuries or fractures have the capacity to heal without leaving any scar (Dimitriou et al., 2011). However, bone is also prone to injury and defects resulting from many different reasons. For example, trauma, infections, and tumors can result in bone injury, which is a major public health problem (Best et al., 2008). Hence, it is logical to say that large bony defect due to the changes on bone structure caused by injury or diseases can be altered the human body's equilibrium and quality of life (Venkatesan et al., 2017). Thus, bone grafts are required in order to reconstruct major alterations of bone's structure or to treat poor bone-healing conductions (Yoshikawa & Myoui, 2005).

1.1 Bone-Graft Substitutes

Bone grafting is a transplanted bone to person's body via surgical procedure to replace or repair the fractured bones (Venkatesan et al., 2011). Ideally, remodeling is a phenomenon in which the implant should replace the missing tissue, promote new bone growth and reform the repaired fracture (Hing, 2005). An ideal bone graft substitute (BGS) promote bone healing through three mechanism: osteoconductive (ability to

support tissue ingrowth and bone formation), osteoinductive (ability to form bone when implanted in non-osseous sites), and osteogenic (ability to form new bone from surviving cells within a bone graft) (Ben-Nissan, 2003; Sutherland & Bostrom, 2005).

To date, there are four common types of bone grafting. Autograft transplants bone from the patient's body; allograft uses bone from a deceased donor; xenograft is bone graft from a species other than human; synthetic graft uses bone that made of synthetic biocompatible materials (Czitrom & Gross, 1992; Salgado et al., 2004).

1.1.1 Autograft

Autogenous bone grafting involves bone transplantation from one part of the patient′s own body to another part. Up to present, autograph is considered as the golden standard among bone grafts. This is due to its obvious advantages which are osteogenic and osteoconductive properties and the immune response in bone allograft (Yoshikawa & Myoui, 2005). One of the drawbacks of using autogenous bone grafting is high medical costing. The patients are also suffering from long surgical operation. Other risks include scar formation at donor site and morbidity related to post-surgical infection (Burg et al., 2000; Mata et al., 2002).

1.1.2 Allograft

Allograft, also referred as allogeneic transplant or homograft, is obtain through bone transplantation from living donor or corpse to patient (Bohner, 2010). Bone grafting became critical during World War II, prompting the US Navy to establish bone banks to better treat fractures sustained in battle (Sutherland & Bostrom, 2005; Ruys, 2013). In fact, the process of incorporation of transplanted bone is similar to normal bone regeneration after fracture or during growth. However, allograft transplantation possesses several risks. A suitable bone is subjected to the availability of a compatible deceased donor, high surgical cost and long operation time have hindered patients for allograft

transplantation. Other drawbacks include delay graft incorporation, disease transmission, immune rejection, and long term graft strength (Bostrom & Mikos, 1997; Burg et al., 2000; Salgado et al., 2004). The higher resorption rate than that observed with autologous bone implants is a factor that often discourages the use of allografts (Baino, 2011).

1.1.3 Xenograft

As an alternative to these two bone grafts, there is also attempting to use animals' tissue (normally from cow or pigs), which is known as xenograft. However, xenograft has rarely been used in human due to its low biocompatibility and high risk of disease transmission. Human xenograft possesses a threat of causing genetic code alterations of animals. Xenograft have also been a topic of discussion in terms of ethical aspects and oppose animal's slaughtering (Platt et al., 1990; Boneva et al., 2001; Salgado et al., 2004; Vagaska et al., 2010; Fernández et al., 2015).

1.1.4 Synthetic Graft

The insertion of man-made materials refers to the synthetic grafts are the preferred choice. Future-oriented approach is more focused on the synthetic BGSs as it has largely solved the problems faced by other graft methods (Bohner, 2010). Therefore, in the field of orthopedic surgery, various kinds of biomaterials have been developed as bone substitute such as ceramics, metals, polymers and composites. Among these materials, the family of calcium phosphate (CaP) mineral, especially hydroxyapatite (HA) has been used extensively as (BGS) due to the their excellent biocompatibility, bioactivity, osteoconductivity, and nontoxicity properties (Bohner, 2010; Baino, 2011). The crystal structure of the unit cell in HA can either be monoclinic or hexagonal. Although HA forms the main constituent of human bones and teeth and considered as a good alternative for bone substitution, the natural bone slightly differs from HA in stoichiometry, composition, structure, crystallinity and biological activity (Zakaria et al., 2009). Despite

HA being osteoconductive, it is not osteoinductive (Yoshikawa & Myoui, 2005). This deficiency could be overcome through doping with selective ions into the structure of HA. The biological apatites are mainly in the form of non-stoichiometric, poorly crystalline and contain several foreign ions mostly carbonate (CO_3^{2-}) along with trace amounts of ions (Na^{2+}, Mg^{2+}, Zn^{2+}, F^-, etc.) in its structure (Bang et al., 2014).

In particular, the introduction of carbonate (CO_3^{2-}) ions in the crystal lattice of HA was reported to be beneficial in enhancing its bioactivity (Gibson & Bonfield, 2002). Carbonated hydroxyapatite (CHA) structure is of special interest, since CO_3^{2-} ion is the main component of bone and dental tissues in humans and many living organisms. Inappropriate of the CO_3^{2-} ion into the apatite structure can lead to the bone and dental disease, since the carbonate ion enhances the ability of the apatite to be dissolved (Frank-Kamenetskaya et al., 2011).

Therefore, many researchers pay close attention on the synthesis of carbonated hydroxyapatite (CHA) bioceramic that emulates the chemical composition of the hard tissue. CHA which is represented as $Ca_{10-x}(PO_4)_{6-x}(CO_3)_x(OH)_{2-x}$ with $0 \leq x \leq 2$ is a prospective material for BGS. It has been established that the amount of carbonate ions found in human bones is age dependent and typically ranges from 2 to 8 wt.% (Ibrahim et al., 2011; Graziani et al., 2017; Wati & Yusuf, 2019).

CHA can be classified either as B-type (CO_3^{2-} substitutes PO_4^{3-}), A-type (CO_3^{2-}substitutes OH^-) or AB-type CHA (CO_3^{2-}substitutes both OH^- and PO_4^{3-}) (Lafon et al., 2008). Biological apatites are predominantly B-type CHA with A/B-type ratio of 0.7-0.9. Higher A/B-type ratio was observed in old tissue as compared to the young one (Landi et al., 2003). These substitution of carbonated apatites are expected to reveal improved structural, mechanical and biological properties when compared to monolithic

hydroxyapatite (Narayan, 2009). Furthermore, the CHA has been found to be easily resorbed by living cells and also to possess higher solubility than HA (Rajesh et al., 2012).

Significant increase in solubility by substitution of CO_3^{2-} anion in HA structure could be attributed to the lower degrees of crystallinity, which causes by increasing in lattice disorder (Boanini et al., 2010). Therefore, in order to mimic the natural bone structure, development of lattice structure of synthetic HA by ionic substitution is of special interest.

The uniqueness of HA crystal structure has enabled it to be doped with multi-ions. The structure of HA consists of an array of PO_4^{3-} held together by Ca^{2+} and hydroxyl ions which allows the substitution of the Ca^{2+} site by Zn^{2+}, Na^{+}, etc., and the phosphate site by CO_3^{2-}, SiO_4^{4-}, etc. The OH^{-} site can be substituted by C^{-}, F^{-}, CO_3^{2-} etc. Such ionic substitutions affect the surface charge, lattice parameters, crystallinity and the morphology of HA, which in turn can result in changes in thermal stability, mechanical properties, solubility and bioactivity of HA (Kumar et al., 2012; Uysal et al., 2013). Multi-ions substituted CHA allows a better development of new calcium phosphate-based materials for biomedical applications (Gasqueres et al., 2008).

Numerous researchers have investigated the effects of ionic substitutions in HA as well as simultaneously co-substitute other cations or anions together with CO_3^{2-} to form single or multi-ions doped CHA. Single-ion doped CHA such as, Mg^{2+}/ CO_3^{2-} (Landi et al., 2004; LeGeros et al. 1995; Gibson & Bonfield 2002), Sr^{2+}/ CO_3^{2-} (Landi et al., 2008), Zn^{2+} / CO_3^{2-} (Mayer et al., 1994; Kumar et al., 2012), SiO_4^{4-} /CO_3^{2-} (Bang et al., 2014), Ag^{+} /CO_3^{2-} (Lysenko et al., 2015), and multi-ion doped CHA such as, Mg^{2+}/ SiO_4^{4-} /CO_3^{2-} (Sprio et al., 2008), Na^{+}/CO_3^{2-}/SiO_4^{4-} (Mostafa et al., 2011), Na^{+}/Mg^{2+}/K^{+}/F^{-}/Cl^{-}/ CO_3^{2-} (Lin et al., 2011) have been reported.

The competition between the ions for occupation the same crystal structure is the one main issue in simultaneous multi-ions substituted CHA. However, a few research works have been focused on the synthesis of multi-ions such as Mg, Si, Zn and Cu doped CHA, there has been little investigation on simultaneous co-substitute multiple elements along with CO_3^{2-} in the wet chemical precipitation method (Jamuna-Thevi et al., 2014).

1.2 Problem Statement

HA with the chemical formula of $Ca_{10}(PO_4)_6(OH)_2$ has been widely used as a material for biomedical application due to its similarity with the chemical composition of natural bone (Matsunaga et al., 2010; Gopi et al., 2012). Nevertheless, HA ceramic materials suffer from drawbacks such as slow formation of new bone tissue *in vivo* and poor mechanical properties compared to the living bone tissue. The natural bone contains a variety of trace ions such as magnesium (Mg^{2+}), zinc (Zn^{2+}), copper (Cu^{2+}), iron (F^-) and CO_3^{2-}.

Moreover, CO_3^{2-} ion is the main element found in human bone mineral. It is believed that substitution some ions in the HA structure enhance the biological and mechanical properties of HA (Palard et al., 2008). Introduction of co-substituted ions in HA would improve solubility rate and bioactivity than stoichiometric HA (LeGeros, 2002; Pietak et al., 2007; Lafon et al., 2008).

On the other hand, to produce densified ceramic part from powders, a high sintering temperature is required. However the stability of CHA is challenging elaborate as reported by Barralet et al. (2000) and Panda et al. (2003). Sintering has considerable influence on the final properties of CHA such as density, porosity and the resulting internal nanostructure. Poor control of thermal treatment during sintering of CHA could lead to partial or total decomposition of materials, resulting in carbonate loss and subsequently affecting the physical and mechanical properties of synthetic material

(Landi et al., 2000; Yanny-Marliana & Ahmad-Fauzi, 2011; Ahmad-Fauzi & Zainudin, 2016). Therefore, the aim of this research was to synthesize and produce a highly dense multi-substituted CHA nanomaterials with good physical and mechanical properties.

1.3 Objective of the Research

The current research was conducted with the aim of producing multi-ion doped CHA via wet chemical method with good physical and mechanical properties in order to mimic the natural human bone mineral. With this main goal, the followings are:

1. To synthesize CHA with different carbonate content by using a wet chemical technique.
2. To evaluate the sintering behavior of the derived CHA under carbon dioxide atmosphere.
3. To optimize the mechanical and biological properties of the sintered CHA compacts
4. To study the bioactivity (*in-vitro*) of the sintered samples via simulated body fluid (SBF).

1.4 Scope of Research

The current study contained three parts, starting with synthesize of CHA with various carbonate content. In the synthesis of CHA powders, wet chemical technique was applied. The optimized synthesized CHA was designated to investigate the effect of different sintering temperature. Sintering was under the dry CO_2 atmosphere to compensate the carbonate loss during the sintering. Lastly, synthesize multi-ions doped CHA via wet chemical method and sintering at the optimum sintering temperature. Wet CO_2 was injected at the cooling stage of the sintering.

The synthesized powder and sintered CHA will be characterized to determine the various physical and mechanical as well as biological properties.

1.5 Structure of the Thesis

Chapter 2, literature review on biomaterials and bioceramics are presented, followed by explanation of different types of bioceramics. Subsequently, a general literature on carbonated hydroxyapatite and its classification with its importance are addressed. Type of the synthesis methods of CHA and the synthesis parameter involved in wet chemical method are extensively discussed. Besides that, the sintering theories and introduction to potential usage wet CO_2 atmosphere on CHA have been reviewed. This is followed by evaluation of biological properties of CHA using SBF.

Chapter 3 presents the materials and methodology of synthesis CHA. This chapter contains three parts of research study, at the first part, synthesizing CHA with variant carbonate content, followed by sintering pressed pellet with different sintering condition, and characterization. The characterization involves the use of X-Ray Diffractometry (XRD), Fourier Transform Infra-Red (FTIR), Carbon-Hydrogen-Nitrogen and Sulfur (CHN/S), Field Emission Scanning Electron Microscopy (FESEM), Energy Dispersive X-Ray (EDX), Linear Shrinkage, Density, Thermal Analysis (TGA), Micro Hardness (Hv) and Fracture Toughness (K_{IC}), Biological Properties (SBF) are further discussed in this chapter. The experimental results are explored and discussed in Chapter 4. This chapter mainly focused on the comparison between different carbonated hydroxy apatite and sintering in CO_2 atmosphere. Based on the results of this study, the sample that exhibited overall best properties was selected for further studies. Then the effect of sintering temperature on the selected CHA is deliberated. Additionally, the effect of multi-substituted CHA on structure of CHA is evaluated. Lastly, Chapter 5 presents the conclusion drawn from the current research findings and suggestions for future work.

CHAPTER 2: LITERATURE REVIEW

This chapter provides a brief overview on biomaterials, followed by different type of bioceramics, whereby a comparison is made of the advantages and disadvantages of each type of bioceramics. The carbonated hydroxyapatite (CHA) presented, as a type of bioceramics is the most compatible material for BGS. Following that, the chapter introduces the wet chemical method used to synthesize CHA. The variation for carbonate (CO_3^{2-}) to phosphate (PO_4^{3-}) of CHA is also discussed. In addition to that, a review of the multi-substituted ions in the structure of CHA and the effect of sintering temperature and carbonate atmosphere on CHA was evaluated. Finally, the chapter concludes with a review of the mechanical properties and bioactivity behavior of CHA in simulated body fluid (SBF).

2.1 Biomaterials

Biomaterials has been defined as the biocompatible materials which is used for biomedical applications. In order to heal, enhance, or substitute damaged tissue or a biological function. It involves not only natural materials like tissues, proteins and cells but also synthetic materials such as metals, ceramics, polymers and composites.

For selecting biomaterials it must be emphasize that biological properties are the most important consideration as opposed to superior mechanical properties (Basu & Nath, 2009; Basu & Ghosh, 2017). To date, many synthetic materials such as, biopolymers, biometals, bioceramics and biocomposites have been considered as biomaterials. Table 2.1 presented the category of biomaterials with its advantages and disadvantages. Amongst them, bioceramics shown better tissue responses and biocompatibility compared to polymer and metal biomaterials (Hench, 1998). Nonetheless, a common drawback to all bioceramics is their brittleness and low mechanical properties that limited their clinical use to non-load bearing application

(Dorozhkin, 2010; Baino et al., 2015). Higher solubility *in vivo* of bioceramics remains an important characteristic, which could accelerate local mineralization of new bone (Eliaz & Metoki, 2017).

Table 2.1: Class of materials for use in the body (Park & Lakes, 2007)

Materials	Advantages	Disadvantages	Example
Polymers (Nylon, Silicones, Rubber, Teflon, Dacron)	Resilient, easy to fabricate	Not strong, deform with time and may degrade	Sutures, sockets, blood, vessels, nose, ear and other soft tissues
Metals (Ti and its alloys, Au, Co-Cr alloys, Ag stainless steels, etc.)	Strong, tough and ductile	May corrode, dense and difficult to manufacture	Bone plates and screws, pacer, dental implant and wire
Ceramics (alumina zirconia, Carbon, CaP, HA and carbon)	Very biocompatible, inert and strong in compression	Brittle, not resilient and weak in tension	Dental and orthopedic implants
Composites such as carbon-based composites or fiber-reinforced bone cement	Strong, tailor-made	Tough to manufacture	Bone cements, heart valves and dental resin

2.1.1 Bioceramics

Ceramics that are designed for use as BGSs, dental implants, and medical are termed bioceramics (Baino, 2015). Calcium phosphates, bioactive glasses, glass–ceramics, alumina and zirconia are genuine examples of bioceramics (Hench, 1991). In the last 50 years there have been a significant advance in the development of bioceramics.

The biocompatibility concerns overcome in 1960s and used in orthopaedic surgery associated with the metallic implants (Vallet-Regí & Arcos, 2013). Recently, ceramic

materials exhibited a number of different applications in biomedical engineering due to their physico-chemical properties (Vallet-Regí, 2014).

The biocompatibility of some ceramic materials made them an ideal materials for hard tissue replacement, such as cranial, maxillofacial, dental, middle ear, spinal, as well as otolaryngology surgery (Diaz-Rodriguez et al., 2018). However, many of these biocompatible ceramic materials are still subjected for further improvement. In order to be used for implant application, the bioceramics should be non-allergic, non-toxic, and non-carcinogenic. Ideally, the bioceramics should be able to form a strong chemical bond with host after transplantation (Wong et al., 2012). In general, these bioceramics can be classified according to their reactivity as nonresorbable, bioactive and bioresorbable (Ben-Nissan, 2003; Khang et al., 2008), as displayed in Table 2.2.

Table 2.2:Classification bioceramics according to their reactivity (Vallet-Regí, 2014)

Classification	Implant tissue Reaction	Example
Nonresorbable/bioinert	Tissue forms a non-adherent fibrous capsule around the implant	Carbon, Silicon carbide, Alumina and Zirconia
Bioactive/surface-reactive/semi-inert	Tissue forms an interfacial bond with the implant	Hydroxyapatite, Glass ceramic (A-W), Bioglass
Bioresorbable/biodegradable Non-inert	Tissue replace implant	Carbonated hydroxyapatite, Hydroxyapatite, α- & β-tricalcium phosphate, Calcium carbonate

Among these classes, bioresorbability and bioactivity are two important requirements of bioceramics. These properties of bioceramics depend on their interaction with collagen. Aggregation of proteins and cells at the interface with the bioceramics would

result in the resorption of the material, leading to the formation of bone tissue (Thamaraiselvi & Rajeswari, 2004).

The major inorganic component of hard tissues is apatite with a profound biological and clinical significance. Apatite name derives from a Greek word apate, which means "deceive ", since apatite is similar in appearance to many other minerals (Duminis et al., 2017). Apatite is a group of phosphate minerals containing isomorphic hexagonal structure and space group of $P6_3/m$ despite the wide range of composition, exist in several forms of calcium phosphate (Legeros et al., 2009). The calcium phosphates are abundant in nature and living systems.

2.1.1.1 Calcium Phosphates

Calcium phosphates or CaP_2O_6 describes a group of mineral having calcium cations (Ca^{2+}) together with phosphate anions (PO_4^{3-}) and sometimes hydroxide (OH^-) ions (Wang & Nancollas, 2008). Calcium phosphate mineral defined as a ca-deficient apatites with an apatitic structure appears as the main components of the bones and teeth (Gross & Berndt, 2002). The calcium phosphates (CaP) occur abundantly in nature in several forms, which are tabulate in Table 2.3. In particular, they constitute the main inorganic components of the hard tissues (Hughes, 1996; Boanini et al., 2010).

Variation in the calcium to phosphate (Ca/P) molar ratio may lead to formation of multivalent calcium phosphate such as mono, di-, tri- and tetra-calcium phosphate, as well as its composition in hydroxyapatite and carbonated hydroxyapatite. CaP bioceramics commercialized as bone repair materials in the 1980s. The first attempt to *in vivo* of tricalcium phosphate (TCP) was made in 1920 by Fred Houdlette Albee (Albee, 1920; Eliaz & Metoki, 2017). In the following years, in 1951, for the first time Ray et al. (1952) implanted HA in guinea pigs and rats. However, it was only in the 1970's when the other CaPs mostly HA, were synthesized, characterized, and applied in medicine.

Consequently, the attention on these materials has been increased. The presence of carbonate in bone and tooth mineral and hydroxyapatite was observed directly by infrared spectroscopy in the 1960s (Legeros, 1965).

Table 2.3: Calcium phosphates and their applications (LeGeros & LeGeros, 2003)

Compound	Chemical formula	Ca/P	Applications
Monocalcium phosphate monohydrate (MCPM)	$Ca(H_2PO_4)_2$	0.5	Cement, polyphosphate
Dicalciumphosphate dihydrate, DCPD	$CaHPO_4.2H_2O$	1	Cement, coating
Dicalciumphosphate anhydrous, DCPA	$CaHPO_4$	1	Cement, coating
Octacalciumphosphat, OCP	$Ca_8H_2(PO_4)_6.5H_2O$	1.33	Coating, bonegraft
Alpha tricalcium phosphate, (α-TCP)	$Ca_3(PO_4)_2$	1.50	Cements
Beta-tricalcium phosphate, β-TCP	$Ca_3(PO_4)_2$	1.50	Cement, bonegraft, composite
Calcium-deficient apatite, CDA	$Ca_3(PO_4)_2$	<1.67	Bonegraft, cement, coating
Biphasic calcium phosphate, BCP	HA/β-TCP	1.55-1.66	Bonegraft, coating
Fluorapatite, FA	$Ca_{10}(PO_4)_6F_2$	1.67	Bonegraft, coating
Hydroxyapatite (HA)	$Ca_{10}(PO_4)_6(OH)_2$	1.67	Bonegraft, coating, composite
Carbonate hydroxyapatite	$(Ca, Na)_{10}(PO_4, CO_3)_6(OH)_2$	1.7-2.6	Bonegraft
Tetracalcium phosphate, TTCP	$Ca_4(PO_4)_2O$	2.0	Cement

Hydroxyapatite (HA) and β-tricalcium phosphate (β-TCP) are the most commonly form of calcium phosphate ceramics. Slight difference in chemical composition and structure of calcium phosphate compounds can influence their applications significantly (Billotte, 2003). The stability of calcium phosphate is reported to have increased with increasing Ca/P molar ratio (Park & Lakes, 2007). HA with Ca/P higher than 1.67, will be present along with calcium oxide (CaO) phase (Best et al., 2008). However, HA with Ca/P molar ratio lower than 1.67, resulted in the formation of secondary phases such as β-TCP in the sintered material, depending on the temperature and condition of sintering (LeGeros & LeGeros, 1993). The second phase may negatively affect the biological responses of the implants (Best et al., 2008).

Several calcium phosphates may reprecipitate as hydroxyapatite and β-TCP. The process not only depend on the Ca/P ratio but also on the presence of water, impurities, and temperature. Hydroxyapatite will form in a wet chemical preparation environment and lower temperature (< 900 °C). In a dry atmosphere and high temperature (> 900 °C), calcium phosphates readily transformed into β-TCP or β-TCP biphasic (BCP) mixture (Park & Lakes, 2007).

2.1.1.2 Tricalcium Phosphate

Tricalcium phosphate (TCP) is also known as Whitlockite. It is a calcium phosphate ceramic with a chemical formula of $Ca_3(PO_4)_2$ and a Ca/P ratio of 1.5. It is widely used as a bioceramic material due to its good osteoconductivity. TCP has four polymorphous: α, β, γ and supper α. The γ and supper α phase are of no interest because obtained at high pressure and temperature (above 1500 °C) respectively (Kumta et al., 2005).

Consequently, the most commonly noted TCP polymorph in the field of bioceramics are α and β-TCP. While, β-TCP is a stable phase at room temperature and transforms into

α-TCP at ~1125 °C and above this. The α-TCP phase becomes stable above 1430 °C until the melting point of 1756 °C (Mirhadi et al., 2011).

In the early 1970s, Driskell et al. (1973) proposed β-TCP to repair hard tissues. Theoretically, a resorbable TCP is an ideal material for implantation. After implantation, TCP presents degradation over a period of time and progressively replaced by the natural host tissues to form HA according to the following reaction:

$$4Ca_3(PO_4)_2 + 2H_2O \rightarrow Ca_{10}(PO_4)_6(OH)_2 + 2Ca^{2+} + 2HPO_4^{3-} \quad (2.1)$$

Both TCP-ceramic and HA are highly biocompatible. However, they are different in the biologic response at the host site, HA is more permanent as bone grows into the scaffold (Giannoudis et al., 2005).

2.1.1.3 Hydroxyapatite

Hydroxyapatite (HA) ($Ca_{10}(PO_4)_6(OH)_2$) is a natural mineral form of calcium apatite with a Ca/P molar ratio of 1.67. The lattice parameters for HA were found to be $a = b =$ 9.418 Å and c = 6.884 Å, with a theoretical density of 3.16 g/cm^3 (Griciuc et al., 2005). The structure of HA is depicted in Figure 2.1.

In the 1920s, Jong (1926) observed that the X-ray diffraction patterns of bone mineral very similar to the hydroxyapatite. Later the crystal structure of hydroxyapatite and bone mineral were identified by Posner and co-workers (Posner et al., 1958; Kay et al., 1964; Posner, 1969). Its affinity to bone minerals has received significant attention since the past two decades mainly because of their biocompatibility, bioactivity and osteoconductivity (Liu, 1997; Bouyer et al., 2000; Riman et al., 2002; Afshar et al., 2003; Murugan & Ramakrishna, 2006; Rajabi-Zamani et al., 2008; Boanini et al., 2010;Chang et al., 2011; Kumar et al., 2012; Saber-Samandari et al., 2016).

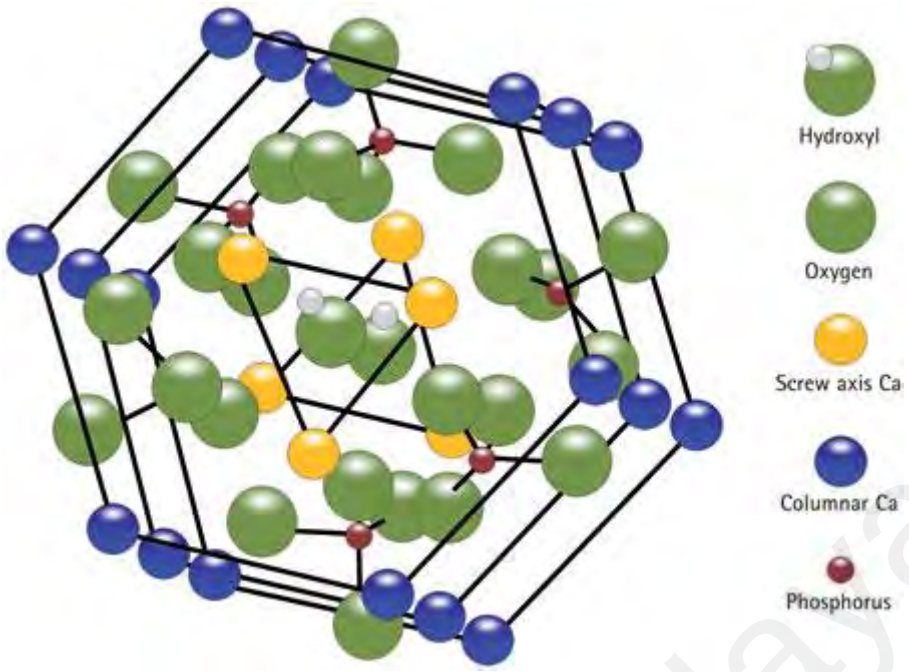

Figure 2.1: Structure of hydroxyapatite (Brunton et al., 2013)

Synthetic HA can be employed in forms of granules, blocks or porous, as coating in biomedical application, or as composite with polymers or other ceramics to fill bone defects or voids (Ishikawa et al., 2003; Gergely et al., 2010; Radovanović et al., 2014).

The most common use of HA is in application of bone grafts and coating of implants for its osteoconductive properties (Shepherd et al., 2012). A porous structure of hydroxyapatite can be used as scaffold for new bone formation or else as a socket filling after tooth extraction (Kolmas et al., 2014).

Despite noticeable attention paid to HA for its ability to directly bond with bone, it has some disadvantages compared to biogenic apatite. Low solubility and sluggish bone resorption considered as serious drawbacks to induce a massive new bone formation (Kovaleva et al., 2008). Besides, HA is osteoconductive (ability to support tissue ingrowth and bone formation) and not osteoinductive (ability to form bone when implanted in non-osseous sites) (Yoshikawa & Myoui, 2005; LeGeros et al., 2008).

Furthermore, inadequate mechanical strength of dense HA ceramics particularly when exposed in aqueous medium, hindered its application as load-bearing implant. However, it has been used for dental and as coatings on orthopedic prostheses because of its biocompatibility and osteoconductivity. As shown in Table 2.4, the Young's modulus of HA ceramics is higher than that of human bond. It ranges from 4.0-117 Gpa. High Young's modulus of HA is undesirable as this makes the bioceramic very brittle (Park & Lakes, 2007). As a result, HA can only be used in non-load bearing parts of the skeleton due to their inferior mechanical properties. Nevertheless, HA still can be used as filler in bone or teeth (Jarcho, 1981; Shin et al., 1992; Teraoka et al., 1998; Riman et al., 2002).

Table 2.4: Typical mechanical properties of synthesis HA (Park & Bronzino, 2003)

Properties	Values
Youngs modulus (GPa)	4.0-117
Compressive strength (MPa)	294
Bending strength (MPa)	147
Hardness (Vickers, GPa)	3.43

The crystallite size of hydroxyapatites are very small in human bone and can be considered as nanostructured materials. Hence considerable attention and efforts have been focused on producing synthetic nano HA materials. Moreover, It has been revealed that nanosized HA powders would improve densification and better bioactivity than coarser crystals (Rajabi-Zamani et al., 2008).

In order to develop synthetic BGSs, it is desirable to understand the bioresorbability of synthesized HA the over a period of time to be replace with the regenerated bone. Murugan & Ramakrishna (2006) indicated that the resorbability of HA could be promoted by ionic doping agents, or smaller crystallite size.

The major difference between biological bone apatites and HA is the presence of significant amounts of carbonate ions in natural bone tissue. Many recent studies have focused on synthetic carbonated hydroxyapatite as carbonate ion is a part of the biological apatite structure (LeGeros, 1991; Combes, 2016).

2.1.1.4 Carbonated Hydroxyapatite

Human bone mineral differs chemically in composition from stoichiometric hydroxyapatite (HA) in that it contains additional trace ions, of which carbonate CO_3^{2-} is the most abundant species (Barralet et al., 1998; Merry et al., 1998; Tadic et al., 2002; Gibson & Bonfield, 2002; Landi et al., 2004;Vallet-Regí & González-Calbet, 2004).

Synthetic carbonate containing hydroxyapatite (CHA) has emerged as a promising bone-substitute ceramic material for biomedical application. Carbonated hydroxyapatite (CHA) with chemical formula $Ca_{10-x}(PO_4)_{6-x}(CO_3)_x(OH)_{2-x}$ where $0 \leq x \leq 2$ is a preferred material for bone repair. These carbonated apatites are expected to exhibit improved structural and biological properties when compared to monolithic hydroxyapatite (Lafon et al., 2008). Carbonate ion is the main component of dental and bone tissues in humans (Siddiqi & Azhar, 2020). It has been established that the amount of carbonate ions found in human bones is age dependent and typically ranges from 2 to 8 wt.% (Zhu et al., 2015; Graziani et al., 2017).

The increase in the CO_3^{2-} content occurs in older bone. The aging is accompanied by a reduction in the HPO_4^{2-} content and an increment in the Ca/P molar ratio (Rey et al., 1991). Such compositional changes have attracted attention to evaluate carbonated apatite to provide support for structural changes in the mineral phase that accompany aging.

Carbonate ion CO_3^{2-} was detected for the first time in 1850 as Carbonate-fluorapatite in the UK and was named francolite. Incorporation of the CO_3^{2-} ion into the apatite

structure has received much interest in various biomedical applications because the carbonate ion increases the solubility of hydroxyapatite and also has an impact on bone and dental health (Frank-Kamenetskaya et al., 2011).

In early 1960s, the influence of CO_3^{2-} on the morphology and lattice structure of apatite started to study by LeGeros (LeGeros, 1965; LeGeros et al., 1967; Liao et al., 2007). It is known as a potential biomaterial for bone regeneration applications because of its similarity to natural bone mineral (Kovaleva et al., 2008).

In particular, as compare to stoiciometric HA, the carbonated hydroxyapatite (CHA) exhibits better biocompatibility, bioactivity, bioresorbability and more similar to the inorganic component of bone (Morales-Nieto et al., 2013). It has been revealed that partial substitution of carbonate anions (CO_3^{2-}) in HA lattice has considerable decrease in crystallinity due to the lattice defects and increase in surface area due to the nanosized particles (He et al., 2008; Vallet-Regí, 2014). Thus, in general biological apatite are referred as carbonated hydroxyapatite (CHA).

2.1.2 Classification of Carbonated Hydroxyapatite

CHA can be classified either as B-type (CO_3^{2-} substitutes PO_4^{3-}), A-type (CO_3^{2-}substitutes OH^-) or AB-type CHA (CO_3^{2-}substitutes both OH^- and PO_4^{3-} (Lafon et al., 2008). For biomedical applications, most of the carbonated apatites are mainly B-type CHA with A-type/B-type ratio of 0.7–0.9, depending on the age of the tissue (with higher ratios normally observed in older tissues) (Rey et al., 1989; Kumar et al., 2000).

Studies have shown that the synthesis method and processing conditions can result in the formation of different type of CHA. The A-type CHA can be synthesized by thermal treatment of HA over a range of temperature (800 to 1000 °C) in dry CO_2 atmosphere (Gibson & Bonfield, 2002; Lafon et al., 2008). According to the Equation 2.2, addition

of carbonate group would balance the loss of OH group in order to maintain charge balance.

$$Ca_{10}(PO_4)_6(OH)_2+xCO_2 \leftrightarrow Ca_{10}(PO_4)_6(OH)_{2-2x}(CO_3)_x +xH_2O \quad \text{(with } 0\leq x\leq 1\text{)} \quad (2.2)$$

The B-type CHA nanoparticles can be synthesized by both the wet and dry methods. Amongst them, the wet method has raised much interest owing to its good homogeneity of the product. The resulting B-type CHA would have a chemical formula of $Ca_{10-x}(PO_4)_{6-x}(CO_3)_x(OH)_{2-x}$ with $0 \leq x \leq 2$ (Lafon et al., 2008).

As the substitution of CO_3^{2-} in HA crystal structure would lead to changes in the Ca/P ratio and crystal lattice parameters (LeGeros, 1965; Bang et al., 2014), LeGeros & LeGeros (2002) and Landi et al. (2004) hypothesized that the Ca/P ratio of CHA would be high in the B-type CHA due to the substitution of CO_3^{2-} for PO_4^{3-}.

The substitution of CO_3^{2-} to PO_4^{3-} in HA crystal structure can be evidenced by the shifting of the (300) Miller's plane to higher angles, indicating a contraction of the *a-axis*. The substitution also resulted in the shift of the (002) Miller's plane to lower angles, indicating a slight expansion of the *c-axis* (LeGeros et al., 1969). This phenomenon is due to the difference in ionic radius between PO_4^{3-} (2.38 Å), OH^- (1.1 Å) and CO_3^{2-} (1.76 Å). When the substitution of CO_3^{2-} to PO_4^{3-} happens, a contraction of the *a-axis* would be expected, resulting to an increase in the *c-axis* /*a-axis* ratio (Aminian et al., 2011; Madupalli et al., 2017).

The A-type and B-type can also simultaneously occur to form AB-type CHA in accordance to the following relationship: $Ca_{10-x}(PO_4)_{6-x}(CO_3)_x(OH)_{2-x-2y}(CO_3)_y$ with $0 \leq x \leq 2$ and $0 \leq y \leq x/2$, where x and y corresponds to the B-type and A-type CHA, respectively (Gibson & Bonfield, 2002; Lafon et al., 2008). Table 2.5 shows the comparison between the A-type and B-type CHA. The B-type substitution having lower

A-type/B-type ratio (0.7–0.9), is prefred compared to A-type. To take into account B-type CHA shown to cause a reduction in crystallinity and enhance in solubility with no changing on the surface polar property of the material (Landi et al., 2004; Krajewski et al., 2005).

Table 2.5: Comparison between A- and B-type CHA (Elena Landi et al., 2004)

Properties	A-type CHA	B-type CHA
CO_3^{2-}substitution	OH^- site	PO_4^{3-}site
A-type/B-type ratio	Higher	Lower
Most abundant species	Old tissues	Young tissues
Preparation	Heating in dry CO_2 atmosphere	Synthesized by dry and wet technique
Synthesis temperature	High (>800 °C)	Low
Unit cell parameters *a-axis* (Å) *c-axis* (Å) *c/a* ratio	 Increase (>9.418) decrease (<6.884) Lower (<0.73)	 decrease (>9.418) Increase (<6.884) Higher (<0.73)
Miller's plane (300) (002)	 Move to lower angle Move to higher angle	 Move to higher angle Move to lower angle
Chemical formula	$Ca_{10}(PO_4)_6(OH)_{2-2y}(CO_3)_y$ with $0 \leq y \leq 1$	$Ca_{10-x}(PO_4)_{6-x}(CO_3)_x(OH)_{2-x}$ with $0 \leq x \leq 2$
Preference	Less preferable, lower affinity for human trabecular osteoblastic cell as compared to HA	Preferable, decrease in crystallinity and increase in solubility without changing surface polar property in both *in-vivo* and *in-vitro* test
Infrared spectrum (CO_3^{2-} bands)	877-880, 1500, 1540-1545 cm^{-1}	870-875, 1410-1430, 1450-1470 cm^{-1}

Barralet et al., (1998) indicated that for carbonate content of below 4 wt.%, the carbonate ions would be present in the A site, while at higher contents (> 4 wt.%), carbonate was located predominantly in the B-site.

Both the A- and B-type CHA can also be characterized fourier transform infrared (FTIR) spectroscopy. The vibrations of carbonate can be observed in two regions: ν_2 =850-890 cm^{-1} and ν_3=1400-1650 cm^{-1}. Existence of the carbonate bands at 877-880, 1500 and 1540 - 1545 cm^{-1} in the spectrum indicates A-type CHA, whereas carbonate bands at 870-875, 1410-1430, and 1450-1470 cm^{-1} are attributed to the B-type CHA (Rey et al.,1989; Landi et al., 2004; Ślósarczyk et al., 2005; Yanny-Marliana & Ahmad-Fauzi, 2011). The AB-type CHA shows a characteristic band at 1515 cm^{-1} (Barralet et al., 1998).

2.1.3 Physical Properties of Nanocrystalline CHA

The prefix ‘‘nano-’’ precisely refer to 10^{-1} m (Dorozhkin, 2010). Karch et. al. (1987) reported that, with nano grain size, a brittle ceramic could permit a large plastic strain up to 100%. In addition, nanostructured ceramics can be sintered at a lower temperature. Nanosized and nanocrystalline bioceramics are promising for use as orthopedic and dental implant with improved biological and biomechanical properties. Thus, in order to mimic the natural bone, researchers have attempted to synthesize nanosized CHA materials by various methods, aiming to achieve low crystallinity and nanometer crystal sizes (Liao et al., 2007).

Nanocrystalline CHA, with typical grain sizes < 100 nm powders have greater surface area, thus they displayed better bioactivity and sinterability than coarser crystals. In addition, nanosized CHA powders exhibit enhanced densification and as a consequence, improved mechanical properties (Siddiqi et al., 2018). The nanosized inorganic phase of the synthesized CHA material has a low degree of crystallinity which resembles that of natural bone. Therefore, because of its excellent biocompatibility and biodegradation properties and exhibiting nanostructure of natural bone, it is desirable for the stimulation and regeneration of new bone formation (Webster, 2001).

2.1.4 Variation in Amount of Carbonate to Phosphate of CHA

Nano-CHA material with variant carbonated content have been studied by some researchers. Liao et al. (2007) indicated that the morphology of CHA changed with increasing of carbonate content from flat platelet, needle-array platelet, particle consisted platelet, smaller platelet and finally spherical particle with increasing CO_3^{2-}/PO_4^{3-} ratio from 0 to 10. However, Ezekiel et al. (2018) reported that no significant changes in morphology was observed with increasing CO_3^{2-}/PO_4^{3-} molar ratios from 0.67 to 1.00. Structural information showed increasing carbonate content resulted in amorphous phase, increased in surface area and reduction in size of the of particles. Furthermore, increasing carbonate content has been reported to promote a rapid formation of apatite layer which may result in improving the biological properties of the implants (Kovaleva et al., 2009).

There are some reports showing the formation of secondary phase ($CaCO_3$) as a result of an increase in carbonate content. Kee et al. (2013) observed the $CaCO_3$ secondary phase at a ratio of $CO_3^{2-}/PO_4^{3-} = 5$ by using XRD ($2\theta = 29°$). Barinov et al. (2006) revealed an approximately 3 wt.% increase in carbonate content that resulted in the formation of secondary phase (0.04 wt.% $CaCO_3$). The secondary phase was presented in sintered AB-type CHA up to 900 °C sintering temperature but vanished at 950 °C and above due to the partial phase decomposition of CHA structure.

Lafon et al. (2008) observed the formation of $CaCO_3$ with a high (CO_3^{2-}/PO_4^{3-}) molar ratio of 2 (~7.5 wt.%) by using $(NH_4)HCO_3$ as carbonate source by precipitation method. Formation of $CaCO_3$ was attributed to the restriction of PO_4^{3-} available for substitution CO_3^{2-} in apatite structure, consequently excess amount of CO_3^{2-} ions could have reacted with Ca^{2+} to form $CaCO_3$.

Merry et al. (1998) indicated that Ca/P increased with increasing carbonate due to the substitution of CO_3^{2-} for PO_4^{3-} that confirmed the B-type CHA. The higher ratio of CO_3^{2-}

the lower temperature required to achieve a density of 95%. Secondary phases of CaO and TCP were observed at the temperature of 900 °C in CHA with higher carbonate (10.2 wt.%) but appeared at 1100 °C in CHA with lower carbonate (7.6 wt.%).

Some researchers have been investigated the effects of the carbonate content on the sintering temperature. The first evidence that presence of carbonate in apatite structure decreases the sintering temperature of apatite was reported by Ellies et al. (1988). It was revealed an inverse linear relationship between initial carbonate content of the CHA samples and sintering temperature. Hence, suggested that the presence of carbonate can lowers the activation energy for surface diffusion. Consequently, with increasing carbonate content in the CHA samples, the reactivity increased, and this resulted in lower sintering temperature. They also reported that, the amount of the Knoop hardness number increased with increasing carbonate from 630 to 661 for 3% to 6% carbonate respectively.

A study by Doi et al. (1993) has been demonstrated that the presence of carbonate ion in apatite structure resulting in a decrease in the sintering temperature. They also reported that, higher amounts of carbonate ions in the CHA led to finer particles and a greater specific surface area. According to the diffusion mechanism, the sintering temperature is proportional to the initial particle size. The decrease in the sintering temperature may due to the increasing of the surface diffusion (Zyman & Tkachenko, 2011).

The mechanical properties of various weight percetage of carbonate, ranging from 0 to 0.62 wt.% of the A-type CHA was examined by Teraoka et al. (1998). It was concluded that the strength of CHA significantly decreased with increasing carbonate content, although the solubility increased. Therefore, they suggested that for a load-bearing purpose, HA are superior to A-type CHA as a biomaterial.

The substitution of carbonate ions in the apatite crystal lattice can affect the biological and materials properties. It has been reported that sintering temperature required for a given degree of densifcation decreased gradually with the increasing carbonate content. Studies have also shown that the bioactivity of samples increased when carbonate content increased due to the higher dissolution rates of synthetic CHA compare with pure HA (Garskaite et al., 2016).

2.1.5 Multi-Ion Doped CHA

In addition to carbonate (CO_3^{2-}) substitution, co-doping of trace elements such as Zn^{2+}, Na^{+}, Ti^{4+}, Sr^{2+} and Mg^{2+} into the structure of CHA can affect the crystallite sizes, crystallinity level, lattice parameters, solubility, morphology, thermal stability and bioactivity of the bioceramic. These changes would improve its mechanical strength, accelerate bone formation and enhance the resorption rate of bone mineral (Lin et al., 2011). The compositions and lattice parameters of bone and stoichiometric HA is compared in Table 2.6.

Several researchers investigated the effect of co-substitution of a metal and carbonate ions (Shepherd et al., 2012), for example Mg^{2+}/ CO_3^{2-} and Na^{+}/ CO_3^{2-}, comprising of single type of cation and anion substitution in HA (Lafon et al., 2008). Numerous researchers have also attempted to simultaneously co-substitute multiple elements such as Mg, Na, Si and K together with CO_3^{2-} to form multi-ions doped CHA (Rey et al., 1989; Kumar et al., 2000; Lafon et al., 2008; Uskoković, 2020).

The major hurdle with co-substitution of multiple ions is the competition that would occur amongst the atoms to occupy the HA lattice (Lin et al., 2011). Nevertheless, researchers have tried to synthesize anionic-cationic co-substituted HA in the form of di-substituted, tri-substituted or multi-substituted HA (Bang et al., 2015). In particular, attention was given on several ions which includes Mg^{2+}, SiO_4^{4-}, Zn^{2+} and Cu^{2+} for their

pronounced biological role. For instance, magnesium ions played an important role in calcified tissues that indirectly influences mineral metabolism through activation on alkaline phosphatase (ALP) (Bigi et al., 1992). On the contrary, silicon substituted HA enhanced the bioactivity and dissolution rate of HA (Mostafa et al., 2011). The presences of copper and zinc ions in minute quantities acts as stimuli for various metabolic processes in organisms and also enhanced antibacterial activity (Shanmugam & Gopal, 2014; Stanić et al., 2010). In addition, zinc has also a stimulatory effect on bone formation (Stanić et al., 2010).

Table 2.6: Comparison between the compositions and lattice parameters of bone and stoichiometric HA (Šupová, 2015)

Composition	Concentration level	Bone	Stoichiometric HA
Calcium (Ca)	(wt.%)	34.80-36.60	39.6
Phosphorus (P)		15.20-17.10	18.5
Carbonates (CO_3)		4.80-7.40	_
Sodium (N)		0.90-1.0	
Magnesium (Mg)		0.60-0.72	
Chlorine (Cl)		0.10-0.13	
Fluoride (F)		0.03-0.10	
Potassium (K)		0.03-0.07	
Strontium (Sr)		0-0.05	
Silicon (Si)	(ppm)	0-500	
Zinc (Zn)		0-39	
Chromium (Cr)		0-0.33	
Cobalt (Co)		0-0.025	
Manganese (Mn)		0-0.17	
Lattice parameter			
a-axis	(nm)	0.9410	0.9430
c-axis		0.6890	0.6891

2.1.6 Magnesium Cation Doped CHA Structure

Magnesium cation (Mg^{2+}) plays an important role in bone metabolism. The incorporation of Mg^{2+} with the organic phase was first reported by Driessens, (1980). The concentrations of Mg in the dentine and bone are about 1.23 wt.% and 0.73 wt.%,

respectively (Percival, 1999). The magnesium concentration of bone decreases with age (Šupová, 2015). Diminution in magnesium adversely affect bone metabolism, cessation of bone growth, and increased bone fragility (Landi et al., 2006).

According to some authors Mg substitute the Ca(I) position (parallel to *c-axis*) (Yasukawa et al., 1996; Tampieri et al., 2004; Sprio et al., 2005; Ren et al., 2010) whereas some literatures reveal the substitution of Mg in the Ca(II) position (at the *c-axis*) (Bigi et al., 1996; Laurencin et al., 2011). The substitution of Mg^{2+} ions associated with the contraction of the *c-axis*, due to the smaller atomic radius of Mg^{2+} (0.69 Å) when compared to Ca^{2+} (0.99Å). Also, magnesium hinders apatite crystallization and destabilize the apatitic structure. These changes lead to amorphization which resulted in an increase in solubility and biodegradability of HA in physiological fluids (Bigi et al., 1992; Bertoni et al., 1998; Laurencin et al., 2011).

Larson et al. (2013) synthesized CHA doped with Mg^{2+} and Na^{+} at pH of 7 and temperature between 60–70 °C. The SEM images (Figure 2.2) showed the carnation-like morphology and increasing the BET surface area of the powders with substitution of Mg^{2+} and Na^{+} into the CHA structure.

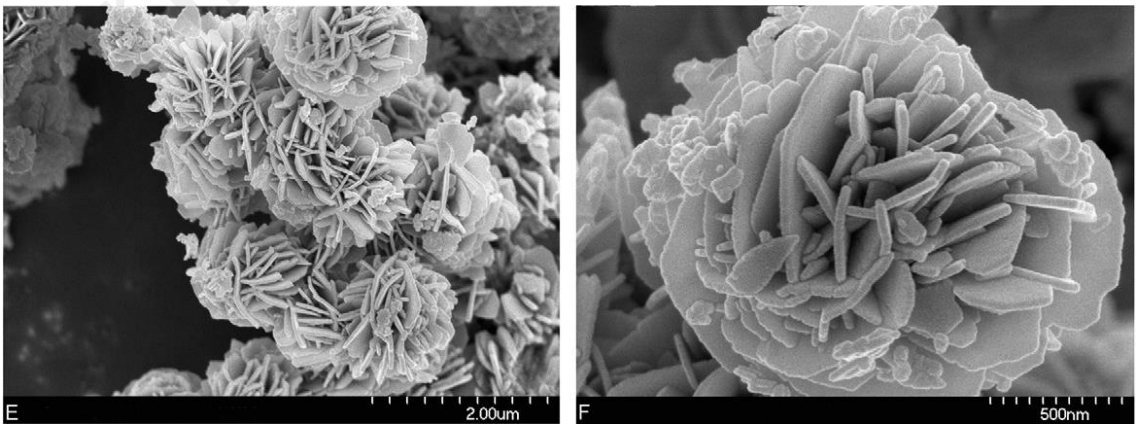

Figure 2.2: SEM of doped CHA powders, synthesized by soaking precipitated $CaCO_3$ in 0.5 M PO_4^{3-} buffer solution (Larson et al., 2013)

Lala et al. (2016) was synthesized nanocrystalline Mg doped A-type CHA by mechanical alloying (ball milling) and suggested that the substitution of Mg^{2+} ions to Ca^{2+} ions in HA lattice could be represented by the following equation;

$$(4\text{-}x)\ CaCO_3 + 6\ CaHPO_4.2H_2O + x\ MgO \rightarrow Ca_{10-x}\ Mg_x\ (PO_4)_6(OH)_{2-2y}(CO_3)_y \qquad (2.3)$$

where $0 < x < 4$ and $0 < y < 1$. The results revealed that the presence of Mg^{2+} ion in CHA structure enhance the biocompatibility, as indicated in the MTT assay test. In addition, incorporation of Mg^{2+} ion in CHA structure enhanced the amorphous phase in CHA and resemble the natural mineral bone.

2.1.7 Silicate Anion Doped CHA Structure

Silicate ions $(SiO_4)^{4-}$ can replace the phosphate ions in the HA lattice. The chemical formula for SiHA can be represented as $Ca_{10}(PO_4)_{6-x}(SiO_4)_x(OH)_{2-x}$, where $x \sim 0.05–1.38$. The negative charge of the $(SiO_4)^{4-}$ anions substituted PO_4^{3-} anions are balanced by the hydroxide vacancy formation (Gibson et al., 1999). It has been established that the maximum amount of Si can be incorporated into HA is 5 wt.% (Vallet-Regí & Arcos, 2005; Gasqueres et al., 2008). The substitution of silicon in the HA lattice lead to a small contraction in the *a-axis* and an expansion in the *c-axis* of the unit cell.

Silicon is one of the trace elements known to be essential in biological processes. Studies on animals have shown that silicon has a specific metabolic role in connection to bone growth. Hence, incorporation of Si in HA has been considered to be a promising way of improving the bioactivity of hydroxyapatite (Gasqueres et al., 2008). Studies carried out by Vallet-Regí & Arcos (2005) have shown that silicon substituted hydroxyapatites (SiHA) are more bioactive than pure hydroxyapatites. The resulting SiHA bonds faster to the bone after implantation, ensuring the functional connection between the implant and the living bone.

Mostafa et al. (2011) studied the crystal structure of Na^{+}, SiO_4^{4-} and CO_3^{2-} co-substitution in HA. It was reported that, SiO_4^{4-} and CO_3^{2-} groups were substituted for two PO_4^{3-} groups. This substitution could be described by the formula;

$$Ca_{10-x}Na_x(PO_4)_{6-x-y-2z}(SiO_4)_{y+z}(CO_3)_{x+z}(OH)_{2-y} \quad (2.4)$$

2.1.8 Zinc Cation Doped CHA Structure

Zinc ion (Zn^{2+}) is an essential trace element in human bone in order to promote the bone metabolism, formation and resorption. Zinc is also essential for DNA replication, bone growth, bone mineralization and improve its clinical applications (Li et al., 2008). Metals such as silver (Ag), gold (Au), copper (Cu) and zinc (Zn) are well known for their antibacterial activities (Jaiswal et al., 2012; Chung et al., 2006). Zinc substitution for Ca sites in the apatite structure can induce contraction of the lattice parameters a and c which was due to the fact that the Zn^{2+} had smaller ionic radius (0.74 Å) than Ca^{2+} (0.99Å) (Miyaji et al., 2005).

The effect of Zinc doped CHA on structural and electrical properties of CHA was studied by Refaat et al. (2017). They revealed that the substitution of Zn^{2+} into the CHA structure would change the physical properties such as ionization potential, and molecular dimensions. It is likely that such changes are due to the disruption of electronic distribution and dipole moment.

2.1.9 Copper Cation Doped CHA Structure

Copper (Cu^{2+}) presents in hard tissues in mammals as an essential trace element (Erol et al., 2012; Radovanović et al., 2014) which stimulates many enzymes activity and plays an important role in processes for bone formation (Habibovic & Barralet, 2011; Huang et al., 2015). A slight decrease in the lattice parameters *a* and *c* is attributed to the smaller

ionic radius of copper (Cu^{2+} (0.73 Å)) compared to the calcium (Ca^{2+} (0.99 Å)) (Shanmugam & Gopal, 2014).

Copper is essential ion for blood vessel formation, and it has been offered good antimicrobial activity at low Cu^{2+} concentration. For these reasons copper substituted HA has attracted researchers. Copper-substituted CHA coating on titanium (Ti) substrate have been studied by Huang et al. (2015). They found that the Cu-CHA coating demonstrated better corrosion resistance in SBF solution in compared with pure HA coating. Cu-substituted CHA also exhibited greater ability to reduction of the bacterial adhesion on the Ti implant surfaces. Thus, Cu-CHA is known as a potential candidate for biomedical applications with good antibacterial property and bone bonding ability.

2.2 Synthesis of Nano Carbonated Hydroxyapatite Powder

Various methods have been proposed to synthesis nanocrystalline CHA, including microwave irradiation (Kumar et al., 2000; Murugan & Ramakrishna, 2006; Zou et al., 2012; Gandou et al., 2015), sonochemistry and microwave (Stanislavov et al., 2018), mechanochemical–hydrothermal (Suchanek et al., 2002; Riman et al., 2002), mechanochemical (Fahami et al., 2015; Lala et al., 2016; Youness et al., 2017), hydrothermal (Roy et al., 1974; Teraoka et al., 1998; Riman et al., 2002; Guo et al., 2013; Xue et al., 2015), hydrolysis (Pieters et al., 2010), vapour diffusion (Iafisco et al., 2010), nonalkoxide sol–gel (Rajabi-Zamani et al., 2008), emulsion (Du et al., 2018) and wet chemical precipitation methods (Lafon et al., 2008; Zhou et al., 2008; Kee et al., 2013). Generally, there are two routes of synthesizing CHA powder, i.e. wet and dry method. The wet method is regarded as the common synthesis route to produce B-type CHA powder (Lafon et al., 2008).

2.2.1 Wet Methods

The wet technique can be divided into six main groups that are hydrothermal, hydrolysis, sol-gel, neutralization, emulsion and chemical precipitation method (Liu et al., 2001). Each method has its own advantages over the others. Among these techniques, the wet chemical precipitation method is most popular for synthesizing B-type CHA, as it presents advantages of precise control over the size and morphology of the particles, simplicity of the reaction system, low reaction temperature and good reproducibility.

2.2.1.1 Hydrothermal Method

Hydrothermal process is defined as a chemical reaction in aqueous media inside an autoclave at elevated pressure and temperature. As one of the most common methods for synthesis of CHA, it has been indicated that hydrothermal treatment resulted in highly crystalline and relatively stoichiometric of CHA nanoparticles (Sadat-Shojai et al., 2013). So far, several research papers has been published regarding the hydrothermal synthesis of CHA. Han et al. (2002) synthesized CHA by hydrothermal method for coating on a titanium alloy. For the hydrothermal synthesis CHA, 0.01M carbonate concentration of $(NH_4)_2 CO_3$ were used at the pH of 13. Subsequently, solution was added to an autoclave, and coated on titanium alloy substrates. In comparison with HA coatings, the CHA coatings are expected to show much more biological efficacy.

In another study, Guo et al. (2013) fabricated hollow CHA microspheres with mesoporous structure (HCHA) by hydrothermal method. According to the results, the hierarchically porous microspheres HCHA have great potentials for bone-implantable drug-delivery applications.

Furthermore, several studies have shown that hydrothermal method can resulted in A-type or B-type CHA. Ren & Leng (2011) synthesized CHA by various methods, including precipitation method, hydrothermal reaction and solid-gas reaction at high temperature.

They have been demonstrated that hydrothermal method and solid-gas reaction resulted in A-type substitution CHA and precipitation resulted in B-type CHA.

Roy et al. (1974) studied the hydrothermal synthesis of CHA with carbonate in both A- and B- type, although simultaneous AB-type carbonate substitution are also observed by Barralet et al. (1998) via precipitated method when carbonate contents were low (< 20 mol%) (Kumar et al., 2000).

Ana et al. (2010) synthesized B-type CHA with hydrothermal method, using gypsum added Ca-hydroxide powders. It was demonstrated that the higher hydrothermal temperature, the faster transformation of gypsum added Ca-hydroxide into CHA. However, decarbonation occurred at higher temperature which resulted in a major loss of carbonate ion (CO_3^{2-}) in the product.

Porous A-type CHA spheres was reported by He et al. (2008) through high-pressure hydrothermal system, using $Ca(NO_3)_2$, $(NH_4)_2HPO_4$, $(NH_2)_2CO$ and Na_2EDTA as precursors. They showed that the flakelets of porous A-type CHA spheres were completely decomposed into the nanoparticles after calcination at 1173 K for 8 h.

The mesoporous B-type carbonated hydroxyapatite with tunable nanoscale characteristics achieved through a microwave-assisted hydrothermal method by Karunakaran et al. (2019). Oxalic acid and sodium dodecyl sulfate (SDS) also used to produce mesoporous CHA nanoparticles. $Ca(NO_3)_2 \cdot 4H_2O$ and K_2HPO_4 were introduced as precursors and pH was adjusted to 13 using a KOH solution. This synthesized method have been proposed as a prospective advanced process in the field of bone regeneration as fillers, tissue engineering scaffolds with tunable features.

Highly crystalline nanorods B-type CHA with different carbonate contents were synthesized via hydrothermal process by Xue et al. (2015). It was reported that by

increasing the carbonate content, the widths of nanorods increased while lengths decreased. In addition, the crystallinity of CHA nanorods decreased due to lattice defects caused by substitution of CO_3^{2-} ions. The results of biocompatibility test proved that CHA nanorods are promising biomaterials in bone-tissue engineering application.

In all these researches, the hydrothermal method has been shown to be viable in producing CHA with good repeatability and crystallinity control (Xue et al., 2015). However, hydrothermal method would require equipment setup that can operate at high temperature and pressure thus hydrothermal method can be defined as a more expensive process comparing with the wet chemical precipitation method. In addition, another disadvantage of hydrothermal method is the poor ability to control the morphology of particles (irregular spherical and rod-shaped) with a broad size distribution.

2.2.1.2 Sol-gel Method

Non alkoxide sol-gel is another method to synthesize nanocrystalline CHA powder. Sol–gel is a wet chemical process that involves dispersion of particles (colloids) into a colloidal solution (sol) and then into an integrated network (gel) which does not need high pH value or high sintering temperatures. Layrolle et al. (1998) synthesized nanosized amorphous AB- type CHA via sol–gel method by using calcium diethoxide and phosphoric in ethanol. The amorphous CHA powder crystallized to a HA phase after heating at 600 °C. Studies by Liu et al. (2002) have shown that fusion among the calcium and phosphate colloids occurs at low temperature calcination. They synthesized B-type CHA through low temperature sol–gel process without measuring the pH. Rajabi-Zamani et al. (2008) also prepared CHA by using a non-alkoxide sol gel without pH control using ethanol to stable the sol. However, many reported sol–gel processes require a strict pH control to obtain good CHA powder (Padmanabhan et al., 2009).

Fathi et al. (2008) synthesized CHA with low-crystallinity (20–30 nm size) by sol-gel method, showed desired in vitro behavior. According to their study, the prepared CHA showed CO_3^{2-} bands at 1462cm^{-1}, 1418cm^{-1} and 876cm^{-1} in FTIR spectra which confirm the B-type substitution and in agreement with previous researchers. They also claimed that crystallinity and crystallite size of the CHA nanoparticles increased with increasing of sintering temperature.

One of the main disadvantageous of this method is the complicated and lengthy process includes the mixing of alkoxide precursors in aqueous or organic phase, followed by gelation, aging, drying, stabilization and post heat treatment (calcination). Apart from that, the high cost of the raw materials especially alkoxide-based precursors limits this method at the lab scale (Kim & Kumta, 2004). In addition, the generation of secondary phase like calcium oxide are inevitable in sol-gel derived CHA (Sadat-Shojai et al., 2013).

2.2.1.3 Emulsion Method

In general, this method refers to a phenomenon that occurs when an organic phase is poured into an aqueous phase, which yield the spontaneous formation of fine droplets by rapid diffusion of organic solvent from the oil phase into the aqueous phase. This method allows the precipitate of nanospheres when the organic phase (containing oil, surfactant and/or a water-miscible solvent) is mixed with aqueous phase (Zhou et al., 2008).

Emulsions are classified as oil-in-water (O/W) or water-in-oil (W/O), whether the constitutes phase is water or oil (Forgiarini et al., 2001) and are generally unstable. However, the stability can significantly increase by the addition of surfactants (typically over 20%). The process of preparing emulsions is termed emulsification which form through energy input such as shaking, stirring, homogenizing or spraying.

Du et al. (2018) synthesized CHA/chitosan composite spherical like particles with the typical size in the range of 100-200 and 300-400 μm via a water in oil (W/O) emulsion technique by using plant oil as the oil phase. It was demonstrated that the size range of the composite spheres was not affecting the biodegradation rate, but it seems to have influenced significantly the pH value of the buffer saline. The degradation of composite spheres was little under the neutral condition (pH=7.4), however under the acidic condition (pH=4.5) was well degraded.

The smaller crystallite size of CHA formed by microemulsion could be attributed to the nanosized microreactors that inhibited crystals growth. Microemulsion stabilized by the presence of surfactants. Some attempts have been used microemulsion method to achieve a powder with nanosized structure. For example, Koumoulidis et al. (2003) applied microemulsion system in combination with the pH–shock wave method to synthesize A-type CHA by using n-octane as oil phase. Amorphous CHA was crystallized after heating at 650 °C with the grain size of 40–120 nm and no internal porosity. Sintering process took place at the temperature of 900 °C, resulting in the larger particles and phase transformation of CHA to HA and β-TCP.

Nanosized B-type CHA was synthesized in oil/water emulsion and microemulsion method consisting of petroleum ether (PE) as the oil phase (Lim et al., 1999). After calcination at 650 °C, particle and crystal underwent little coarsening (i.e. the average particle size was about 25 nm). The bands at 1470, 1414 and 872 cm^{-1} in spectra attributed to the carbonate substituted phosphate positions is termed as B-type substitution.

One major set-back with microemulsions is that the process requires large concentration of surfactants (i.e. typically over 20 wt.%) if compared to conventional emulsions methods. On the other hand, nanoemulsions offer the possibility of forming microemulsion-like dispersion at a much lower surfactant content.

Nanoemulsion, also referred as miniemulsions, ultrafine emulsions, submicron emulsions, consist of narrow size distributions with droplets ranging typically from 20-200 nm although in some nanoemulsions up to 500nm has been reported (Solans et al., 2005).

2.2.1.4 Neutralization Method

Neutralization is a chemical reaction in which acid and base react to form salt and water. Celotti et al. (2004) synthesized CHA powder via the neutralization method by introducing a CO_2 as a source of carbonate through flux in the HA synthesis process, based on the neutralization reaction between $Ca(OH)_2$ and H_3PO_4. CO_2 gas was bubbled into the basic suspension of $Ca(OH)_2$ which heated at 40 °C and at the same time a solution of H_3PO_4 were added dropwise for 4 hours. The system was sealed off, and the CO_2 was bubbled (5 ml/min) into the suspension and then Then, it was stirred for two hours without the CO_2 stream and aged overnight at room temperature. The precipitate was washed (2000 ml×2), filtered, dried (80°C) and sieved (400 and 150 μm mesh).

Xu et al. (2007) synthesized acicular nanocrystal B-type CHA powder (20 nm diameter × 70 nm length) via a neutralization reaction method with aid of ultrasonic irradiation by using $Ca(OH)_2$, H_3PO_4 and $CaCO_3$ as the starting materials. The results showed that the CHA was partly decomposed into HA and CaO and removed CO_2 at above 1100 °C. It was found that neutralization with ultrasonic (sonochemical) method is a rapid and effective method for synthesis of nanosized CHA with high thermal stability.

Landi et al. (2004) synthesized predominantly B-type CHA powder with high yield by using neutralization method. The synthesis was performed in different conditions (temperature, dropping rate, reaction time, CO_2 gas, ageing time). It was found that increase in CO_2 gas increased A-type CHA formation, while increase in dropping rate resulted in a lower carbonate content and more substitution of A-type CHA. Additionally,

increase of temperature from 40 °C to 90 °C resulted in decrease the amount of carbonate. Therefore, in order to obtain the highest carbonate content and the B-type CHA precipitation, process conditions have to be optimised.

Although this neutralization method is promising to synthesis CHA at low temperature without pH control and by-products, it has to pay for high costs of consuming and controlling the CO_2 flow to form the suspension. In addition, the possibility of the carbonate ion to partially substitute both side of the hydroxyapatite structure and form the B-type and A-type is high.

2.2.1.5 Hydrolysis Method

B-type CHA can also be synthesized via hydrolysis method. In the study by Maeyer et al. (1994), CHA containing Na^+ were prepared by the hydrolysis of monetite ($CaHPO_4$) in Na_2CO_3 solutions at 95 °C for 5h and dried at 25 °C under vacuum. Single phase B-type CHA containing Na^+ without contamination under homogeneous precipitation condition was obtained. The results of the chemical and physical analyses of the samples reveal that all the water was removed after heating at 400 °C.

Pieters et al. (2010) prepared a homogeneous precipitation of B-type CHA by the hydrolysis of monetite ($CaHPO_4$, DCP) in Na_2CO_3 solutions. After hydrolysis process, the precipitates were filtered, washed (distilled water, ±95 °C) and lyophilized overnight to remove adsorbed water. The main advantage of this method is the reproducibly prepare single phase CHA with the lowest and the highest carbonate content found in bone mineral (3.2– 13 wt.%). However, High drying temperatures are required to remove adsorbed water molecules. Therefore, some studies suggested that such a heating process could lead to physical and structural changes, especially a loss of CO_3^{2-}.

2.2.1.6 Wet Chemical Precipitation Method

Precipitation referred as a creation of a solid from two solutions. The reaction take place in an aqueous solution to form a solid that is called precipitate. The chemical that causes the solid to form is known as the precipitant. Chemical precipitation process can be used to prepare a wide variety of inorganic salts.

The wet chemical precipitation method has been considered the most common synthesis method to produce B-type CHA powder owing to its low cost, low temperature, low risk of contamination and ease of operation (Lafon et al., 2008; Ślósarczyk et al., 2005). Precipitation also known as the simplest method for the synthesis of nanosized CHA (Merry et al., 1998).

The wet chemical precipitation method was originally investigated by Hayek et al. (1963). They succeeded in producing HA at normal temperature and pH of 12. Later on, several researchers developed and improved this method to achieve better properties of hydroxyapatite ceramic. For example, Jarcho et al. (1976) produced a dense polycrystalline hydroxyapatite with improved mechanical properties through precipitation method and also Merry et al. (1998) synthesized B-type CHA using wet chemical precipitation method at temperature about 20 °C and pH of 11, by adding dropwise the diammonium hydrogen orthophosphate solution to the calcium nitrate solution.

According to the Vignoles et al. (1988) during the CHA synthesis, under a high pH condition (basic), the possibility of carbonate to substitute phosphate groups in apatite structure was higher. Since excessive OH^- ions present in the reaction resulted in more competitive to fill apatite structure easily than (CO_3^{2-}) ions. Consequently, the partial replacement of (CO_3^{2-}) at (PO_4^{3-}) sites instead of OH^- groups led to the development of B-type CHA.

Othman et al. (2016) synthesized CHA via precipitation method by using three calcium sources (carbonate, hydroxide and nitrate) as the starting material for Ca^{2+} and di-ammonium hydrogen phosphate as the starting material for PO_4^{3-}. It was found that amongst them, only the calcium nitrate tetrahydrate precursor formed a single phase CHA, whereas the other two precursors formed a secondary calcite phase or did not react fully. This was attributed to the low solubility of the calcium hydroxide and the partial reaction of the calcium carbonate. It was also observed that increasing the pH of the solution led to higher CO_3^{2-} content and smaller crystallite size.

Mohammad et al. (2016) synthesized mesoporous carbonated hydroxyapatite (m-CHA) by precipitate method and compared with nonporous carbonated hydroxyapatite (np-CHA). They found that m-CHA exhibited better cytotoxicity properties and excellent osteinductive properties in comparison with np-CHA. This result indicates that m-CHA is suitable for drug delivery since it does not induce cytotoxicity after two weeks incubation, and moreover, supported cell proliferation.

Porous A/B type CHA (4.4 wt.% carbonate) via precipitation method with the chemical formula of $(Ca_{9.5}(PO_4)_{5.5}(CO_3)_{0.5}(OH)(CO_3)_{0.25})$ was synthesized by Germaini et al. (2017). The CHA raw powders were calcined at 400 °C and 2h to obtain a specific surface area of around 30 m^2g^{-1} to facilitate the compaction of powders. Afterwards, pellets were sintered at 935 °C for 30min under a controlled flowing atmosphere of CO_2 gas (145 ml min^{-1}) to compensate decarbonation.

Zhu et al. (2012) prepared the CHA powder via precipitation method at the temperature of 60 °C and pH ≥10 by mixing of $(NH_4)_2HPO_4$ and $NaHCO_3$ solution into a reactor containing $Ca(NO_3)_2{\cdot}4H_2O$ solution. The molar ratio of Ca^{2+}/PO_4^{3-}= 1.667, and CO_3^{2-}/PO_4^{3-} = 0.03, 0.22 and 0.88. After mixing, the solution was vigorously stirred for

about 3h and then aged for 24h at room temperature. Consequently, the precipitate was washed, filtered and dried.

Nanosized B-type CHA powders produced using acetone solution comprising of $Ca(NO_3)_2.4H_2O$ mixed with $(NH_4)_2HPO_4$ and NH_4HCO_3 were first prepared by Zhou et al. (2008) with a molar ratio of Ca^{2+}: PO_4^{3-}: CO_3^{2-}= 1.67:1:0.5. Subsequently as-synthesized CHA powder was calcined at the temperature of 900 °C for 4h in air to incorporate into the PLA matrix for producing CHA/PLA nanocomposite. They also indicated that the wet chemical is a very promising method for the synthesize nanosized B-type CHA with the chemical formula of $Ca_{10}(PO_4)_4(CO_3)_2(OH)_2$.

In this method, ethanol (EtOH) and acetone $(CH_3)_2CO$ are the common solvent for $Ca(NO_3)_2.4H_2O$. Some researchers (Cheng et al., 2001; Liu et al., 2001) used ethanol to synthesize HA via sol-gel method. However, EtOH is a protic solvent, and could incorporate into the apatite structure by substitution of ethoxide groups with some nitrate groups.

Acetone is referred as a non-protic solvent which would not contaminate the synthesized CHA powder. Since acetone is normally present in minute amounts in urine and blood (a product of the breakdown of body fat), thus the purpose of selecting acetone as reaction medium is to promote the formation of natural apatite (Reisman, 1998; Zhou et al., 2008).

Kee et al. (2013) also synthesized nanosized and low crystallinity B-type CHA at room temperature by using acetone medium of $Ca(NO_3)_2.4H_2O$. The authors found that during the synthesis process, direct pouring was more effective than dropwise, due to the time saving and higher crystallinity. In addition, increasing the carbonate content decreased the crystallinity of powder and the particle size.

Prekajski et al. (2016) applied wet chemical technique to synthesize spherical nanoparticles carbonated strontium hydroxyapatite (CSrHA) with the formula of $Sr_{10}(PO_4)_6(OH)_{0.60}(CO_3)_{0.70}$ at room temperature. In this work, an acetone solution of $Sr(NO_3)_2$ was mixed with an aqueous solution of $(NH_4)_2HPO_4$ and NH_4HCO_3 at a molar ratio of Ca^{2+}:PO_4^{3-}:CO_3^{2-} = 1.67:1:0.5. They achieved better crystallization with prolonged stirring time while formation of CSrHA was independent. They also indicated that the total 2.19 wt.% weight loss in the temperature range of 600 to 1100 °C was attributed to the decomposition of the carbonate.

In recent work conducted by Ion et al. (2019) CHA synthesized by wet chemical method at a molar ratio of Ca^{2+}:PO_4^{3-}:CO_3^{2-} = 1.67:1:0.5. and doped with different metal ions (Ag^+, Sr^{2+}, Ba^{2+}, Zn^{2+}, K^+) to apply a coating to the surface of the stone. The result revealed the substitution of Ca (0.99 Å) with Zn (0.74 Å), Sr (1.12 Å), Ag (1.26 Å), Ba (1.35 Å), and K (1.38 Å) in CHA lattice could increase in *a* and *c* lattice parameters (except for Zn, which has a smaller ionic radius than Ca). And also, Zn-CHA shown the highest values of compressive strength.

The wet precipitation method has the potential to be upscale to produce mass amount of CHA with the correct stoichiometric composition as the reaction involves no foreign elements and the only by product is water (Nagai et al., 1992). However, non-stoichiometric and poor crystalline CHA were reported by wet precipitation method (Sadat-Shojai et al., 2013).

2.3 Sintering of Carbonated Hydroxyapatite

Sintering is the process of heating the green body ceramics in order to transform loose particles into a dense tough ceramics (Barsoum, 1997; Kang, 2005). In fact, the sintering technique is one of the oldest yet, dating to prehistoric times with the firing of pottery.

Nevertheless, only after the 1940s, sintering has been studied fundamentally and scientifically leading to major progress in sintering science (Kang, 2005).

In general, the aim of sintering is to prepare a fully dense body with a fine grain structure. It can happen by reduction of the total surface area and an increase in the average size of the particles, which leads to coarsening and elimination of solid/vapor interfaces and the creation of grain boundary, followed by grain growth, which leads to densification (Barsoum, 1997). After removal of the gases the pore get smaller with time and disappear, then the compact shrinks and densifies, leading to significant strengthening (German, 2010).

Hence, a high sintering temperature is required to reach a near-maximum density and hardness in the ceramic composition. It is followed by a decrease in porosity until the optimum sintering temperature is reached (Youness et al., 2017). However, in case of CHA sintering at high temperature pose a problem due to the dissociation of the carbonate ions. Therefore, to ensure the adequate amount of carbonate content remain in the sintered CHA, a precise control over the sintering conditions is always advised to minimize the carbonate loss or to compensate it (Tonsuaadu et al., 1995). Barralet et al. (2002) reported that the loss of carbonate from CHA at high temperature is time dependent. They suggested that rapid high temperature treatment would minimize the carbonate loss.

Studies have shown that decomposition of carbonate begins at ~500 °C, and the carbonate is completely decomposed at temperature of 800-1000 °C. The duration of sintering and composition site of CHA are equally important in this process (Ivanova et al., 2001). Of note, heating of B-type CHA at 500-800 °C resulted in the migration of carbonate ions and the tendency of switching to A-type CHA.

Based on a study of Landi et al. (2000), carbonate ions can promote sintering of calcium phosphate ceramics, especially for the B-type CHA. According to their study, B-type carbonation required a lower sintering temperature as compared to the A-type carbonation (Ślósarczyk et al., 2010; Champion, 2013).

It has been reported that the loss of carbonate in CHA would trigger the formation of CaO and HA. Ivanova et al. (2001) hypothesized that if the Ca:P molar ratio is less than 1.67, the loss of carbonate in CHA may resulted in the formation of whitlockite $Ca_3(PO_4)_2$. A higher Ca:P molar ratio (> 1.67) would end up decomposition of CHA into HA and CaO (Joschek et al., 2000).

Merry et al. (1998) found that decomposition of B-type CHA, which contained a higher level of CO_3 substitution (10.2 wt.%) would happen at ~1000 °C under the wet CO_2 atmosphere. However, Barralet et al. (2000) reported that sintering B-type CHA under similar conditions at temperature up to 1200 °C did not show any formation of new phases.

The main challenge in the sintering of CHA is to prevent decomposition of carbonate that occurs at low temperatures from ~500 °C and nearly completed at 1000 °C (Koda et al., 1993; Lafon et al., 2003; Champion, 2013). Furthermore, several studies have shown that sintering atmosphere is one of the important factors during sintering of CHA to minimize or avoid the decomposition of carbonate in CHA structure (Barralet et al., 2000; Barralet et al., 2002; Landi et al., 2004; Lafon, et al., 2008; Ślósarczyk, et al., 2010; Champion, 2013).

2.3.1 Sintering Atmosphere

Sintering of CHA with the desired degree and type of substitution of carbonate, faced some challenges. Since carbonate content highly influenced by variable parameters,

including the concentration of carbonate, starting precursor, and also the sintering temperature, heating rate, soaking time and atmosphere of sintering (Barralet et al., 2000; Zyman & Tkachenko, 2011).

The sintering atmosphere revealed a strong effect on processes such as decomposition, densification and microstructural evolution of the ceramics. These effects are associated with both physical phenomena (when atmospheric gas trapped in isolated pores in the final stage of sintering), and chemical phenomena (particularly when the volatility, ionic oxidation state, and defect chemistry of the system can be modified) (Rahaman, 2007). Control of the sintering atmosphere is important, and precise control of the gas partial pressure as a function of temperature in some cases can be beneficial or essential.

Therefore, in order to achieve high density, good physical, mechanical and biological properties with minimal decomposition of CHA various atmospheres have been investigated, including nitrogen, carbon dioxide (wet and dry), air, water vapor and wet oxygen.

2.3.1.1 Sintering CHA in Air atmosphere

Sintering in air and N_2 atmosphere have no effect on the mass loss which accompanies densification (Zyman & Tkachenko, 2011). However, the introduction of dry CO_2 enhances densification. Lafon et al., (2003) reported that decarbonation in N_2 atmosphere occurred about 750 °C and 800 °C, while decarbonation peaks were shifted to higher temperature under CO_2 atmosphere (around 900 and 1150 °C).

Barralet et al., (2002) performed the sintering experiments in various gas atmospheres, including nitrogen, carbon dioxide, air, water vapor, and wet oxygen. It was revealed that the gas atmosphere could significantly affect the rate of CHA decomposition and demonstrated that when CHA sintered in the air atmosphere, rather than in the CO_2

atmosphere, phase decomposition occurred. Consequently diffraction peaks corresponding to both CaO and HA phase were observed (Gibson & Bonfield., 2002).

Studies have shown that sintering CHA at elevated temperatures in normal air atmosphere would eliminate the functional groups in the CHA structure, resulting to the phase transformations of CHA into calcium oxide (CaO), hydroxyapatite (HA), α-tricalcium phosphate (α-$Ca_3(PO_4)_2$, α-TCP), β-tricalcium phosphate (β-$Ca_3(PO_4)_2$, β-TCP) and tetracalcium phosphate ($Ca_4(PO_4)_2O$, TTCP) (Zhou et al., 1993; Gibson & Bonfield, 2002).

2.3.1.2 Sintering CHA in CO_2 atmosphere

During sintering process, the reaction between the sintering atmosphere and CHA samples take place. According to the Zyman & Tkachenko. (2011) supposition, there are two opposite streams of CO_2, from the atmosphere into the bulk and vice versa. Due to the CO_3^{2-} decomposition in the lattice, partial exchange between the crystallites and the CO_2 medium could have facilitated CHA nanoparticles consolidation thus leading to sintering.

In order to prepare an appropriate functional CHA with the desire properties, the sintering conditions should hinder or at least decelerate the decomposition of CHA (Kang, 2005). A number of researches have been directed towards the influence of CO_2 (dry or wet) atmosphere on sintering CHA. For example, Haberko et al. (2009) studied the heat treatment of CHA at elevated temperatures up to 1000 °C in O_2 and CO_2 atmospheres. They found that, CO_2 atmosphere compensate carbonate ions in the CHA.

Rau et al. (2004) reported that the control of the sintering atmosphere with respect in the CO_2/CO ratio was necessary to prepare CHA ceramics. Merry et al. (1998) reported that sintering CHA under a wet CO_2 atmosphere would minimize carbonate loss and

promote densification. This process can be conducted by bubbling dry CO_2 gas through a flask containing distilled water before being introduced into the furnace. The resulting CHA with 95% density was attained at 880 °C. A 94% dense CHA body was obtained when the sintering process occurred at 1000 °C in dry CO_2 atmosphere (Tkachenko & Zyman, 2008). Above 1100 °C, partial decomposition of the B-type CHA occurred, and calcium oxide was detected. The resulting CHA ceramics have a higher porosity, but their density and mechanical strength are compromised. It was also reported that the shrinkage of the compact was dependent on sintering temperature but not CO_2 atmosphere. This means that the CO_2 atmosphere stabilizes the sintering process.

Barralet et al. (2000) investigated the sintering behavior of CHA under dry and wet (3% water) CO_2 atmospheres by using 7.8 wt.% and 5.8 wt.% carbonated CHA. They concluded that a highly dense (93 %) CHA (5.8wt%) was obtained in wet CO_2 atmospheres at 700 °C for 4h. However, bloating occurred at temperature above 900 °C and the relative density dropped below 80%. On the other hand, little densification occurred in dry CO_2 even at temperature up to 1000 °C. Under such conditions, CHA with 84% density can only be obtained at 1200 °C. Beyond 1200 °C, bloating occurred immediately. In conclusion, both dry and wet CO_2 atmosphere cause an increase in carbonate content in CHA.

Similarly, Landi, et al. (2000) discussed the ability of the substituting carbonate to decrease the densification temperature of the CHA. It was found that wet CO_2 sintering atmosphere yielded fully dense translucence ceramics and presence of water increases the densification in the sintering atmosphere (Yasumoto, 1984). Similarly, Barinov et al. (2006) confirmed that B-type CHA did not show evidence of decomposition by sintering in wet CO_2. Landi et al. (2004) shown the best result in terms of high carbonate residue

with low A/B ratio in the range of the biological CHA at the thermal treatment of 900 °C in wet CO_2.

The highest relative density of CHA was achieved by Yanny-Marliana and Ahmad-Fauzi (2011) with addition of $Mg(OH)_2$ as the sintering aid at a low temperature of 800 °C in wet CO_2 atmosphere. Wong and Fauzi (2016) investigated the effect of cooling down temperatures on dense CHA with two kind of wet CO_2 atmospheres: direct wet CO_2 and dry CO_2 through water. The result revealed that using dry CO_2 through water at 200 °C compensated more carbonate ions in the CHA lattice compared to the direct wet CO_2.

Lafon et al. (2003) claimed that, the decomposition of CHA into CaO under N_2 atmosphere occurred at the temperature between 750 °C and 800 °C, then at 1250 °C CaO disappeared and formed tetracalcium phosphate monoxide (TCPM). Conversely, when sintered under CO_2 atmosphere neither crystalline change nor secondary phase formation was detected up to 1250 °C. On the other hand, the decomposition of carbonate shifted to higher temperature (around 900 °C and 1150 °C). This work confirmed by Barralet et al. (2002), who investigated the effect of (wet and dry) carbon dioxide and nitrogen, (wet condition containing 3% water) on phase composition of carbonated hydroxyapatite at temperatures ranging from 700 to 1400 °C. It was found that in dry CO_2 atmosphere, crystallization occurred at 900 °C, while it occurred at 1100 °C in wet CO_2 atmosphere. Also, β-TCP was formed at 1300 °C and 1500 °C respectively.

Moreover, it was revealed that presence of CO_2 atmosphere during sintering (900 °C for 1 h) compensate the carbonate loss in CHA structure and led to dense CHA ceramic (relative density >97% of theoretical). It has also shown that the surface area decreased when sintering CHA in a declining CO_2 atmosphere (from 20.2±1.2 to 2.7±0.8 m^2/g) (Ślósarczyk et al., 2010). As a conclusion, the presence of CO_2 atmosphere is important in sintering process.

Lafon et al. (2008) synthesized AB-type CHA dense ceramics with sintering under nitrogen, dry and wet CO_2 atmosphere. The main difference between the two nitrogen and dry CO_2 atmospheres was the decomposition of CHA shifted towards higher temperature ~1000 °C in dry CO_2, against 900 °C in argon. On the other hand, the sintering was enhanced with introducing of a partial pressure of water vapor H_2O in the CO_2 atmosphere. For example, achieved nearly fully dense (up to 97%) at 900 °C for 1 h in wet CO_2 condition, while 950 °C was needed to attain 95% dense body in dry atmosphere. However, when a partial pressure of water vapor is present in the sintering atmosphere, this could cause the decomposition of B-type carbonated apatites.

According to Zyman & Tkachenko. (2011) study, sintering in CO_2 atmospheres (wet or dry) have an effect on the shrinkage rate, sintering temperature, chemical and phase compositions as well as structural changes such as type of carbonate ion substitution in the CHA lattice.

Zyman & Tkachenko. (2011) sintered CHA compacts in CO_2 gas flowing at 4 mL/min. They reported that CO_2 atmosphere compensated the decomposition of carbonate from the lattice structure at lower temperature ~ 900 °C and consequently improved densification. Sintering at temperatures > 1000 °C resulted in carbonatation on the A-sites and led to a decreased in bulk density as well as mechanical properties.

2.4 Mechanical Properties of Sintered CHA

Substitution of CO_3^{2-} ions into the HA lattice has been found to improve the mechanical properties of the bioceramic (Landi et al., 2003). Several studies have been conducted on mechanical properties of sintered CHA. Teraoka et al. (1998) used hydrothermal gradual heating method in a range from 200 to 300 °C to sinter CHA. It was found that the bending strength ranged from 450 to 513 MPa and were nearly constant over all the carbonate contents and the measured average Young's modulus was from 54

to 79 GPa. The effect of carbonate on the mechanical strength properties of CHA at temperature between 800-1000 °C in wet CO_2 atmosphere was studied by Merry et al. (1998). Mechanical properties of CHA indicated a reduction in flexural strength from ~63 MPa to ~57 MPa with increasing carbonate content and both compositions showed lower flexural strengths compared with HA ~66 MPa with relative density of 96%.

Tkachenko & Zyman (2008) achieved highest CHA density of 94% at the temperature of 1000 °C in dry CO_2 atmosphere. All the mechanical properties increased as the sintering temperature rose from 800 to 1000 °C and dropped sharply above this temperature. The Vickers microhardness of 127 MPa at 800 °C increased to 171 MPa with increasing temperature to 1000 °C.

Doi et al. (1993) demonstrated that CHA with 8 wt.% carbonate could be sintered at a lower temperature (650 °C) than that of pure HA (1050 °C). The resulting sintered CHA samples showed a relative density of 90% with Knoop hardness of 380 Hk

Zyman & Tkachenko (2011) indicated that CHA with 3.4 wt.% CO_3^{2-} content can sinter at a temperature 200 °C lower than that required for HA. The resulting CHA has 94% relative density and 1.7 GPa *H*v. Firing at temperatures > 1000 °C resulted in a declined in both density and mechanical properties.

Zhu et al. (2012) studied the influence of the carbonate content on the relative density and mechanical properties of CHA pellets. The results revealed that the sintering temperature decreases with increasing initial carbonate content. This process is associated with the following aspects; - increase in lattice defects lead to the decrease in diffusion activation energy, promotes the movement of the structure element thus decreases the sintering temperature, -decrease in particle size lead to the decline in atomic diffusion

distance consequently decrease in sintering temperature. And also, wet CO_2 atmosphere would lead to increases the diffusivity of anion and the sintering process accelerates.

In addition, flexural strength decreased from 34.27 Mpa, 31.89 Mpa to 26.78 Mpa with decreasing carbonate content of CHA from 10.36 wt.% to 7.35 wt.% and 2.8 wt.% respectively, while increased in compare with HA (20.05 Mpa). The decrease in flexural strength is due to the increase in porosity and stress concentrations around the pores subsequently decrease in density.

Youness et. al., (2017) worked on mechanical properties of nanocrystalline B-type CHA prepared by mechanochemical synthesis. Microhardness and compressive strength revealed that with increasing the milling time, microhardness and compressive strength increased. These results can be attributed to the fact that the increase in density is related to the increase of mechanical properties as they are influenced by the small particle size which increases the specific surface area and is the driving force for densification thus contributing to high mechanical properties. Therefore, the high density as well as high mechanical properties can be marked by the bonding amongst the grains in the sintered CHA samples.

2.5 Bioactivity Evaluation of CHA

The most important properties of biomaterials is their biocompatibility. Biocompatibility can be defined as the ability to accept an artificial material by host tissue at the interface (Park & Bronzino, 2003).

Since CHA is the inorganic part of human bone, *in vitro* tests with biological systems and *in vivo* animal studies are needed to better assess their compatibility as a bio-resorbable bone substitute (Fathi et al., 2008). Most of the literatures have been reported the *in vitro* behavior of CHA in phosphate buffer saline (PBS) and simulated body fluid

(SBF) at 37 °C with a controlled pH condition at 7.4. Therefore, the bioactivity of the sintered CHA samples can be evaluated by ability of bone-like apatite formation on their surface when immersed in SBF or PBS solution.

Some researchers have been investigated on difference between SBF and PBS solution. They compared the effect of ionic content of PBS and SBF on the biological properties of apatites. Kaewsichan et al. (2011) indicated that SBF has been suitable for evaluating the *in vitro* bioactivity of silicate-based ceramics, but not for other types of bioceramics. While, Jamuna-Thevi et al. (2017) and Kokubo & Takadama, (2006) presented that *in vitro* degradation in SBF is closely mimic the *in vivo* bone regeneration which its ion concentrations simulate the human blood plasma.

In comparison to SBF, ionic species such as Mg^{2+}, Ca^{2+}, and HCO^{-3} are absent in PBS (Table 2.7). The osmolarity and ion concentrations of SBF is very similar to that of blood plasma (isotonic). Hence, to evaluate the effect of carbonate on degradation of CHA ceramics, *in vitro* bioactivity test could perform by immersing CHA pellets in SBF solution with ion concentrations nearly equal to human blood plasma at 37 °C similar to biological fluids , over time (Kokubo & Takadama, 2006).

Table 2.7: Ion concentrations of human blood plasma, SBF and PBS (Kaewsichan et al., 2011)

	Ion concentration (mM)						
Type	Na^+	K^+	Mg^{2+}	Ca^{2+}	Cl^-	HCO_3^-	HPO_4^{2-}
Blood plasma	142.0	5.0	1.5	2.5	103.0	27.0	1.0
SBF	142.0	5.0	1.5	2.5	148.8	4.2	1.0
PBS	157.0	4.5			140.0		10.0

Horváthová et al., (2008) investigated the *in vitro* bioactivity and mineralization behavior by soaking the octacalcium phosphate (OCP) coated on titanium alloys

(Ti6Al4V) substrates into SBF at various soaking times ranging from 10 to 168h. The transformation of OCP into CHA occurs via hydrolysis and partial dissolution of the crystals. The thickness of the plate-shaped morphology of the OCP crystals increased with soaking time. After 100h soaking in SBF, CHA formed onto OCP via a dissolution–precipitation process. Thus, OCP coatings would enhance the osteoconductivity of orthopedic titanium-based implants by transforming into CHA.

2.6 Summary

In general, this chapter has provided an overview of structure and properties of biomaterials. Followed by fundamental understanding of bioceramics as a part of biomaterials in detail. Bioceramics and its derivatives have been general importance for several decades in many fields of science. The review will be then focused further on the carbonated hydroxyapatite. Substitution of carbonate in HA resulted in changes in lattice parameters, crystallite size, degree of crystallinity, mechanical properties and in solubility.

In addition, ionic doping or ionic substitutions have received great interest as a mean of improving the mechanical and biological properties of the CHA. Hence, many different synthesis techniques have been experimented to produce nanosized CHA. By contrast, wet chemical method posed many advantages when used to synthesize B-type CHA under controlled atmosphere. The amount of carbonates content can significantly influence the sintering temperature and mechanical properties. Moreover, it has been shown that sintering under CO_2 atmosphere (wet/dry) can compensate the carbonate loss. It also stated that the incorporation of ions into the HA structure will enhanced the biological properties *in vitro* and/or *in vivo*.

CHAPTER 3: MATERIALS & METHODOLOGY

3.1 Introduction

This chapter describes the synthesis of carbonated hydroxyapatite (CHA) with different molar ratio of CO_3^{2-}/PO_4^{3-} and multi-ions (Mg^{2+}, SiO_4^{4-}, Zn^{2+} and Cu^{2+}) doped CHA via direct pouring wet chemical precipitation method followed by pelletizing, sintering in CO_2 atmosphere (wet and dry) and polishing. Finally, the studies were directed towards the characterization of CHA samples.

3.2 Synthesis of CHA and Multi-Ion Doped CHA

In this study, the nanosphere B-type CHA powders were synthesized by a direct pouring wet chemical precipitation method (Zhou et al., 2008) using ≥99% purity materials comprising of di-ammonium hydrogen phosphate $(NH_4)_2HPO_4$, ammonium bicarbonate NH_4HCO_3 and calcium nitrate tetrahydrate $Ca(NO_3)_2{\cdot}4H_2O$ as the precursors for PO_4^{3-} ; CO_3^{2-} and Ca^{2+} ions, respectively. For the multi-ion doping, compounds of magnesium nitrate hexahydrate $Mg(NO_3)_2{\cdot}6H_2O$, tetraethyl orthosilicate (TEOS) $SiC_8H_{20}O_4$, zinc nitrate hexahydrate $Zn(NO_3)_2{\cdot}6H_2O$ and copper (II) nitrate trihydrate $Cu(NO_3)_2{\cdot}3H_2O$ were used as the source for Mg^{2+}, SiO_4^{4-}, Zn^{2+} and Cu^{2+}, respectively during the synthesis process.

All these chemicals were purchased from Merck, Germany. Ammonium and nitrate salts in this study is that they do not interact with the apatite structure and can readily be removed from the separated precipitate by washing (Elliott et al., 1994; Ma et al., 1994; Admassu & Breese, 1999). The analytical grade acetone was used as a solvent for synthesizing nanosphere CHA. Table 3.1 lists all the chemicals for synthesizing CHA and multi-ion doped CHA via wet chemical method.

Typically, to make 0.1 mol of CHA powder, 1M of each reagent solution was needed. During the synthesis process, the Ca/P ratio was kept constant at 1.67 with Ca^{2+}: PO_4^{3-}: CO_3^{2-} of 1.67: 1: 1 (Appendix A), based on the following equation

$$6(NH_4)_2H(PO_4) + 6(NH_4)HCO_3 + 10Ca(NO_3)_2 + 2H_2O \rightarrow Ca_{10}(PO_4)_6(CO_3)_6(OH)_2 + 18(NH_4^+) + 20(NO_3^-) + 14(H^+)$$

The flowchart showing the CHA synthesis process is given in Figure 3.1. In a typical synthesis process, the procedure involves preparing an aqueous transparent solution of (4.74 gr, 60 mmol) NH_4HCO_3 and (7.92 gr, 60 mmol) $(NH_4)_2HPO_4$, in 60 ml of deionized (DI) water respectively were mixed for 15 min at a stirring rate of 450 rpm. Next, 1M NaOH solution (dissolved 40 g NaOH in 1000 ml water to get 1mol/L NaOH solution) was added into the mixture until pH 11. Subsequently, the organic solution of $Ca(NO_3)_2.4H_2O$ (23.615 gr,100 mmol) in 100 ml of acetone was poured directly into the previously stirred aqueous solution at a rate of 450 rpm, resulting in the formation of a slightly milky solution (Appendix B 1-5). Six different CO_3^{2-}/ PO_4^{3-} molar ratios, i.e. 0.5 to 5, were prepared and the synthesized CHA powders were subsequently labelled as 0.5CHA, 1CHA, 2CHA, 3CHA, 4CHA and 5CHA, respectively.

For the preparation of multi-ion doped CHA powders, small amounts of magnesium nitrate hexahydrate, TEOS, zinc nitrate hexahydrate and copper (II) nitrate trihydrate were added to the stirring milky solution in a ratio of 0.72, 0.05, 0.0039 and 0.003 wt.%, respectively in accordance to the composition of mineral phase in human bone (Šupová, 2015). Four different combination of multi-ion doped CHA powders were prepared and designated as follows: SA1(CHA+Mg+Si), SA2 (CHA+Mg+Si+Cu), SA3 (CHA+Mg+Si+Zn) and SA4 (CHA+Mg+Si+Cu+Zn).

After that, the mixed milky solution was filtered (Whatman, Grade1) and washed with DI water (500 ml × 3) to remove byproducts. The obtained white cake was dried (100 ºC, 20 h) in a box oven, ground (agate mortar and pestle) and sieved (100 µm mesh) to obtain fine CHA/ multi-ion doped CHA powder.

Table 3.1: Raw materials used in wet chemical method for CHA synthesis

Name	Formula	Molecular weight (g/mol)	Purity (%)	Function
Calcium nitrate tetra hydrate	(Ca $(NO_3)_2.4H_2O$)	236.15	≥99.0	Calcium source
Di ammonium hydrogen phosphate	$((NH_4)_2HPO_4)$	132	≥99.0	phosphate source
Ammonium hydrogen carbonate	(NH_4HCO_3)	79.06	≥99.0	Carbonate source
Magnesium nitrate hexahydrate	Mg $(NO_3)_2$ $.6H_2O$	256.41	≥99.0	Magnesium source
Sodium hydroxide	NaOH	40.00	≥99.0	PH adjustment
Tetraethyl orthosilicate (TEOS)	$SiC_8H_{20}O_4$	208.329	≥99.0	Silicate Source
Zinc nitrate hexahydrate	Zn $(NO_3)_2 \cdot 6H_2O$	297.4815	≥99.0	Zinc source
Copper (II) nitrate trihydrate	Cu $(NO_3)_2 \cdot 3H_2O$	241.6016	≥99.0	Copper source
Acetone	$(CH_3)_2CO$	58.08	100	Solvent for Calcium source

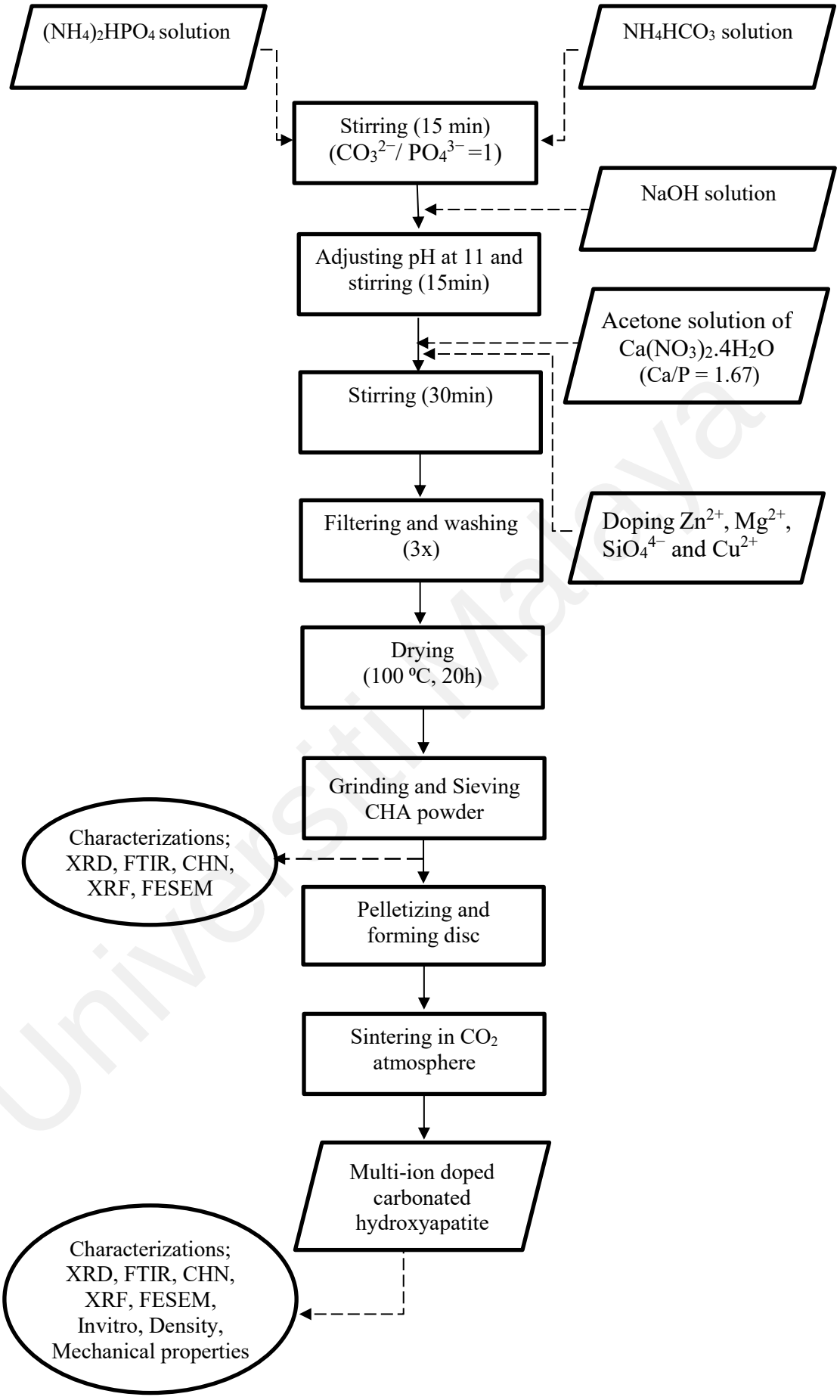

Figure 3.1: Flowchart of the synthesizing multi-ions doped CHA via wet chemical precipitation method

3.3 Pelletizing synthesized CHA powders

The synthesized CHA powders were compacted to produce green circular pellets (20 mm diameter× 5 mm thickness). The powders were weight (2 gr) and then subjected to cold isostatic pressing (CIP), pressed at a pressure of 200 MPa and held steadily for 120s to ensure uniform pressure applied on the pellets and allowing the powders to rearrange and deform. Green pellets exhibit spring back effect due to recovery of elastic strain on withdrawal of pressing load which is high for non-plastic materials. So, to control the crack defects that mainly contribute to pellet rejection, the pressure was slowly released and pushed out from the die. Five samples were prepared for each composition.

3.4 Sintering of CHA with Various Carbonate Content

The disc samples were then sintered in a CO_2 atmosphere (flow rate of 4 ml/min) at a temperature of 900 °C for 2h in tube furnace, at a cooling and heating rate of 10 °C/min. Five samples of each composition were prepared for subsequent test. This temperature was chosen in order to ensure that the CHA produced is of the B-type. It has been reported in the literature (Zyman & Tkachenko, 2011) that as the temperature increased beyond 900 °C, this will cause an increase in the *a-axis* parameter which is typical for an A-type substitution in CHA.

3.5 Sintering of Multi-Ion Doped CHA

The compacted disc samples sintered at 900 °C in air atmosphere, using a heating and cooling rate of 10 °C/min and holding time of 2h. On cooling from sintering to 200 °C, the samples were taken out from the furnace and placed in a desiccator containing wet carbon dioxide gas, flowing at a constant rate of 0.5 L/min. This is to compensate any loss of carbonate during the heat treatment process (Wong & Ahmad-Fauzi, 2016). The sintered samples were left in the desiccator to cool to ambient temperature for 24h (Figure 3.2.).

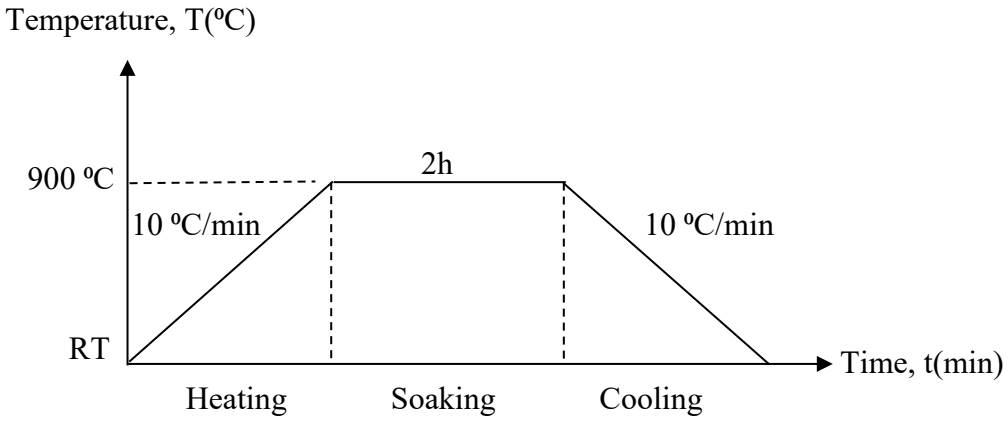

Figure 3.2: Sintering profile of multi-ion doped CHA

3.6 Grinding and Polishing

In order to obtain a smooth surface to ensure the consistency of results, prior to microstructural evaluation, such as Vickers hardness, fracture toughness and FESEM, sintered samples were ground successively using SiC papers with grit sizes varying from 600 (rough) to 1200 (fine) and followed by mirror-polishing with 6-µm down to 1 µm surface finish using diamond paste. During the grinding process, in order to ensure successful fine grinding, the samples were rotated 90º for every grit size whereas polishing was conducted by moving the sample directional figure-eight (inline figure-eight) as shown in Figure 3.3.

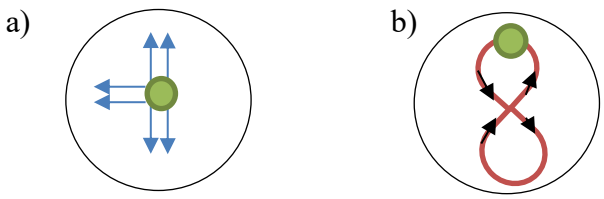

Figure 3.3: a) grinding b) polishing

The microstructure of sintered materials was revealed on mirror polished surfaces by thermal etching for 30min at 50 °C below the sintering temperature and ramp rate of 10 °C/min.

3.7 Sample Characterization

3.7.1 X-Ray Diffraction (XRD)

X-ray diffraction (XRD) was performed to determine phases present, crystallite size and lattice parameters by using Diffractometer (Panalytical X'Pert^3 Powder, Netherland) in the 2θ range of 20–60° (Cu Kα, ƛ=1.5406 Å). The crystallite size of the powders was estimated using the Scherrer's equation as follows (Cullity & Stock, 2001).

$$D = \frac{K\lambda}{\text{FWHM}\cos\theta} \tag{3.1}$$

Where D refers to the crystallite size (nm), K is a constant related to the crystallite shape, which can be 0.89 for the FWHM of spherical crystals with cubic unit cells, λ refers to the wavelength of Cu Kα radiation which equal to 1.5406 Å, FWHM is the full width at half maximum (rad) and θ is the half of the diffraction angle (degree). In this study, the (002) diffraction peak was chosen for calculation of the crystallite size of the CHA (powder and sintered) since it is sharpest peak without overlapping. From Bragg's Law it is clearly stated that the diffraction angle (θ) depends on the wavelength (λ) and the distance (d) between the planes as shown in Equation 3.2.

$$n\lambda=2d\sin\theta \tag{3.2}$$

Phase determinations were made by using Standard International Centre for Diffraction Data (ICDD) card no. #9-0432 for HA. Determination of the lattice constants, crystallite size and phase analysis of the CHA samples were obtained by Rietveld

refinement of the XRD data which is processed by *PANalytical X'Pert HighScore Plus* software according to the procedure described (Yacoubi et al., 2017).

3.7.2 Fourier Transform Infra-Red (FTIR) Spectroscopy

The types of functional groups present in the CHA and mechanism of substitution carbonate within the HA structure were determined by using Fourier Transform Infrared Spectrometry (FTIR; Perkin Elmer, USA) scan over a range of wavelengths (400-4000 cm^{-1}). FTIR spectrometry measures the absorption energy at each wavelength, which excited vibration or rotation of groups of atoms within the molecule. The wavelengths of many IR absorption bands were characteristic of specific types of chemical bonds. The shift in bands wavenumbers and intensities were caused by changes in environments of chemical bonds (Chappard et al., 2016). FTIR performed in transmittance mode (light is passed through the section) (Boskey et al., 2007) thus to the preparation of transparent pellet, the sample powder was mixed with the ratio of 1:100 gr with potassium bromide (KBr) powder and grounded to a fine powder by using agate mortar. Then the mixture was pelletized at 28 Mpa for 2 min and scanned for 3 times.

3.7.3 X-Ray Fluorescence (XRF)

X-ray Fluorescence (XRF) spectrometer is an emitted x-rays technique widely used in determine the elemental composition of materials. To restore the atoms to a more stable state, the holes in inner orbitals are filled by electrons from outer orbitals. Such transitions may be accompanied by an energy emission in the form of secondary x-ray photon. This phenomenon known as fluorescence. In this study, XRF was used to determine the Ca/P ratio of the synthesized CHA samples (Rigaku Rix 3000, Japan).

3.7.4 Carbon, Hydrogen, Nitrogen (CHN) Elemental Analysis

The amount of carbonate present in the CHA samples was calculated from the carbon content measured using the CHNS/O elemental analyzer (Perkin Elmer, USA), where

1mg of sample was combusted in a chamber at a high temperature of 925 °C in the presence of oxygen in order to convert the sample into the gas element. The gas was detected thermal conductivity detection (TCD). The wt.% of carbonate content present in the CHA samples was proportional to the wt.% of carbon content by a factor of 5 (1 mol carbonate (60 g) is five times the weight of 1 mole carbon (12 g)) (Krajewski et al., 2005).

3.7.5 Specific Surface Area Determination

The specific surface area of the CHA powders was calculated using Brunauer–Emmett–Teller (BET) method. BET obtained through physical absorption of nitrogen gas molecules onto their surface (Micromeritics ASAP 2020 V4.00 G, USA). In this technique a monolayer of liquid nitrogen was absorbed onto the surface of the particles. The amount of nitrogen gas released to producing the monolayer was measured using BET equation (Kumar et al., 2018). Surface area per unit mass was obtained from the combination of ideal gas as well as variation in the calculated values.

3.7.6 Field Emission Scanning Electron Microscopy (FESEM)

The morphology, microstructural evolution and grains size of the sintered CHA samples were examined by using Field Emission Scanning Electron Microscopy (FESEM; Carl Zeiss Auriga, Germany). The sample for FESEM was secured on the carbon tape placed on an aluminum stub. The sample were subsequently coated with a thin layer of gold to prevent sample electrical charging during FESEM analysis. Various magnification of the samples was taken using secondary electron (SE) mode operating at 5 to 10 KV.

3.7.7 Energy Dispersive X-Ray (EDX)

EDX which is attached on to the FESEM instrument was used to identify the localized elemental composition of materials by using the X-Ray spectrum emitted by the samples after bombarded by a stream of electrons.

3.7.8 Linear Shrinkage

Shrinkage is part of the densification process (Naceur et al., 2014). During sintering, as the temperature increases, consolidation of the particles proceed as a rapid pace and this result in shrinkage of the sintered body as well as elimination of porosity (Ring, 1996).

In this study, the linear shrinkage was obtained by measuring the changes in the dimensions (i.e .diameter, D and length, L) of the samples before and after sintering. The dimension measurement was accomplished by using a Mitutoyo caliper. Typically, five samples were measured at each temperature and average value was taken. To ensure accuracy of the shrinkage, the dimensions were measured at three different locations on each sample. Shrinkage of the sintered CHA pellets was calculated as follows:

$$\text{Linear shrinkage expressed in \%, } D_S = \left(\frac{D_0 - D_F}{D_0}\right) \times 100 \quad (3.3)$$

Where Do = diameter as measured before firing (mm), D_F = diameter as measured after firing (mm).

3.7.9 Relative Density

In order to obtain good mechanical properties, ceramics needs to be as dense as possible. High strength ceramics can be produced if pores and flaws inside the ceramics body can be eliminated during sintering. The density of the sintered samples was determined by Archimedes' method using distilled water. The relative density was

calculated by taking 3.156 g/cm^3 as the theoretical density of HA. A standard electronic balance (Shimadzu AY 220, Japan) was used. First of all, the dry weights of sample (*Wa*) were measured in air, then sample were immersed in the water and the immersed weight (*Ww*) of samples were measured.

$$\text{Bulk density, } \rho_{bulk}\,(g/cm^3) = \frac{Wa}{Wa-Ww} \times \rho_{water} \quad (3.4)$$

$$\text{Relative density (\%)} = \frac{\text{Bulk density of the sample } (\rho bulk)}{\text{theoretical density } (\rho theoretical)} \times 100 \quad (3.5)$$

3.7.10 Average Grain Size

The average grain size of the sintered CHA samples measured by using the line-intercept method on the FESEM micrographs based on the following equation.

$$\bar{D} = 1.56 \times \frac{C}{M \times N} \quad (3.6)$$

Where $\bar{D}$ is the average grain size and C is the total length of test line used, M magnification of the FESEM and N is the number of intersections (Mendelson, 1969; Wurst & Nelson, 1972). Initially, to calculate the intersection between the grains and the test line, FESEM image was drawn on the A4 paper (Figure 3.4). However, it has been noticed that this measuring grain size method can be used only for polycrystalline ceramics with equiaxed grains and fully dense microstructure.

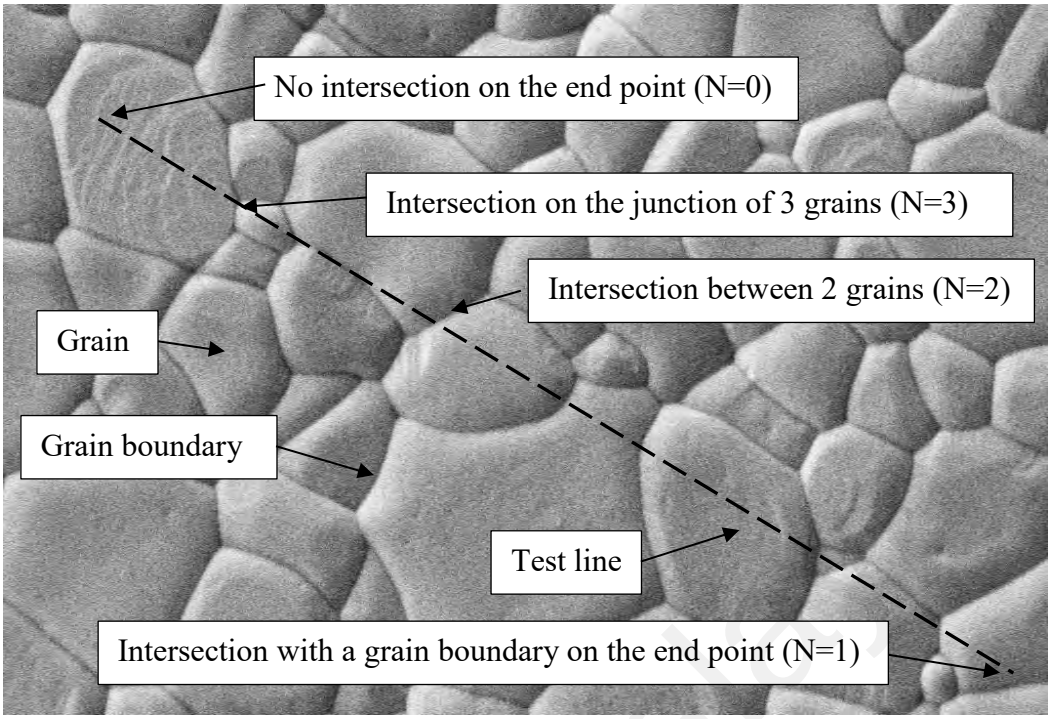

Figure 3.4: Schematic of measuring grainsize by line-intercept method

3.7.11 Thermal Analysis

The weight loss of the samples during heat treatment was measured from room temperature to 1000 °C in nitrogen (N_2) atmosphere with heating rate of 10 °C/min by using a Thermo-Gravimetric Analyzer (TGA; Perkin Elmer Pyris TGA 8000, USA).

3.7.12 Vickers Hardness

Hardness is defined as materials resistance to localized plastic deformation (e.g., penetration or scratching). The Vickers hardness is denoted as H_V, also known as a microhardness, of the sample is obtained by measuring the impression produced by a pyramid shaped diamond indenter (Broitman, 2016). A polished surface is required for Vickers hardness testing, to ensure a well-defined indentation that accurately measured. The Vickers indentation technique was used to determine the hardness of the sintered CHA samples by using diamond pyramid indenter Vickers Hardness Tester (Shimadzu HMV-2, Japan). The load applied at 100 gf and held for 10s (indentation time), which resulted in the formation of a diamond shaped indent on the surface of the sintered sample

(Figure 3.5). The impression was observed under a microscope and the diagonal lengths of the indent were measured. This measurement was then converted into a Vickers hardness number (H_V) and International Standard of Units (MPa) as shown in Equations 3.7 (Broitman, 2016). Five indentations were made on each sample and the average value was taken.

$$\text{Hardness } (H\text{v}) = \frac{1.854f}{\left(\frac{d1 + d2}{2}\right)^2} \tag{3.7}$$

Where f is the load (gf), d_1 and d_2 are the two diagonal lengths of the impression (mm)

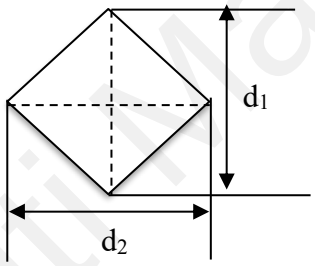

Figure 3.5: The schematic view of the indentation for measuring *H*v

3.7.13 Fracture Toughness

Toughness is indicated of the ability of a material to absorb energy before fracturing. The material's resistance to crack propagation is termed Fracture toughness (Taylor, 2018). Indentation technique was used to evaluating the fracture toughness which involves the measurement of radial crack length as a function of indentation load. The average value was taken from five measurements made for each sample. In principle, it is the same as the microhardness measurement whereby the Vickers diamond indenter was driven into the surface by known load. When the indenter was removed, a

characteristic pattern as in figure should be visible, comprising a central indentation with radial cracks emanating from the corners (Figure 3.6).

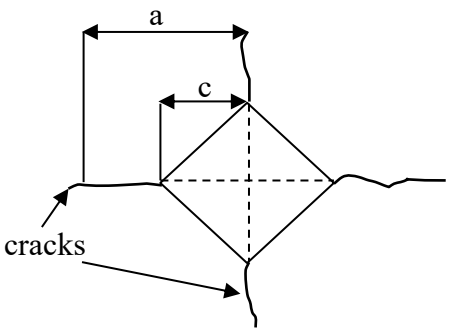

Figure 3.6: Schematic of the radial crack due to Vickers indentation

The fracture toughness value was calculated by using Equation 3.8

$$K_{IC} = 0.203 \left[\frac{c}{a}\right]^{-1.5} (H_V) a^{0.5} \qquad (3.8)$$

Where K_{IC} is the fracture toughness, H_V = Vickers hardness, a and c are the impression radius and length of the indentation crack, correspondingly (Niihara, 1985).

3.7.14 Biological Properties (*in vitro*)

The behavior of calcium phosphate biomaterial in biological environment determines how they can be used *in vivo*. The most important requirement for CaP to be bioactive and bond to living tissue is the formation of bone like apatite layer on their surface. A protein-free solution simulated body fluid (SBF) with ion concentrations similar to those of human blood plasma were prepared to mimic the chemical analysis of human body fluid. It was first used by Kokubo (1990). He applied a load to glass ceramic A-W in a simulated body fluid at 36.5 ºC, which has almost equal ion concentrations (Na^+ 142.0, K^+ 5.0, Mg^{2+} 1.5, Ca^{2+} 2.5, Cl^- 148.8, HO_3^- 4.2, HPO_4^{2-} 1.0, SO_4^{2-} 0.5 mM) to those of the human blood plasma. Bioactive calcium ceramics has also been reported to support osteoblast adhesion and proliferation (Davies, 1996; Anselme, 2000).

The SBF solution was prepared according to the Kokubo & Takadama (2006) procedure. The order and reagents used to prepare 1000 ml of SBF is shown in Table 3.2. Before preparing SBF, for all apparatus thorough cleaning with sterilizing liquid is required. Then the reagents were dissolved (in the order of #1 to #8 as shown in Table 3.2) in 700 ml of DI water using a plastic container. Each chemical was dissolved after the previous one was dissolved completely. The temperature was kept at 36.5 ± 1.5 °C in a water bath and while solution was stirred continuously using a magnetic stirrer. The total solution was brought to 900 ml by adding some DI water. Then the reagent #9 were added into the solution little by little to control the pH 7.45±0.01 at the temperature of 36.5±0.2 °C. Then reagent #10 dropped to lower the pH to 7.42±0.01. The process was repeated until the whole amount of Tris was dissolved and the pH kept within the range of 7.40 at 36.5 °C. DI water was added to SBF solution up to 1000 ml and kept at 20 °C and after falling the temperature to 20 °C, added more DI water up to the marked line. The *in vitro* test was done by immersion the densest CHA samples in SBF solution.

Table 3.2: Reagents used for preparing 1000 ml of SBF solution

Order	Reagent	Amount
#1	NaCl	8.035 g
#2	$NaHCO_3$	0.355 g
#3	KCl	0.225 g
#4	$K_2HPO_4.3H_2O$	0.231 g
#5	$MgCl_2.6H_2O$	0.311 g
#6	1M HCl	39 ml
#7	$CaCl_2$	0.292 g
#8	Na_2SO_4	0.072 g
#9	Tris	6.118 g
#10	1M HCl	Appropriate amount for adjusting pH

CHAPTER 4: RESULTS AND DISCUSSION

4.1 Introduction

The research work in this chapter included in three parts. In the first part, carbonated hydroxyapatite (CHA) with various carbonate (CO_3^{2-}/PO_4^{3-}) powders produced by wet chemical precipitated method and sintered at 900 °C in CO_2 atmosphere. Then, the optimum (CO_3^{2-}/PO_4^{3-}) ratio was selected for the next experiment. Subsequently, evaluated different sintering temperature on the selected CHA with CO_2 atmosphere to minimize decomposition carbonate during heat treatment. At last part, the effect of multi-ions doping on the properties of carbonated hydroxyapatite bioceramic was evaluated. In first and second part sintering conducted in dry CO_2 while third part sintered in wet CO_2.

4.2 Effect of variant CO_3^{2-}/PO_4^{3-} molar ratios on physical and mechanical properties and *in vitro* bioactivity of synthesized CHA

The aim of this research is to evaluate the effect of varying the CO_3^{2-}/ PO_4^{3-} ratio on the invitro bioactivity, physical and mechanical properties of B-type CHA. Direct pouring wet chemical precipitation method has been used to prepare nanocrystalline B-type CHA. Six different variation of CO_3^{2-}/ PO_4^{3-} molar ratios, i.e. 0.5 to 5, were initially prepared and the as-synthesized CHA powders were labelled as 0.5CHA, 1CHA, 2CHA, 3CHA, 4CHA and 5CHA respectively. The single-phase samples (0.5-4CHA) were then subjected to tube furnace for a sintering period of 2h at 900 °C under CO_2 atmosphere. A stoichiometric HA was also synthesized under similar condition for comparison purpose.

4.2.1 XRD Analysis

The XRD signatures of the synthesized HA and CHA powders are as shown in Figure 4.1. The diffraction peaks of the synthesized HA and 0.5CHA to 5CHA powders exhibited a single phase material (except 5CHA) that closely match the ICDD#9-432 standard for hydroxyapatite. Further increased in the CO_3^{2-}/ PO_4^{3-} ratio above 4, however

resulted in the development of calcium carbonate. For the as-synthesized 5CHA powder (CO_3^{2-}/ PO_4^{3-} molar ratio of 5) which exhibited some minor calcite or $CaCO_3$ (ICDD #5-586) as a secondary phase at 2θ = 29°, indexed as (104). Other researchers have also reported the presences of calcite in CHA prepared at different CO_3^{2-}/ PO_4^{3-} ratios using various synthesis methods (Barinov et al., 2005; Liao et al., 2007; Lafon et al., 2008; Kee et al., 2013). This result indicated that the excess amount of CO_3^{2-} ions present in the 5CHA sample during synthesis could have reacted with Ca^{2+} in the apatite lattice to form $CaCO_3$ due to the limited PO_4^{3-} available for the substitution. This composition will not be considered in the sintering study.

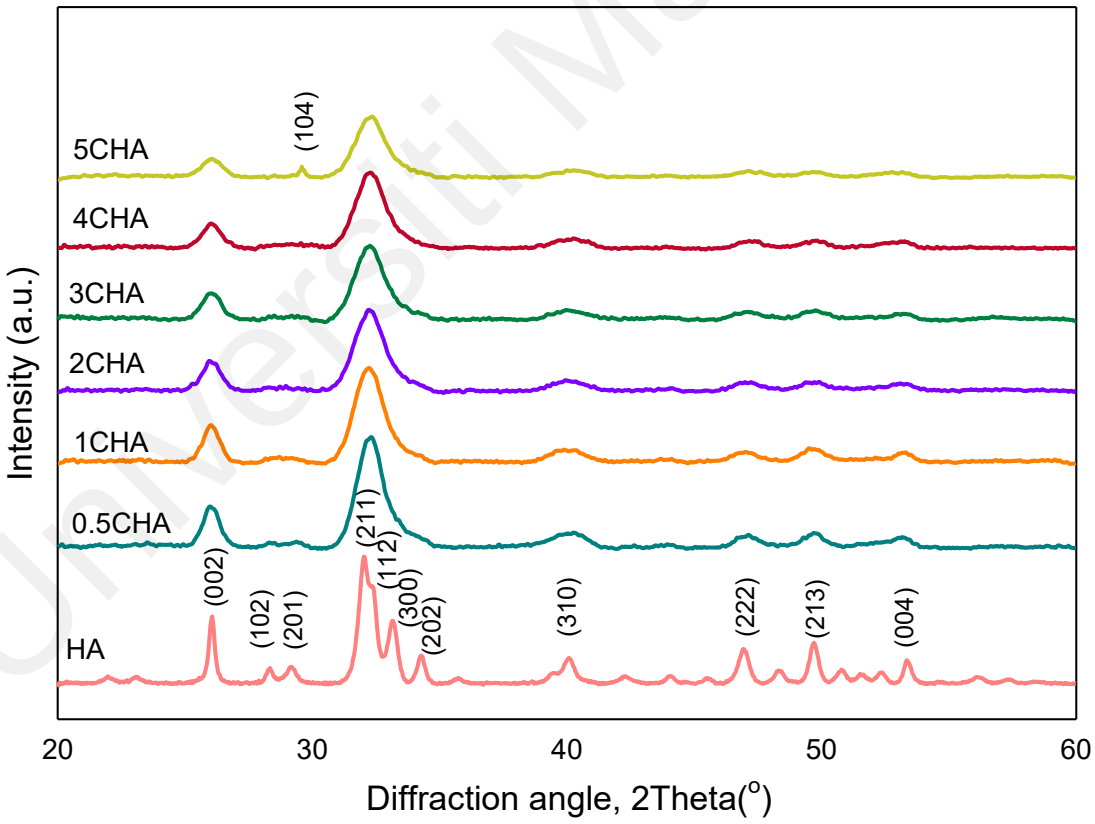

Figure 4.1: XRD diffractograms of as-synthesized HA and B-type CHA (CO_3^{2-}/ PO_4^{3-} = 0.5-5) powders

The major signatures of the synthesized CHA at various ratios i.e. 0.5CHA to 5CHA identified with low intensities are (002) at 26°, (102) and (201) at 28 and 29°, the typical features of the (211) and (112), peaks at 2θ about 32° observed for stoichiometric HA as shown in Figure 4.1 becomes unnoticeable for all the CHA samples due to the peaks overlapping each other and it is the differentiating HA from CHA as indicated by Landi et al. (2003). In addition, two more overlapping peaks reflections around 33-34° indexed (300) and (202) owing to peak broadening. The presence of broad peak between 30° and 35° indicated that as-synthesized CHA powders was in amorphous phase. The peak of (310) at 40° and (222), (213) and (004) at 47°, 50° and 53° respectively was as also detected in XRD pattern.

In agreement with other researchers (Xu et al., 2001; Pasteris et al., 2004; Barinov et al., 2005; Liao et al., 2007; Lafon et al., 2008; Kee et al., 2013), it can be observed in Figure 4.1 that the degree of crystallinity of the CHA powders decreased and the peaks become more broaden with increasing CO_3^{2-}/ PO_4^{3-} molar ratio. This was also confirmed from the analysis of the lattice constants *c/a* ratio (Table 4.1) as determined by Rietveld refinement (Feki et al., 1999).

The structural parameters obtained from the Rietveld refinement of all the samples have been determined based on the unit cell parameters at the hexagonal setting (space group $P6_3/m$) as given in Table 4.1 which further verified the formation of apatite structure. The results show that in comparison to the synthesized HA, the *c/a* parameter increases with increasing CO_3^{2-}/ PO_4^{3-} ratio resulting from a decrease in the *a-axis* and an increase in the *c-axis*, which could be attributed to the replacement of the bigger tetrahedral PO_4^{3-} ion by smaller trigonal planner CO_3^{2-} ion which indicated the B-type CHA (Murugan & Ramakrishna, 2006). Nevertheless, with sintering samples, *c/a* ratio slightly decreased (Table 4.2), which is attributed to the partial loss of carbonate content

from the CHA structure subsequently would reduce the lattice distortion (Rogers & Daniels, 2002).

Table 4.1: Structural parameters for as-synthesized HA and B-type CHA (CO_3^{2-}/ PO_4^{3-} = 0.5-5) powders determined from the Rietveld refinement

Samples	*a-axis* (Å)	*c-axis* (Å)	*c/a* ratio	Crystallite size (nm)
HA	9.4180	6.8822	0.7307	12.8
0.5CHA	9.4153	6.8889	0.7317	8.3
1CHA	9.4132	6.9159	0.7347	7.9
2CHA	9.4125	6.9611	0.7396	7.1
3CHA	9.4115	6.9735	0.7410	6.7
4CHA	9.4012	6.9926	0.7438	6.2
5CHA	9.4031	6.9972	0.7441	5.4

The XRD patterns of the sintered 0.5CHA to 4CHA samples are shown in Figure 4.2. The sharp and narrow peaks, suggesting the relatively crystalline structure of apatite was formed during sintering at 900 °C in CO_2. Guo et al. (2003) also reported similar results of amorphous to crystalline structure during sintering. In general, it can be said that, the higher the CO_3^{2-} content, the lower the crystallinity and sintering temperature (Zyman & Tkachenko, 2011). There was no secondary phase formation and the samples remained as B-type CHA regardless of carbonate content and sintering. This was also confirmed from the higher *c/a* ratio of the sintered samples as compared to that of the synthesized HA (Table 4.2).

All XRD signatures confirmed with the HA reference ICDD #9-432 with a slight shift of the pattern, signifying the formation of CHA. The substitution of carbonate into HA had not affect the structural pattern of HA. However, increasing the carbonate content exhibited significant reduction in intensity. The main peaks of HA on the XRD pattern are; plane (002) at 2θ = 26°, (102) and (201) indexed at 2θ = 28 and 29°, peaks of (211), (112), (300) and (202) located at 32-34°, (301) and (212) at 36 and 39°,one around 40°

indexed (310), peaks of (311), (113), (203) at 42, 44, 45° and peaks of (222), (312), (213), (402) and (004) located at 47°, 48°, 50°, 52° and 53°, respectively.

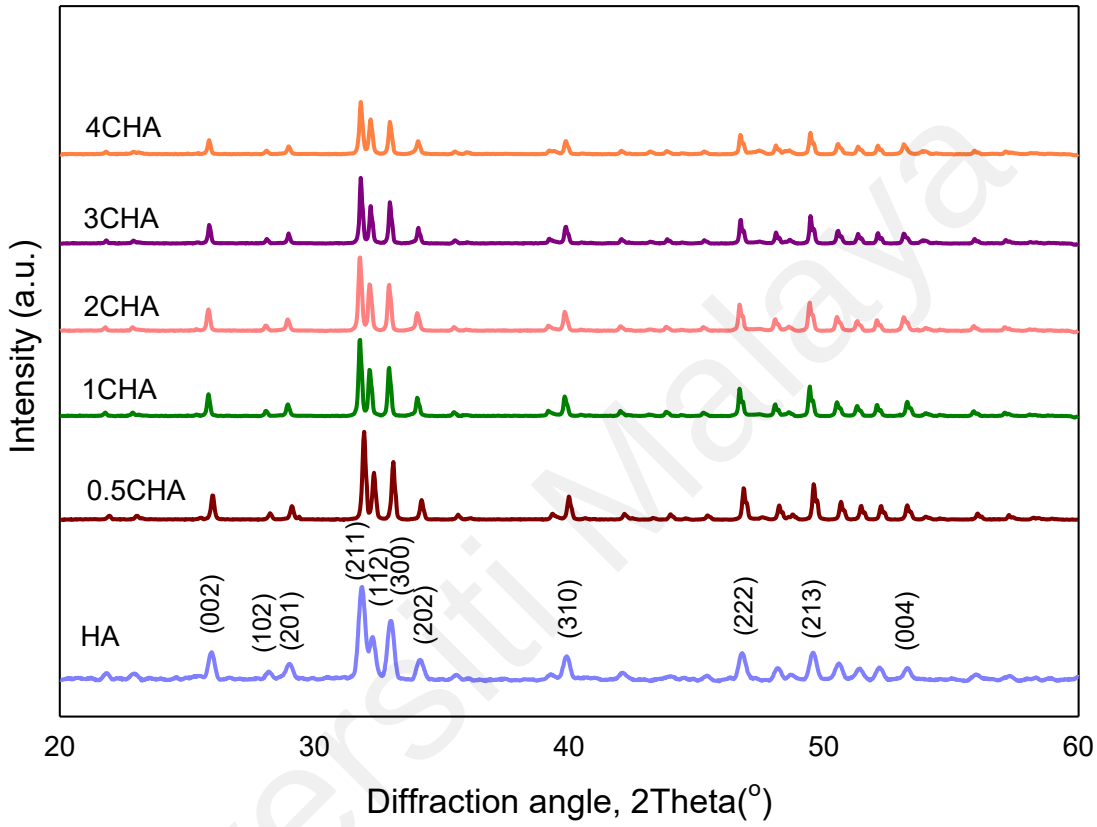

Figure 4.2: XRD diffractograms of sintered HA and B-type CHA (CO_3^{2-}/ PO_4^{3-} =0.5- 4) pellets at 900 °C in CO_2

The carbonate substitution would induce lattice defects in the apatite structure and suppress crystal growth (Xu et al., 2001; Pasteris et al., 2004; Wopenka & Pasteris, 2005). This is evident from the decreased in the crystallite size by using the Scherrer's formula based on the (002) peak (Cullity, 1978) (Table 4.1 & Table 4.2) and the decreased in the crystallinity of the powders with increasing CO_3^{2-}/ PO_4^{3-} ratio as depicted by the XRD peaks (Figure 4.1 & Figure 4.2) which declined in both sharpness and intensity.

Table 4.2: Structural parameters for sintered HA and B-type CHA (CO_3^{2-}/ PO_4^{3-} =0.5- 4) at 900 °C in CO_2

Sample	*a-axis* (Å)	*c-axis* (Å)	*c/a* ratio	Crystallite size (nm)
HA	9.4218	6.8822	0.7305	94.3
0.5CHA	9.4152	6.8883	0.7316	81.5
1CHA	9.4131	6.9145	0.7345	77.2
2CHA	9.4124	6.9603	0.7394	72.0
3CHA	9.4113	6.9724	0.7408	69.1
4CHA	9.4011	6.9895	0.7435	68.5

The Rietveld refinement of the sintered CHA samples presented in Figure 4.3, showing the residual of fittings ($I_O - I_C$) between observed (I_O) and calculated (I_C) intensities patterns of each fitting. A very small differences could be seen between both patterns as shown by the difference curve ($I_O - I_C$) plotted under the respective XRD signatures. There was no secondary phase formation detected and all the samples conformed to the standard ICDD for HA phase. The various *R* factors of these samples are presented in Table 4.3. The quality of the refinement using the Rietveld method is monitored by the reliability index parameter: profile residual (R_p), weighted profile residual (R_{wp}), expected profile residual (R_{exp}) and goodness of fit (χ). R_P and R_{WP} should reach a value of R_{exp} to consider the model acceptable (Shatokha, 2012; Grumezescu & Grumezescu, 2019). Experimental XRD patterns of all sintered CHA samples and HA are fitted by refining the structural and microstructural parameters of the respective simulated patterns with 'goodness of fittings' (GoFs). In general, the GoF values for the CHAs were found to be slightly higher (i.e. 2.10 – 2.22) if compared to the control HA which had a lower value of 1.35, i.e. demonstrating a very good fit exist between the observed and calculated patterns. This is expected since the CHA are non-stoichiometric apatite and their calcium to phosphate proportion was found to increase with increasing CO_3^{2-}/ PO_4^{3-} ratio, from 1.71 for 0.5CHA to 1.96 for 4CHA.

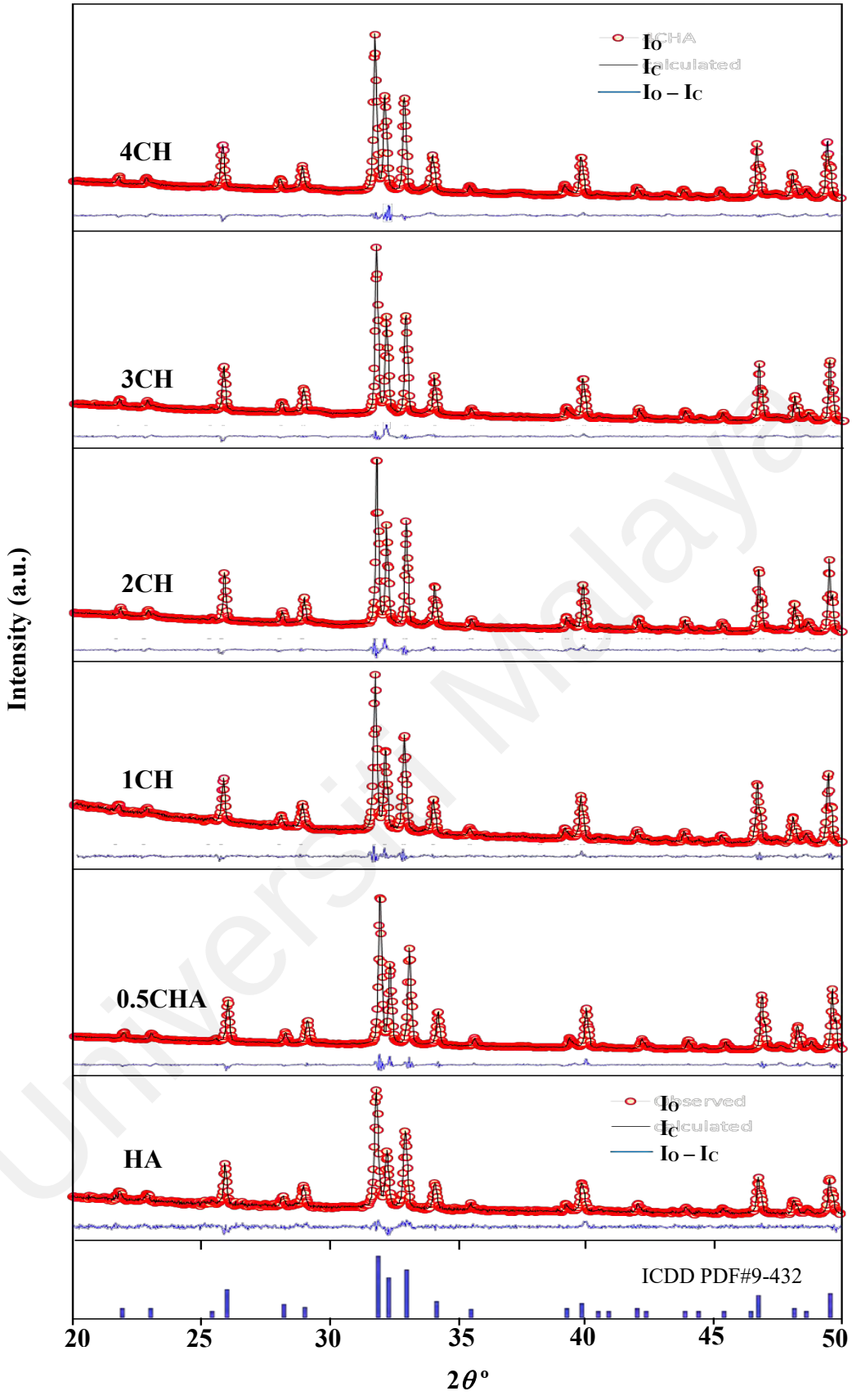

Figure 4.3: Comparison of Rietveld analysis patterns for sintered samples obtained from the XRD data

Nevertheless, Table 4.3 shows that for all samples, both the I_O and I_C patterns are in good agreement with each other and this is considered acceptable in accordance to the basic rule of GoF less than 4% (Sarkar & Kannan, 2014; Yacoubi, et al., 2017; Fahami et al., 2017).

Table 4.3: The various reliability index parameters obtained from the Rietveld refinement for the sintered samples

Sample	R_p	R_{wp}	R_{exp}	χ^2	*GoF*
HA	20.5	16.0	11.85	1.82	1.35
0.5CHA	19.1	13.1	5.91	4.93	2.22
1CHA	18.3	12.6	5.89	4.58	2.14
2CHA	16.5	12.5	5.95	4.41	2.10
3CHA	16.2	12.7	5.97	4.54	2.13
4CHA	16.5	13.2	6.1	4.67	2.16

Note: $\chi^2 = (R_{wp}/R_{exp})^2$

4.2.2 FTIR Analysis

The FTIR spectrums for HA and CHA synthesized powders with variant carbonate content shown in Figure 4.4. It was found that the intensity of the CO_3^{2-} derived bands in the FTIR spectra increased proportionally with increasing CO_3^{2-}/ PO_4^{3-} ratio. Basically, carbonate vibrations are characterized into two regions; 871-873 cm^{-1} (ν_2) and 1416-1486 cm^{-1} (ν_3), representative of the B-type CHA (Krajewski et al., 2005; Lafon et al., 2008). The characteristic vibration of A-type CHA, normally seen at the wavelengths of 877–880 cm^{-1}, 1500 cm^{-1} and 1540–1550 cm^{-1}, and the AB-type CHA (at 1515 cm^{-1}) were not observed for all samples (Ślósarczyk et al., 2005).

Moreover, the broad bands in the range of 3435-3437 cm^{-1} and 1637-1643 cm^{-1} were assigned to adsorbed water, while the bands at 630 and 3540 cm^{-1} which were corresponded to OH groups were not observed for stoichiometric HA (Vignoles et al., 1988; Suchanek et al., 2002). The characteristic bands of PO_4^{3-} groups of the apatite structure was observed at about 566-568 and 603-604cm^{-1} (ν_4), 1039–1046 cm^{-1} (ν_3). The

marker band of $CaCO_3$ at 712 cm^{-1} were not detected for all samples in FTIR (Krajewski et al., 2005). However, it was observed as a secondary phase at the 5CHA sample in XRD analysis. It possibly was because of the present small amount of $CaCO_3$ (7%) in 5CHA sample that overlapped with CO_3^{2-} band at 872 cm^{-1} (Liu et al., 2009). The FTIR analysis verified the formation of single-phase CHA and this is in good agreement with that of the XRD analysis (except 5CHA). The band at 1380 cm^{-1} attributed to residual nitrates was not evident in all spectra (Kovaleva et al., 2008).

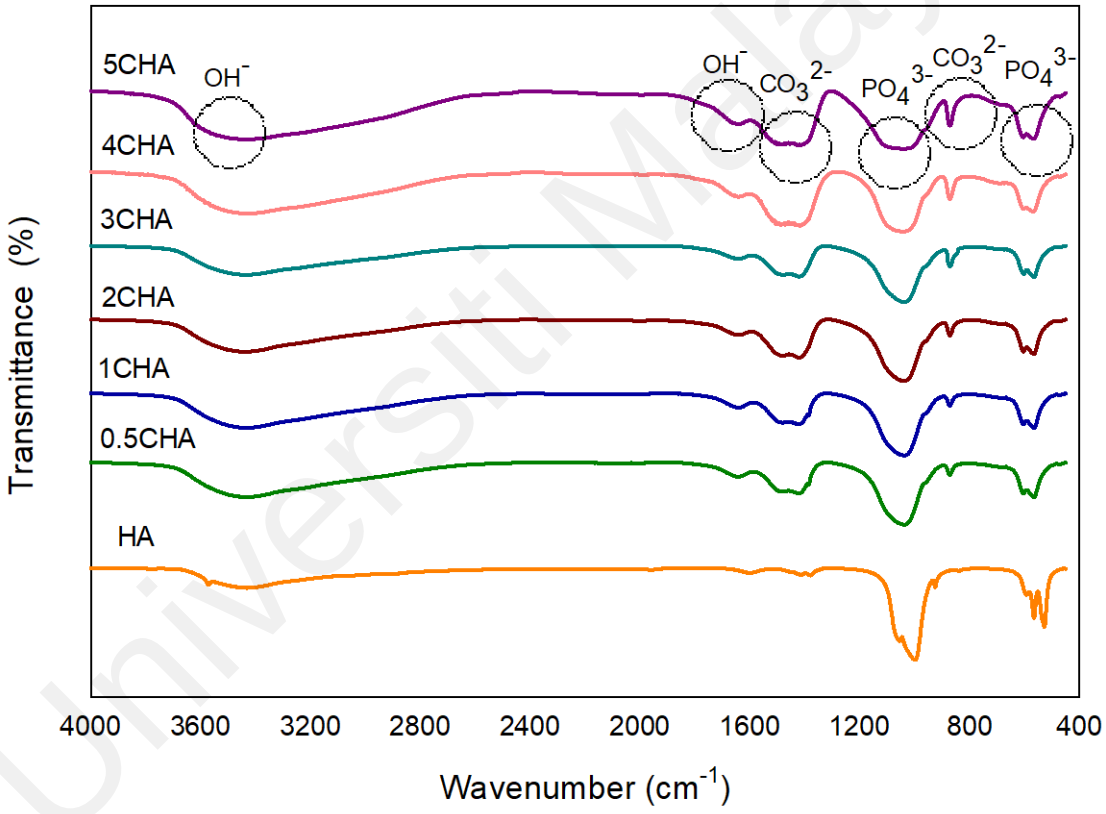

Figure 4.4: FTIR spectra of as-synthesized HA and B-type CHA (CO_3^{2-}/ PO_4^{3-} =0.5- 4) powders

The FTIR spectra of the sintered HA and CHA with variant carbonate content are shown in Figure. 4.5. The trends in IR spectra displayed that all the sintered samples had remained as B-type CHA. It has been proven by the typical characteristic bands of

carbonate group detected at 870-875(v_2) as well as 1410-1430 (v_3) and 1450-1470 cm^{-1} (v_3) which were in agreement with Ślósarczyk et al. (2010) study. The characteristic vibration of A-type CHA at about 880, 1500, and 1540-1545 cm^{-1} (Landi et al., 2003; Rau et al., 2004) as well as the AB-type band at 1515cm^{-1} (Ślósarczyk et al., 2005) were not detected for all sintered samples. In addition, the bands at 566-568 and 603-604 cm^{-1} (ν_4) and 1039–1046 cm^{-1} (ν_3) are attributed to PO_4^{3-} group.

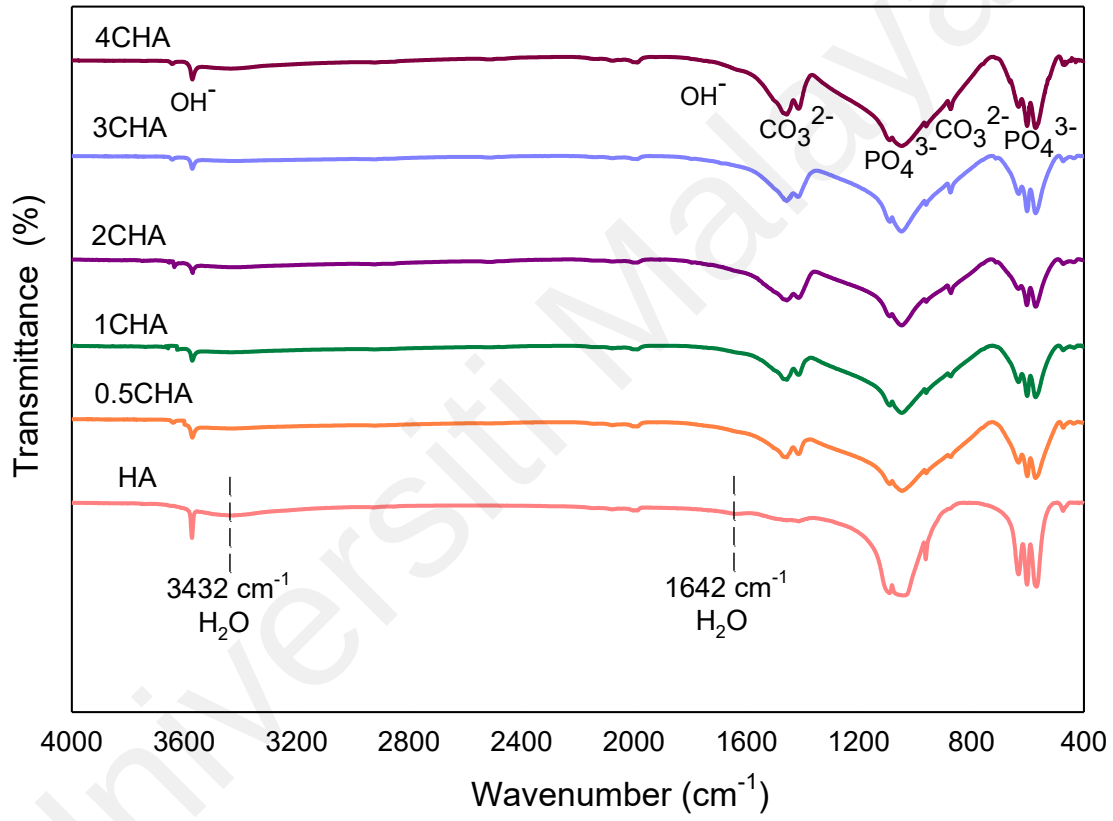

Figure 4.5: FTIR spectra of sintered HA and B-type CHA pellets (CO_3^{2-}/ PO_4^{3-} =0.5- 4) at 900 °C in CO_2

However, the intensity of the CO_3^{2-} derived bands in the FTIR spectra increased with increasing CO_3^{2-}/ PO_4^{3-} ratio, the decrease in intensity of the CO_3^{2-} bands in compare with CHA powders suggesting the decomposition of carbonate at sintering. The synthesized HA has a sharp peak at approximately 3570 cm^{-1} that corresponds to the

stretching vibration of the lattice OH^- ions and the relatively broad peak centered around 3432 cm^{-1} and the minor peak at 1642 cm^{-1} are attributable to absorbed water which is a typical feature observed for stoichiometric HA (Vignoles et al., 1988; Suchanek et al., 2002). The significant changes observed in the spectra of the CHA are the absences of the broad peaks associated with absorbed water and that the OH^- peak at 3570 cm^{-1} appears to be of a lower intensity compared to the HA sample, suggesting less OH groups in the carbonated-substituted HA. This is expected due to the non-stoichiometric nature of the CHA. In addition, the absences of $CaCO_3$ at 712 cm^{-1} in all spectra confirmed that the HA phase was not disrupted after sintering and this is in good agreement with the XRD analysis.

4.2.3 Thermal Analysis

A typical thermal analysis of the sample 4CHA is presented in Figure 4.6. In general, the TG curve shows two stage of significant weight loss occurring during heating. From room temperature to 500 °C (stage I), there was about 12 wt.% loss which can be ascribed to the liberation of absorbed and lattice H_2O (Barinov et al., 2005; Zyman & Tkachenko, 2011). This was followed by another weight loss of about 3.5 wt.% from 500 to 900 °C (stage II) and this could be associated with decomposition of carbonate. There was no further weight loss observed from 900 to 1000 °C for all samples.

A similar trend was observed for all other samples and the total weight loss measured at 900 ºC for the samples did not vary very much as shown in the inset table in Figure 4.6. In general, the amount of carbonate loss during heating of the synthesized powders is considered below the threshold limit for the stabilization of the B-type CHA. It is also believed that the sintering of the samples in CO_2 atmosphere could have compensated the loss of CO_3^{2-} since the characteristics of the CHA phase were preserved as confirmed by the XRD analysis.

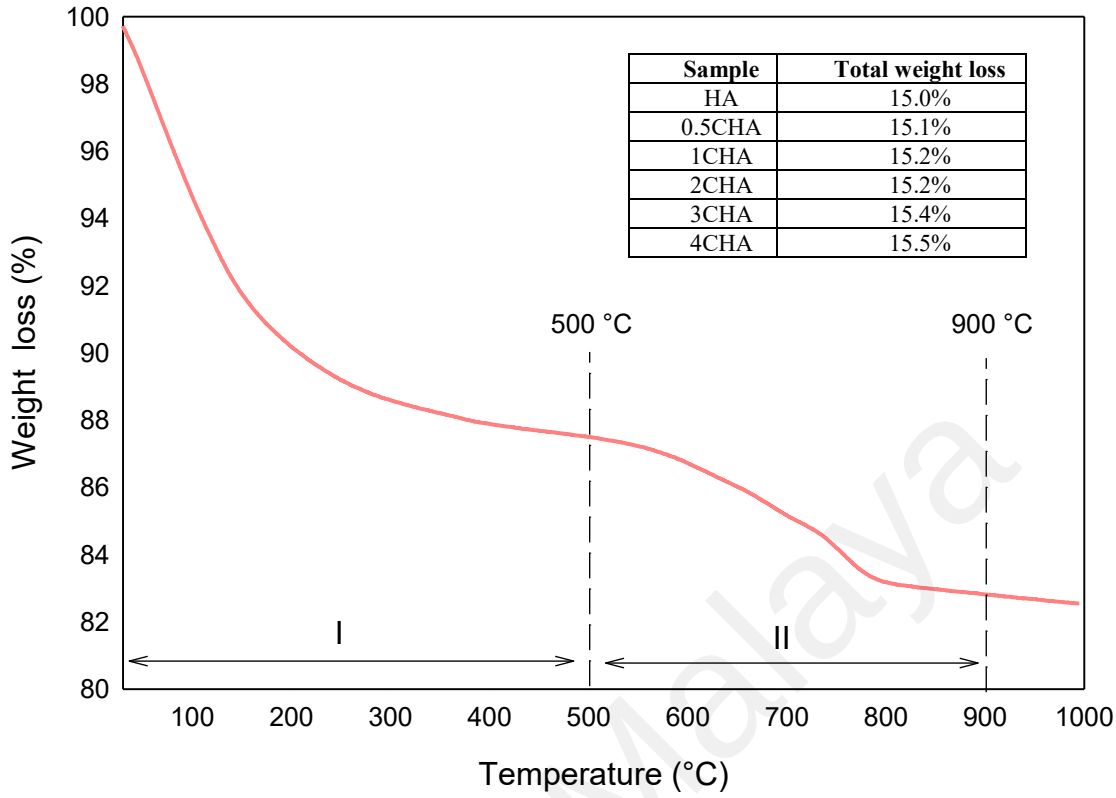

Figure 4.6: TGA curve of B-type CHA (CO_3^{2-}/ PO_4^{3-}=4) subjected to heating from room temperature to 1000 °C. The inset table shows the total weight loss measured for the other samples

4.2.4 Elemental Analysis (CHN & XRF) and Specific Surface Area

The calcium to phosphate (Ca/P) ratio of the as-synthesized 0.5-5CHA samples as determined from the XRF analysis was found to be higher than the stoichiometric HA of 1.67 and increases with increasing CO_3^{2-}/ PO_4^{3-} ratio, from 1.72 for 0.5CHA to 2.07 for 5CHA (Table 4.4). This is expected since the substitution of CO_3 would reduce the phosphate content in the CHA lattice, thus resulting in an increased in the Ca/P ratio. This observation is in good agreement with that of LeGeros & LeGeros (2002) and Landi et al. (2004) who reported that the Ca/P ratio of CHA could vary from 1.7 to 2.6.

As for the Ca/P ratio of all sintered CHA, results in Table 4.4 designated that the Ca/P ratio were not noticeably affected by sintering. The Ca/P ratio for sintered 0.5 -4 CHA was 1.71 – 1.96 respectively, while generally the fluctuation in the Ca/P ratio for all

samples after sintering were about ± 0.01 %. The obtained result for the current CHA varies between 1.7 to 2.6.

The amount of carbonate content present in the sintered samples for 0.5CHA, 1CHA, 2CHA, 3CHA and 4CHA as per the CHNS/O analysis were 2.01, 2.95, 4.10, 5.05 and 5.25 wt.%, respectively. These values are within the limit of 2-8 wt.% normally found in human bones (Barralet et al., 2000).

The specific surface area of HA and 0.5-5CHA powders as measured by the BET method (S_{BET}) is given in Table 4.4. The result shown that the higher amount of carbonate in CHA resulted in a higher S_{BET} value (106.97 m^2/g) which correlated well with the smaller crystallite sizes of these samples.

Table 4.4: Carbonate content, Ca/P ratio and specific surface area of HA and B-type CHA (CO_3^{2-}/ PO_4^{3-} = 0.5-5)

Samples	*As-synthesized powder*			*Sintered pellets*			S_{BET} (m^2/g)
	wt% C	wt% CO_3^{2-}	Ca/P ratio	wt% C	wt% CO_3^{2-}	Ca/P ratio	
HA	-	-	1.67	-	-	1.67	59.52
0.5CHA	1.05	5.25	1.72	0.40	2.01	1.71	65.97
1CHA	1.75	8.75	1.78	0.59	2.95	1.77	67.90
2CHA	2.46	12.30	1.83	0.82	4.10	1.84	80.30
3CHA	2.99	14.95	1.89	1.01	5.05	1.89	82.13
4CHA	3.05	15.25	1.98	1.05	5.25	1.96	86.71
5CHA	3.51	17.55	2.07	-	-	-	106.97

On the other hand, it has been reported that the S_{BET} of the non-stoichiometric HA samples have higher values than stoichiometric (59.52 m^2/g) ones (Krishna et al., 2007). Suggesting that increase in carbonate substitution effectively leads to increase the S_{BET} which would enhance *in vitro* biological activity (Bang et al., 2015).

4.2.5 FESEM Analysis

Morphological characterization of CHA powders and sintered pellets was studied by FESEM. From the Figure 4.7, it was noticed that there was no major difference between variant carbonate of CHA powders. This result appeared similar with Ellies et al. (1988) reports. Highly agglomerated particles were observed in all as-synthesized CHA powders. It can be due to the high surface energy of nanosized primary particles which is associated with the high surface area of the nano particles. However, it was clear from the results, as-synthesized HA powders was consisting of microsized agglomerated rod-like particles, measuring the accurate particle size of the as-synthesized HA and CHA powders was still difficult.

The FESEM microstructure of the fractured cross-sectional area of the HA and various CHA is shown in Figure 4.8. In general, the micrographs show that varying the CO_3^{2-}/ PO_4^{3-} ratio has negligible effect on the sintered microstructure. All the CHA samples exhibited an equiaxed and uniform grain morphology. The synthesized HA exhibited a fine microstructure, composed of almost spherical grains, having an average size of about 0.16 ± 0.02 μm. From the fracture morphology, the HA revealed a smooth fracture associated with an intergranular-type fracture whereas a transgranular-type fracture is observed for the CHA samples.

In agreement with the higher relative density and higher shrinkage values, a much compact structure, comprised of large grains were observed for all the CHA samples. The measured grain size of the sintered CHA was found to decrease monotonically with increasing carbonate content, from an average value of 1.12 ± 0.11 μm to 0.75 ± 0.08 μm (Table 4.5). This decreased in the grain size, however, was found to have effect on the mechanical properties of the samples as depicted in Figure 4.9.

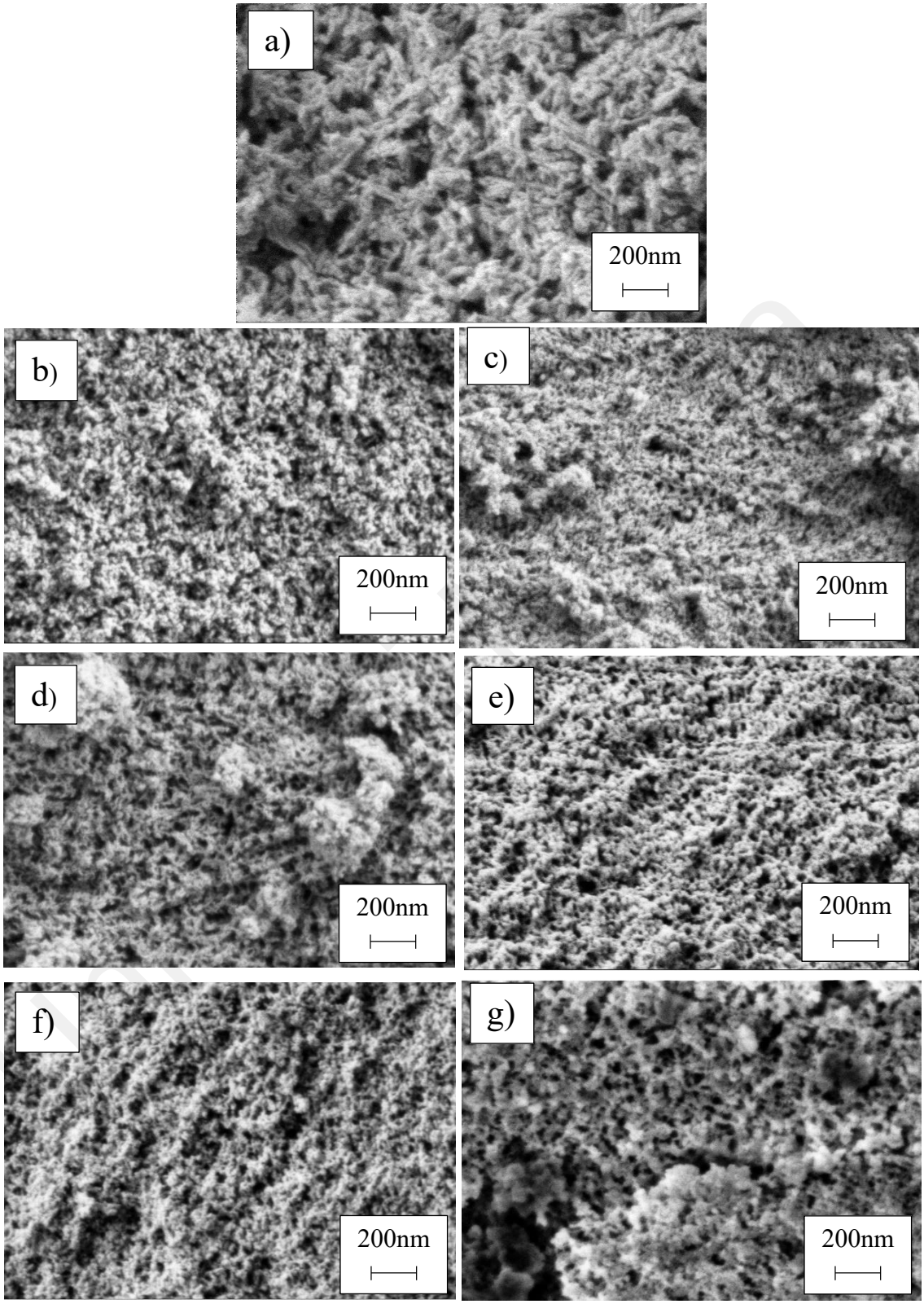

Figure 4.7: FESEM micrographs of as-synthesized powder a)HA, b)0.5CHA, c)1CHA, d)2CHA, e) 3CHA, f)4CHA and g)5CHA (Mag: 50KX)

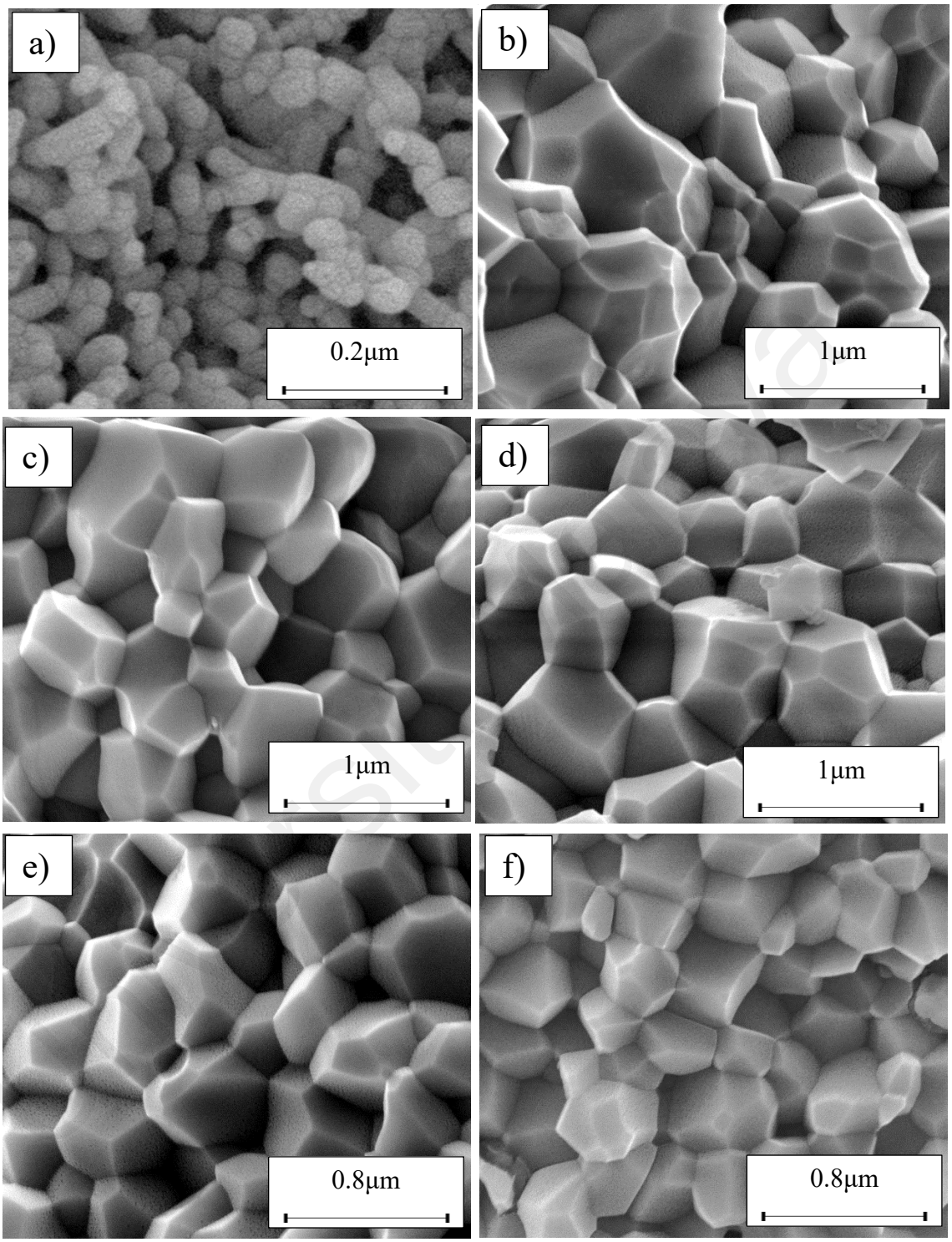

Figure 4.8: FESEM images of the fractured surface of (a) HA, (b) 0.5CHA, (c) 1CHA, (d) 2CHA, (e) 3CHA and (f) 4CHA

4.2.6 Relative Density, Linear Shrinkage and Grain size

The relative density and linear shrinkage of the sintered samples are given in Table 4.5. A relative density of more than 80% was obtained for the CHA samples and this is in good agreement with that reported by other researchers (Zyman & Tkachenko, 2011). The highest relative density of 87% was measured for the 0.5CHA sample and this value decreases slightly with increasing carbonate content. The linear shrinkage correlated well with the relative density and the values were found to be high, at about 13% to 14%. In addition, the carbonate substitution was found to be beneficial in enhancing densification when compared to the unsubstituted HA which exhibited a relatively low density of about 64% which correspond to a low shrinkage of about 10% when sintered under similar conditions. The higher porosity of the HA can be observed from the FESEM of the fractured surface micrograph shown in Figure 4.8.

Table 4.5: Relative density, linear shrinkage and average grain size of the sintered samples

Sample	Linear shrinkage (%)	Relative density (%)	Average grain size (μm)
HA	10.2 ± 0.2	64.0 ± 1.3	0.16 ± 0.02
0.5CHA	14.1 ± 0.3	87.0 ± 1.7	1.12 ± 0.11
1CHA	14.0 ± 0.2	86.2 ± 1.6	0.98 ± 0.10
2CHA	13.6 ± 0.3	83.7 ± 1.6	0.92 ± 0.09
3CHA	13.1 ± 0.3	81.4 ± 1.7	0.88 ± 0.09
4CHA	13.0 ± 0.3	80.6 ± 1.6	0.75 ± 0.08

4.2.7 Microhardness Analysis

As can observed in Figure 4.9, the general trend is that the mechanical properties decrease with increasing carbonate content. In agreement with the density results, the Vickers hardness of the CHA was also higher (> 1.4 GPa) when compared to 1.04 GPa obtained for HA when sintered at 900 °C and 1.17 GPa reported for HA sintered at

1000 °C (Muralithran & Ramesh, 2000). The improvement in the mechanical properties of the CHA could be associated with the improvement in the bulk density of the sintered compact as well as in part to the increased in the *c/a* lattice parameter ratio as depicted in Table 4.1. It is envisaged that the distortion of the *a-axis* in the CHA lattice would create additional dislocation barrier for plastic deformation to proceed, thus resulting in improvement in the mechanical properties. However, with increasing carbonate content, density decreased, resulting in a decrease in mechanical properties.

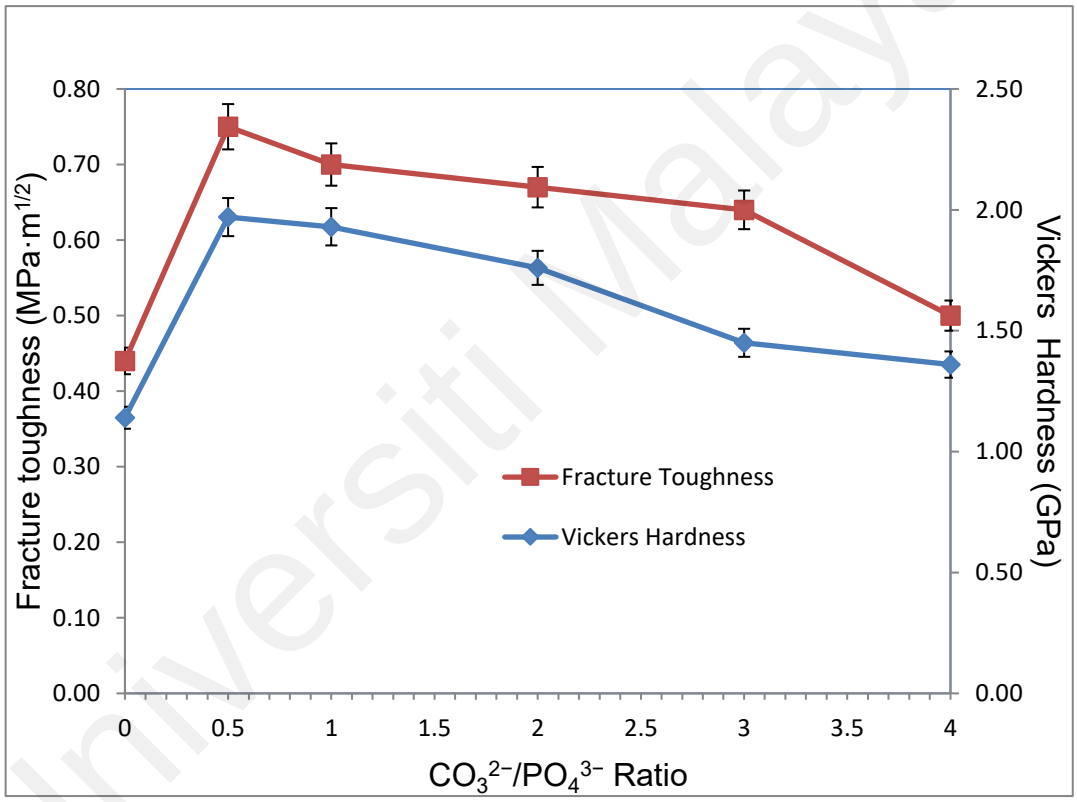

Figure 4.9: Mechanical properties of sintered CHA (CO_3^{2-}/ PO_4^{3-} = 0.5-4) pellets

Fracture toughness is typically associated with the propagation of pre-existing flaws within the product, such as cracks, voids, and weld defects. Therefore, it is assumed that tightly bound grains structure with dense microstructural arrangements could led to shorter crack length and increase in toughness.

The present study also revealed that smaller grain size may not necessarily result in better toughness and there is certainly a combinatory effect between density, grain size and carbonated content. More work is in progress to elucidate this behavior. Other researchers have also reported that carbonate substitution was beneficial in enhancing the mechanical and biological properties compared to hydroxyapatite (Doi et al., 1993; Gibson & Bonfield, 2002) although the exact role of carbonate in enhancing the mechanical properties is not well understood.

4.2.8 *In vitro* Bioactivity Test in SBF

An essential prerequisite for artificial material is the formation of bone-like apatite on its surface when implanted in the living body (Kokubo & Takadama, 2006). Simulated body fluid (SBF) solution was performed to evaluate the *in vitro* bioactivity test in ion concentration closely to human blood plasma as proposed by Kokubo & Takadama (2006). Various types of carbonate ratio CO_3^{2-}/ PO_4^{3-} from 0.5 to 4CHA samples were chosen to soak in the SBF solution at 36.5 ± 0.5 °C accordingly for different periods within 1, 3, and 7 weeks incubation. The formation of calcium phosphate precipitates on the surface of CHA samples with various carbonate ratio of (0.5-4) in SBF was studied.

Figure 4.10 – 4.14 shown the FESEM images (10Kx) of 0.5-4CHA samples were subjected to SBF with different immersion period. It was observed that after first week of incubation, almost no apatite layer on the surface of the 0.5 CHA sample were observed (Figure 4.10). However, the rates of bone-like apatite layer formation were accelerated due to the higher carbonate ion substitution. The required time to form a bone-like apatite layer on the surface of the 4CHA was 1 week in compared to 4 weeks for 0.5CHA. Gibson & Bonfield. (2002) also observed the same results. In Figure 4.14, sample 4CHA with a higher carbonate content showed a more noticeable apatite layer formation on the surface than 0.5-3CHA samples, which could be attributed to a higher dissolution rate of

carbonate containing CHA. After prolonging the soaking time to 3 weeks, the precipitation layer became thicker and have completely covered the surface of the 4CHA sample with an elongated shape after 7 weeks of soaking in SBF.

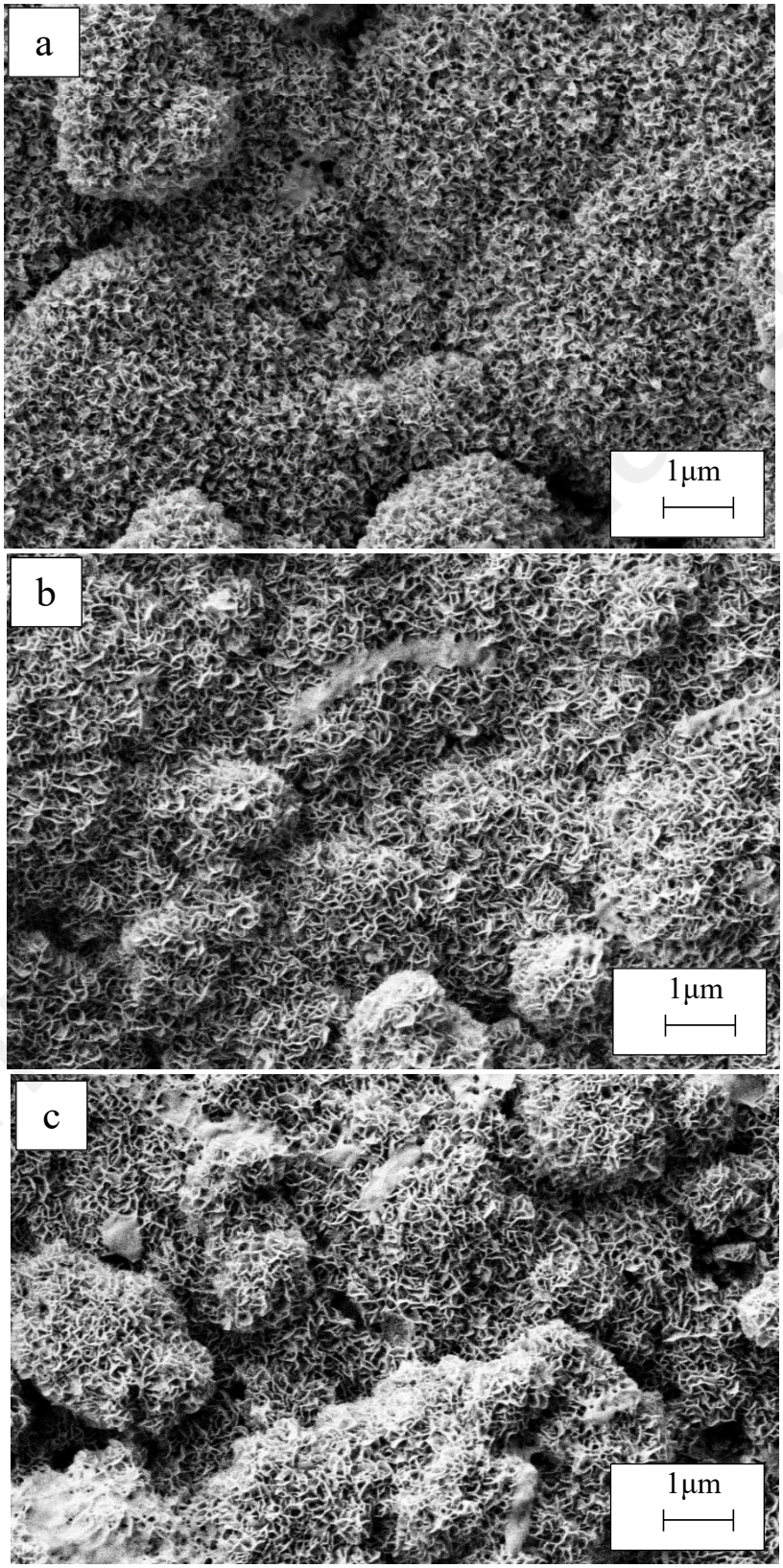

Figure 4.10: FESEM micrograph of apatite layer formed on 0.5CHA immersed in SBF (a)1 week, (b)2weeks and (c)7weeks (Mag:10 KX)

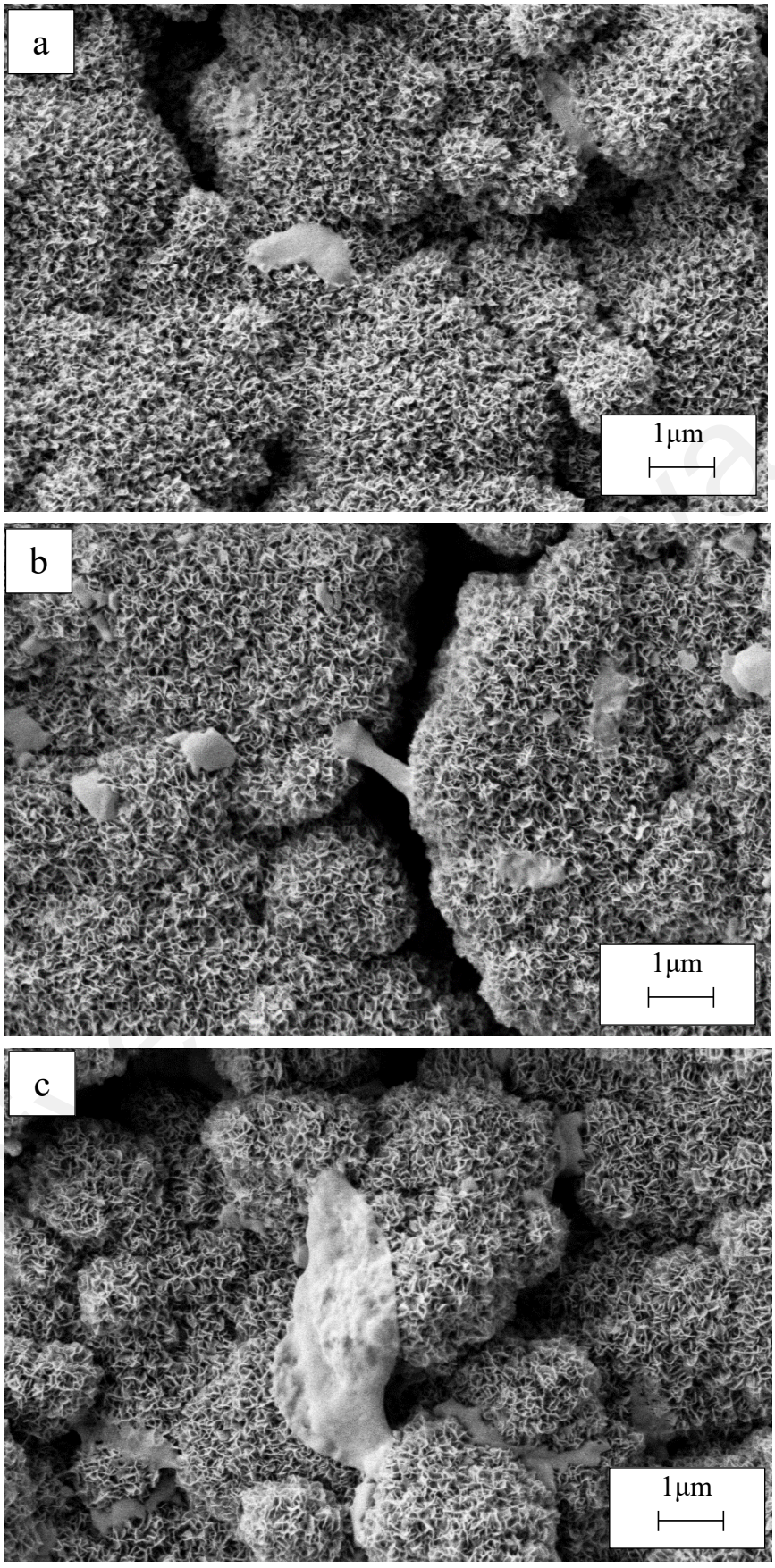

Figure 4.11: FESEM micrograph of apatite layer formed on 1CHA immersed in SBF (a)1 week, (b)3weeks and (c)7weeks (Mag:10 KX)

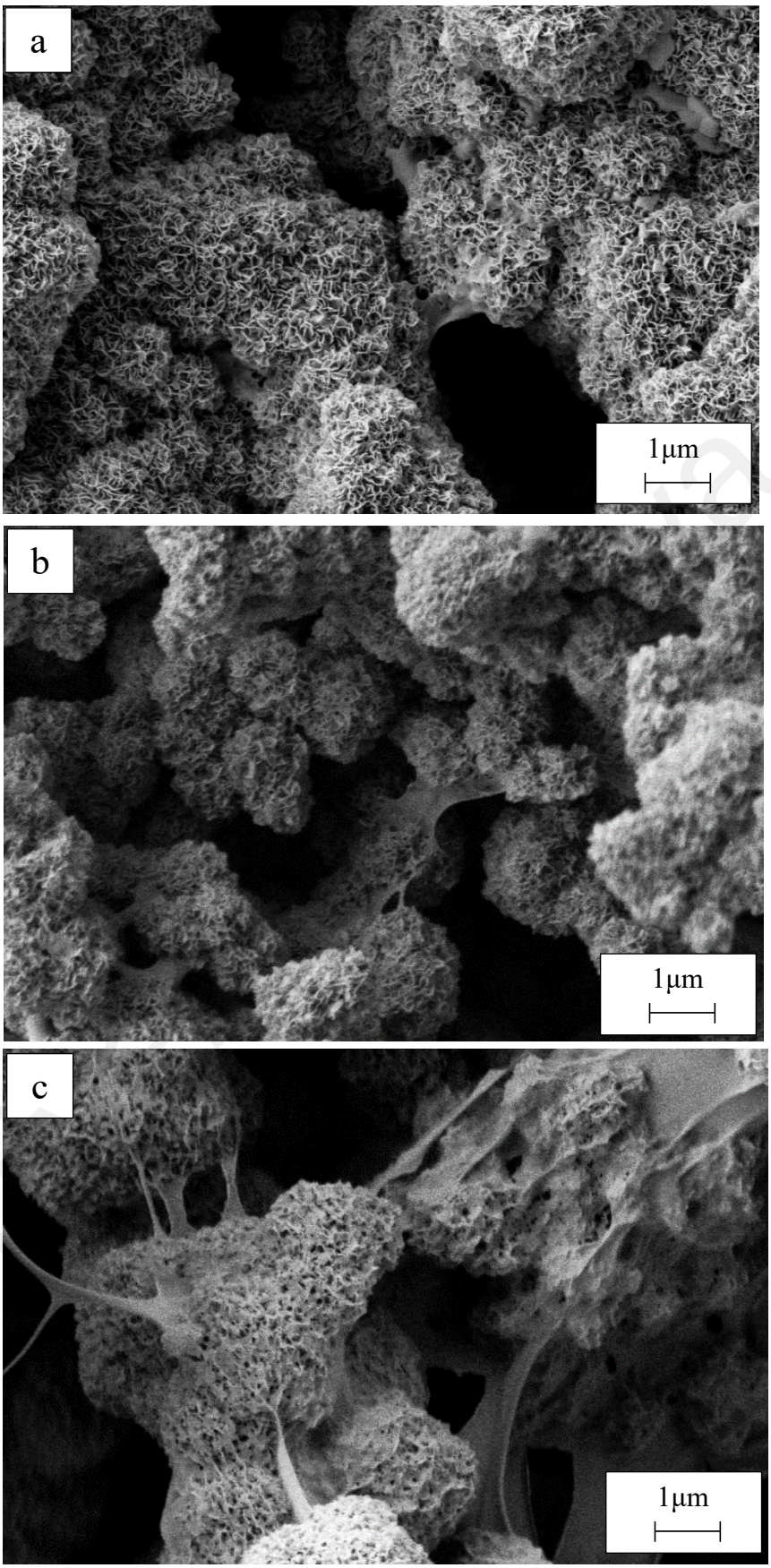

Figure 4.12: FESEM micrograph of apatite layer formed on 2CHA immersed in SBF (a)1 week, (b)3weeks and (c)7weeks (Mag:10 KX)

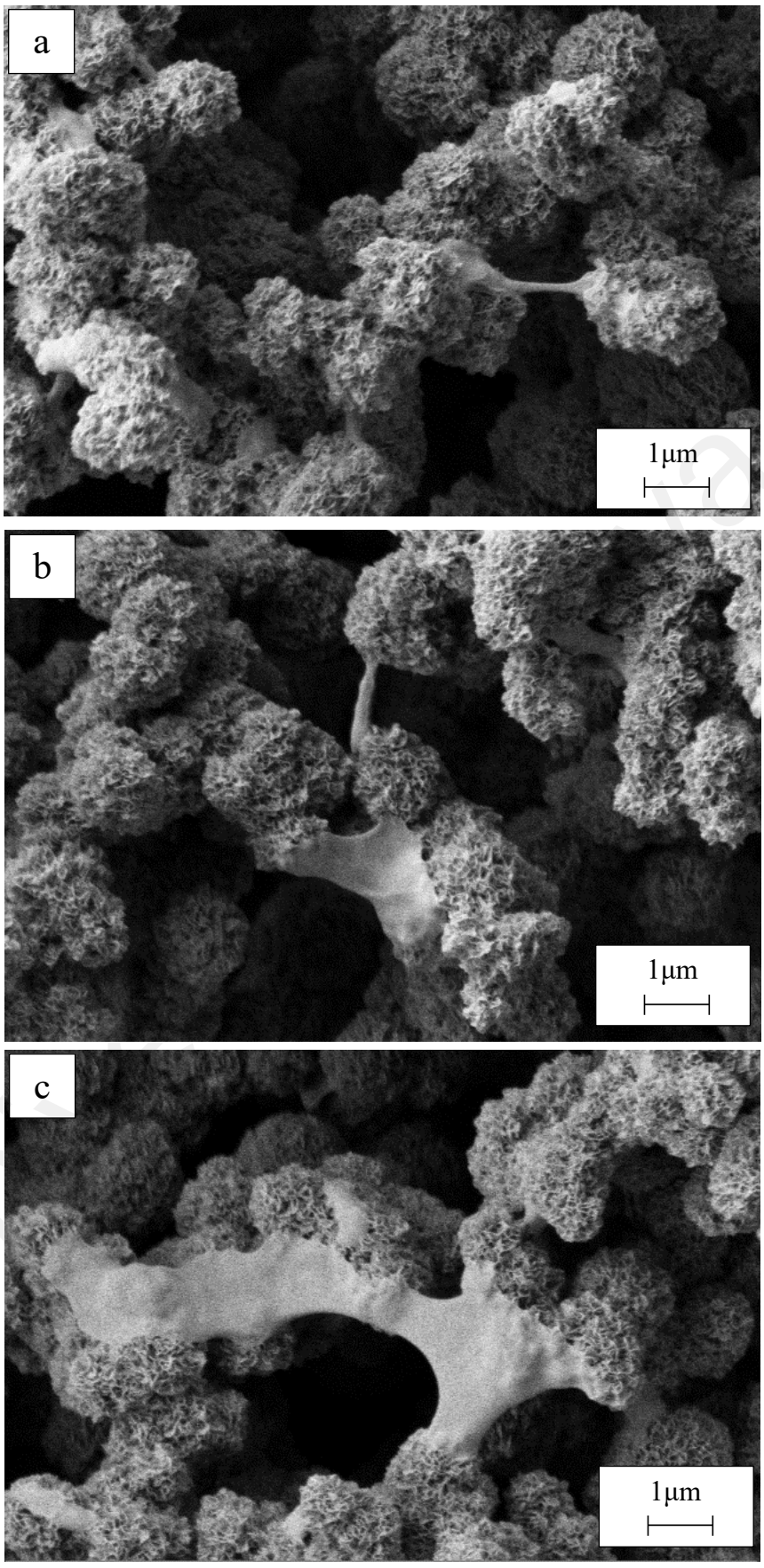

Figure 4.13: FESEM micrograph of apatite layer formed on 3CHA immersed in SBF (a)1 week, (b)3weeks and (c)7weeks (Mag:10 KX)

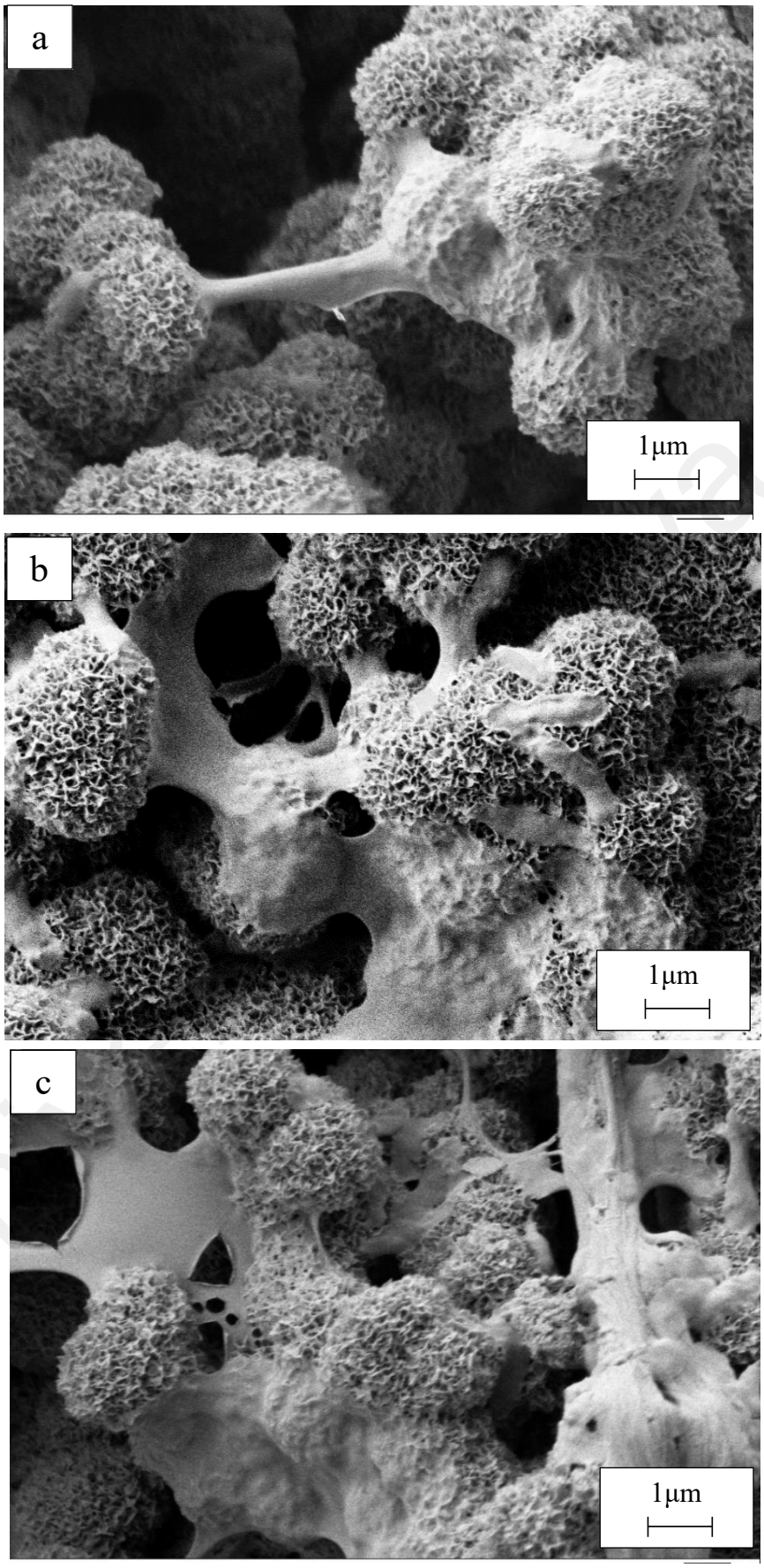

Figure 4.14: FESEM micrograph of apatite layer formed on 4CHA immersed in SBF (a)1 week, (b)3weeks and (c)7weeks (Mag:10 KX)

Guo et al. (2012) reported that the process of the formation of bone-like apatite in SBF can be divided into two stages, including nucleus formation and nucleus growth. The nucleus growth was observed as the immersion time reached 3 and 7 weeks, continues layer of apatite was observed thicker respectively. This results are in agreement with Ellies et al. (1988), Webster et al. (2001) and Porter et al. (2005) findings.

Microstructural study revealed that the rate of the formation apatite layer increased with decreasing the grain size due to the increasing the carbonate content (Porter et al., 2005). Moreover, the mode of the carbonate substitution in the apatite structure plays and important role in solubility. Landi et al. (2004) observed that the B-type substitution enhanced the solubility if compare to A-type CHA.

Furthermore, Nilsson et al. (2004) stated that the formation of apatite layer on the surface were generated by the interaction between the released ions from the sample's surface and ions in the SBF solution. Generally, because of the surface dissolution of samples in SBF, all samples showed decrease in weight after 1 week of incubation followed by slight increase after 3 and 7 weeks since the precipitation of calcium and phosphate layer formed on the sample's surface (Figure 4.14 c).

It was also observed from the Figure 4.15 that higher carbonate content experienced greater weight loss (10.5 wt.%) after 1week incubation in SBF while 0.5CHA, 1CHA, 2CHA and 3CHA samples had weight loss of 3.42wt.%, 6.34 wt.%, 7.9 wt.% and 8.91 wt.% respectively. This clearly shown that the solubility of CHA increased with increasing the carbonate content in its structure. Therefore, sample 4CHA shown the most solubility in compare with 0.5- 3CHA and thicker apatite layer after 7 weeks immersion in SBF.

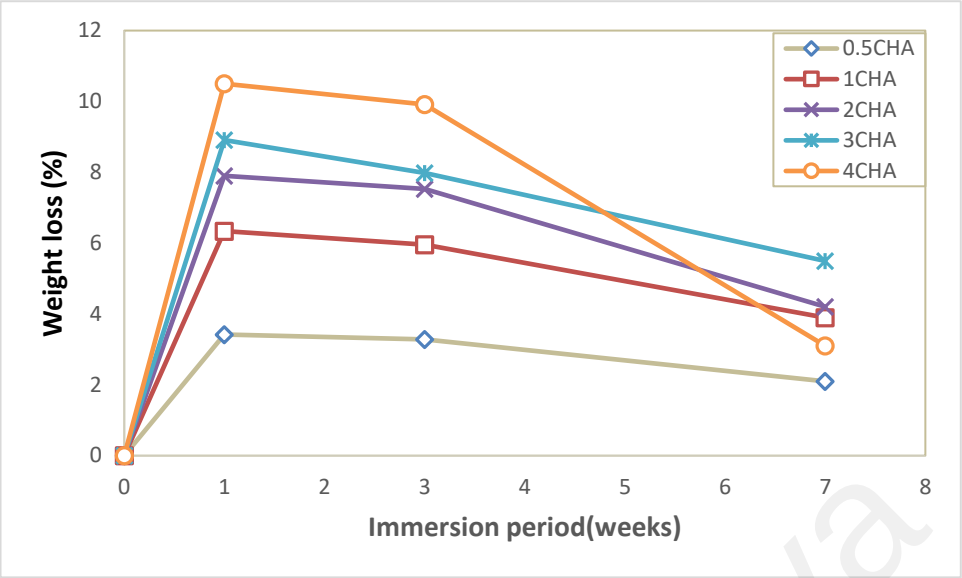

Figure 4.15: Weight loss of 0.5-4CHA as a function of immersion period in SBF at 36.5 ± 0.5 °C

Fluctuation in pH was recorded for different incubation periods of time in SBF solution according to Figure 4.16. Overall, pH value increased within the first period of soaking in SBF as the alkaline ions released from the sample's surface to the SBF solution. It has been reported that the release of Ca ions from the sample leads to an increase in pH value in SBF (Vallet-Regí & Rámila, 2000). The increase in pH indicated the solubility of the CHA samples and alternatively decreased with precipitation of apatite layer after prolonging the soaking time.

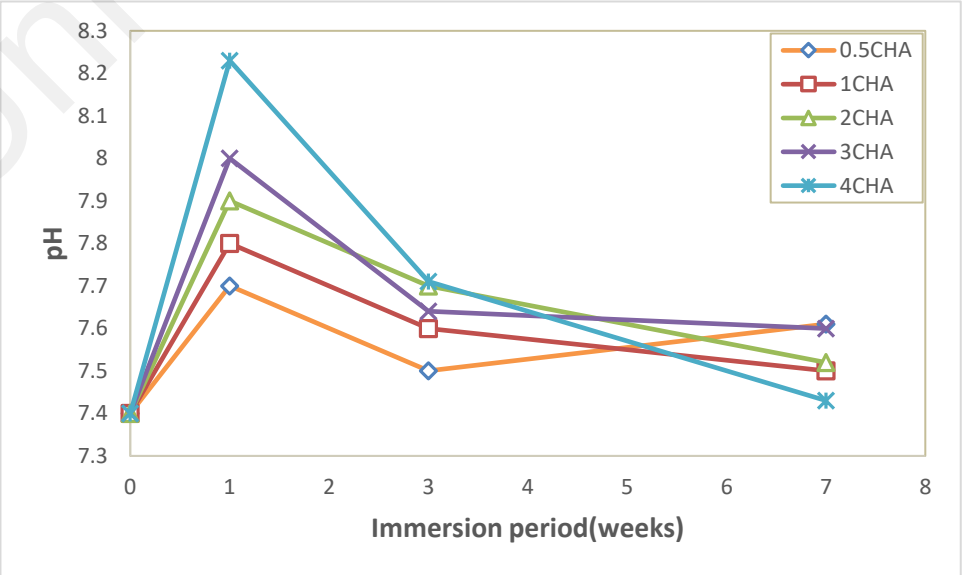

Figure 4.16: The pH value of SBF solution of 0.5-4CHA as a function of immersion period in SBF at 36.5 ± 0.5 °C

Generally, the increase in pH of the solution accommodate the nucleation of apatite (Pan et al., 2010). It was considered that after 1 week, the pH value for SBF of 4CHA displayed higher fluctuation (7.4-8.23) as compared to 0.5CHA (7.4-7.7), 1CHA (7.4-7.8), 2CHA (7.4- 7.9) and 3CHA (7.4-8). In the first week, the highest pH value of 4CHA amongst the other four CHA samples showing the highest dissolution rate, and relatively high weight reduction observed.

After 3 weeks incubation, precipitation of apatite layer increased on the surface of the samples which was accompanied by the decrease in pH value. Sample 4CHA, exhibited the rapid drop in pH value. The drop was contributed with formation of more precipitation layer on the sample. As for samples after 7 weeks incubation, pH was continued to decrease slightly which was signified by the formation of a thicker precipitation layer on the surface of samples which have completely covered the 4CHA sample's surface with an elongated shape. Thus, it can be concluded that sample 4CHA had higher degradation rate and make it suitable to be use in bone application.

It has been suggested that lower crystallinity and crystallite size would affected ion release and consequently solubility (Boanini et al., 2010). Thus, according to Fathi et al. (2008) presence of CO_3^{2-} as foreign ions induced structural disorder and increase insolubility. It has predicted that increasing the carbonate contents induced the transformation of crystalline to amorphous. Therefore, the amorphous apatite grains leads to a faster solubility within the first period of immersion in SBF and subsequently faster rate of apatite nucleation and growth on the sample's surface (Aminian et al., 2011; Bang et al., 2014).

Accordingly, Ca/P ratio is not constant as the surface dissolution increased and continues precipitation apatite layer during soaking in SBF. The EDX analysis after 7 weeks revealed that the formed apatite is reduction in calcium with an average Ca/P molar

ratio 1.83- 1.9 (Guo et al., 2012). According to Figure 4.17 Ca/P molar ratio decreased with dissolution the surface after 1 week and increased with formation of apatite layer after 3-7 weeks incubation in SBF. The Ca/P molar ratio of the samples increased with increasing the apatite layer on their surface.

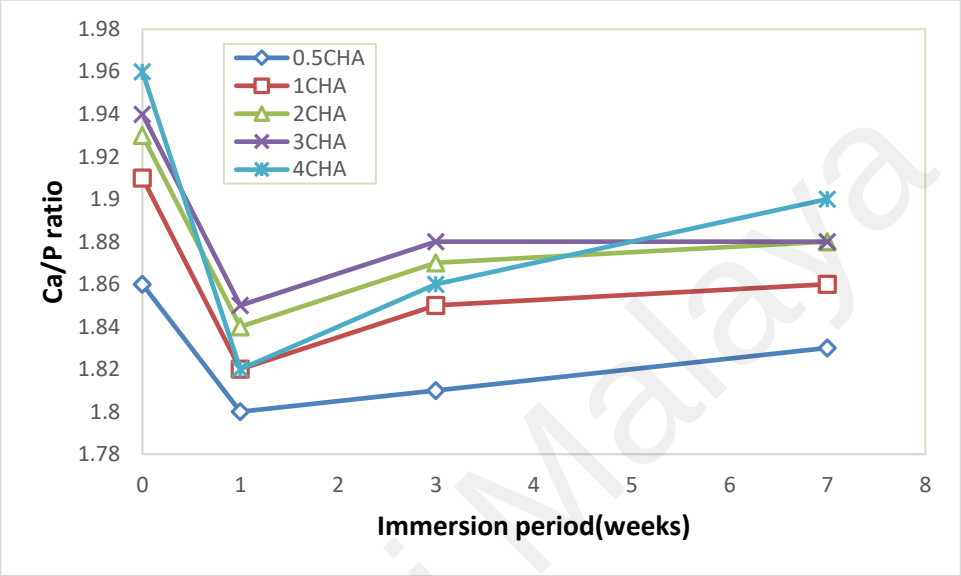

Figure 4.17: The Ca/P ratio changes of 0.5-4CHA as a function of immersion period in SBF at 36.5 ± 0.5 °C

In this part of research, 1CHA sample with molar ratio of CO_3^{2-}/PO_4^{3-}=1 were chosen with the optimum significant parameters which affecting the synthesized CHA properties. It has been found that 1CHA resembled a B-type CHA, having carbonate content of 8.75 and 2.95 for as-synthesize powder and sintered body, respectively. As-synthesized powder was in nanosized has been suggested that the high surface area provides a very high surface energy Relative density of 87.0 ± 1.7 leads the higher hardness value with grain size of 0.98. Therefore, 1CHA were selected to proceed with the next parts of this study.

4.3 Effect of sintering temperatures on the properties of carbonated hydroxyapatite

In the present work, the effect of varying sintering temperature under the CO_2 atmosphere on the morphology, crystallinity and mechanical properties of carbonated hydroxyapatite (CHA) were investigated. Four CHA samples with ratios of CO_3^{2-}/ PO_4^{3-} =1, namely SCHA1, SCHA2, SCHA3 and SCHA4 were sintered at 800 °C, 900 °C, 1000 °C and 1100 °C respectively. Synthesized CHA powder was labeled as ASCHA and used for comparison purpose.

4.3.1 XRD Analysis

The X-ray diffraction patterns of CHA samples sintered from 800 to 1100 °C in CO_2 atmosphere are illustrated in Figure 4.18. The diffraction peaks of all sintered CHA samples closely matched the ICDD#9-432 standard for hydroxyapatite as stated in previous XRD patterns Figure 4.2.

No other phases was formed or detected at temperatures from 800 to 1000 °C. However, due to the partial decomposition of CHA, very little CaO was formed in the CHA pellets sintered at 1100 °C. The presence of an additional weak peak at $2\theta = 37.5°$ is corresponding to the (200) plane of CaO reflections with ICDD No. 37-1497 (Chung et al., 2005; Ingole et al., 2016; Ramacharyulu et al., 2017). Similar XRD diffraction peak of CaO was also observed by Barinov et al. (2006) and Zyman & Tkachenko (2011). Barinov et al. (2006) reported the formation of CaO at sintering temperature of 950 °C. The formation of secondary phase CaO is common at temperature higher than 1100 °C (Landi et al., 2004; Zyman & Tkachenko, 2011). At temperature greater than 1300 °C, the XRD diffraction peak of CaO is shifted to 35° due to the lattice expansion (Barralet et al., 2002).

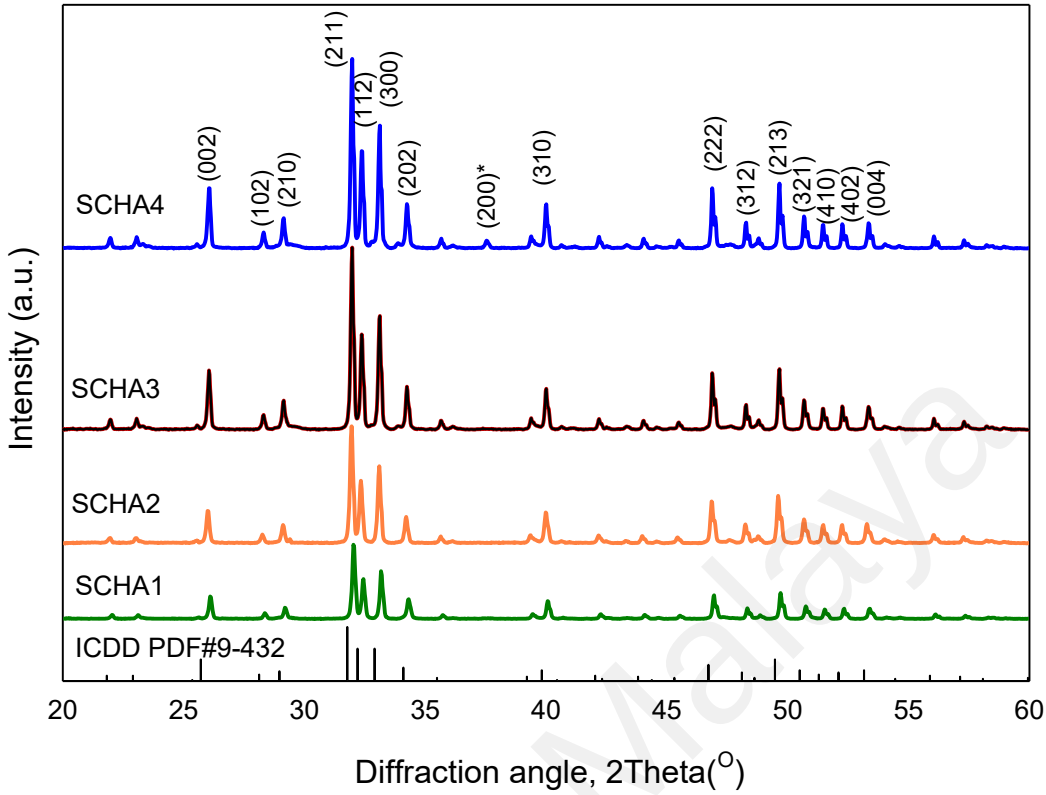

Figure 4.18: XRD diffractograms of B-type CHA pellets sintered at 800- 1100 °C

As the sintering temperature increased higher than 800 °C, the XRD peaks of sintered CHA became sharper and narrower, as a result of the transformation of semi-amorphous hydroxyapatite to crystalline phase. Between 900 to 1100 °C the sintered CHA pellets developed crystallinity. The XRD results are similar to that of Guo et al. (2003) results.

The changes in the crystal lattice parameters is due to the carbonate substitution in HA host structure showed in Table 4.6. The XRD results exhibited that in comparison to the synthesized HA, the *c/a* parameter increased (> 0.7309) resulting from a decrease in the *a-axis* (<9.418 Å) and an increase in the *c-axis* (> 0.6884 Å) for all sintering temperature from 800-1100 °C. These results suggested that all sintered samples were still a B-type CHA regardless of sintering temperatures. A slight decrease in the *c/a* ratio, is attributed to the partial loss of carbonate ion from the CHA lattice and this phenomenon is believed

to reduce the lattice distortion in the apatite structure (Rogers & Daniels., 2002). There was no significant variation for the *a-axis* and *c-axis* of CHA unit cell above 1000 °C (Landi et al., 2004).

As the sintering temperature increases, the crystallite size of CHA pellets increases drastically, i.e. from 7.9 nm for synthesized CHA powder to 81.9 nm for SCHA4 (Fathi et al., 2008). It is noticed that all CHA samples exhibited crystallites in nanosize. The higher temperature needed in order to reach the higher crystalline structure and density. However, sintering of CHA at high temperature would lead to higher decomposition of CHA.

Table 4.6: Structural parameters of CHA pellets sintered at 800- 1100 °C in CO_2 atmosphere

Sample	*a-axis* (Å)	*c-axis* (Å)	*c/a ratio*	Crystallite size (nm)
ASCHA	9.4129	6.9165	0.7348	7.9
SCHA1	9.4130	6.9153	0.7347	74.8
SCHA2	9.4131	6.9145	0.7346	77.2
SCHA3	9.4142	6.9122	0.7342	80.1
SCHA4	9.4143	6.9114	0.7341	81.9

In order to produce dense CHA without harmful CaO, sintering conditions have to be carefully established and controlled (Ślósarczyk et al., 2010). Although, CHA is known to decompose into HA and CaO at temperature above 1000 °C as the equation $Ca_{10}(PO_4)_6(OH)_x(CO_3)_y \rightarrow Ca_{10}(PO_4)_6(OH)_2 + CaO + CO_2$ (Barralet et al., 2002; Ślósarczyk et al., 2010; Sobczak-Kupiec & Wzorek, 2012), some controversial observations (Landi et al., 2004) were reported the formation of CaO and TCP at 1300–1400 °C and some others

(Zyman & Tkachenko, 2011) obtained CHA along with CaO at the sintering temperature above 1100 °C.

4.3.2 FTIR Analysis

The FTIR analysis were performed to determine type of substitution of CO_3^{2-} in hydroxyapatite. The FTIR spectra of all four sintered CHA and synthesized CHA powder are presented in Figure 4.19. The similar observation was found in FTIR analysis of sintered CHA are shown in previous results in Section 4.2.

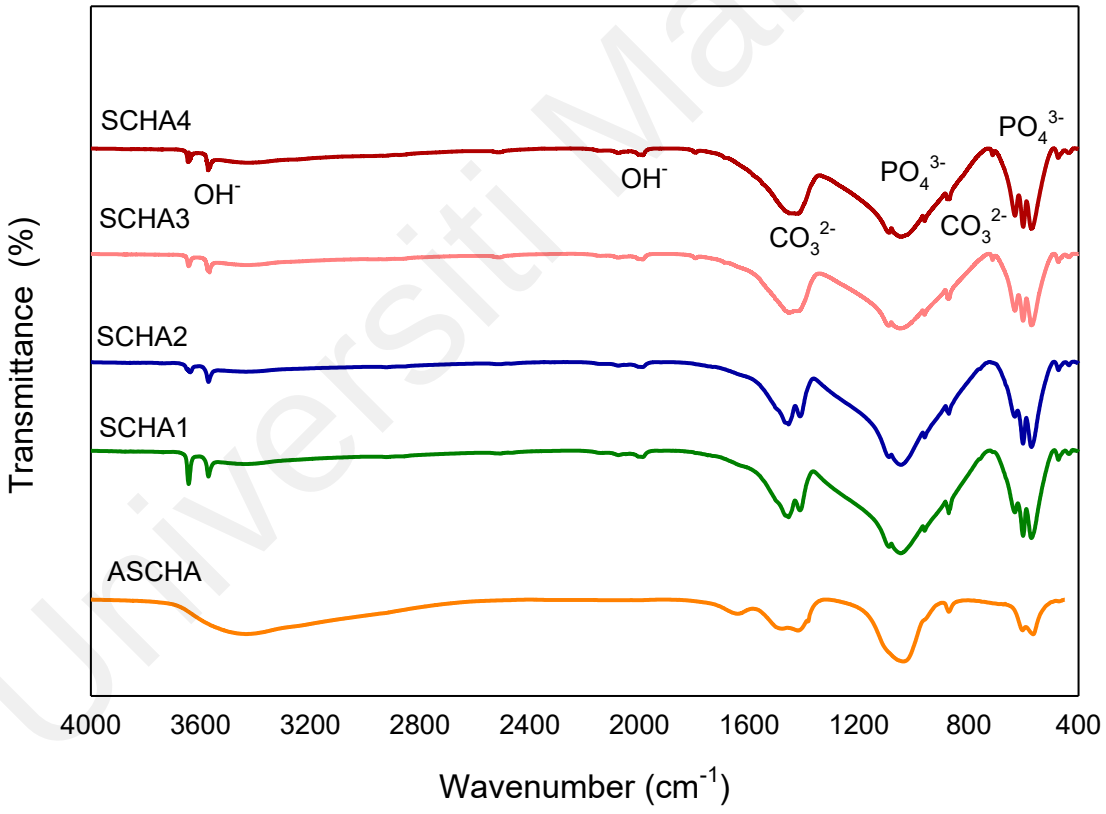

Figure 4.19: FTIR spectra of B-type CHA sintered at 800- 1100 °C in CO_2

The trends of the spectra demonstrated that all sintered samples had remained as B-type CHA. However, as the temperature increases, there is a reduction in the intensity of the carbonate band and at 1000 - 1100 °C, the band at 1410-1430 (ν_3) disappeared for

SCHA3 and SCHA4. This reduction in the band indicates that the carbonate content in CHA decreased with increasing temperature. Nevertheless, although there was reduction in intensity of the carbonate bands, but crystallinity increased by increasing temperature.

The high crystallinity of CHA pellets had been revealed with the sharper PO_4^{3-} (Tadic et al., 2002). It can be easily seen that the crystallinity increased from semi-amorphous to crystalline, particularly on the phosphate bands at 567– 604 cm^{-1} and around 1038 cm^{-1}. Broad bands designate a poor crystallinity, whereas with increasing temperature and subsequently increasing crystallinity, characteristic band were splitting into peaks at 567-572 and 601-604 cm^{-1} (ν_4), 962-963 cm^{-1} (ν_1), and 1040-1090 cm^{-1} (ν_3) respectively. This was also reported by Tadic et al. (2002) and Krajewski et al. (2005).

It is worth noted that neither calcite (at 712 cm^{-1}), aragonite (at 713 and 700 cm^{-1}) nor vaterite (745 cm^{-1}) bands was detected in all SCHA samples. In addition, the characteristic bands of β-TCP (1120, 970, and 940 cm^{-1}) were not presence (Krajewski et al., 2005), indicating, sintered CHA remained single phase. The characteristic vibration bands of A-type and AB-type CHA was not detected in all spectra.

In addition to carbonate and phosphate bands, the bands of absorbed OH^- was also detected typically in range of 3200-3500 cm^{-1} and 1600-1700 cm^{-1} (Kovaleva et al., 2008). The reduction in intensity with increasing temperature, implies that water content was removed from the samples.

4.3.3 Elemental Analysis (CHN & XRF)

The XRF and CHN analyses were carried out on all four samples sintered at various sintering temperature from 800-1100 °C and compared with synthesized CHA at RT. The carbon and carbonate contents and Ca/P molar ratio of CHA samples are tabulated in

Table 4.7. As discussed earlier in Section 4.2.4, sintering may not affect the Ca/P molar ratio, and it remained constant with the molar ration of Ca/P= 1.77 ± 0.01.

The carbonate content of CHA samples was decreased with increasing temperature. The CO_3^{2-} content was decreased from 8.75 wt.% at room temperature to 1.95 wt.% at 1100 °C. This reducing carbonate content observation is in line with the XRD and FTIR results.

Table 4.7: The carbon and carbonate contents and Ca/P ratio of CHA pellets

Samples	wt.% C	wt.% CO_3^{2-}	Ca/P ratio
ASCHA	1.75	8.75	1.78
SCHA1	0.96	4.80	1.76
SCHA2	0.59	2.95	1.77
SCHA3	0.47	2.35	1.78
SCHA4	0.39	1.95	1.76

Considering the amount of carbonate present in human bone (2 - 8 wt.%) (Rey et al., 1991; Krajewski et al., 2005), all four CHA samples to be used as biomaterials in bone substitution.

4.3.4 FESEM Analysis

The fractured surface of sintered CHA pellets at temperatures of 800 to 1100 °C shown the development of the micron sizes grains with increasing sintering temperature (Figure 4.20). All sintered CHA samples displayed a transgranular-type fracture and uniform grain morphology except for the SCHA4 which sintered at 1100 °C. Irregular tiny-sized particles were observed on the surface of grains. The average grain size of the sintered CHA samples, as calculated from FESEM micrograph based on the line-intercept analysis was tabulated in Table 4.8.

The microstructure of the fractured SCHA1 compacts at sintering temperate of 800 °C reveals that the CHA particles fused together and formed grains with some porosity (marked "white arrow") (Figure 4.20 a). The grain size increases with increasing sintering temperature while the number of grains decreases. The grain growth was initiated by filling of necks between contacting grains followed by the movement of the grain boundary (German, 2010). At elevated sintering temperature the grain boundary decreased, and grain growth happened. The CHA compacts started to transform into a dense ceramic at 900 °C (Figure 4.20b).

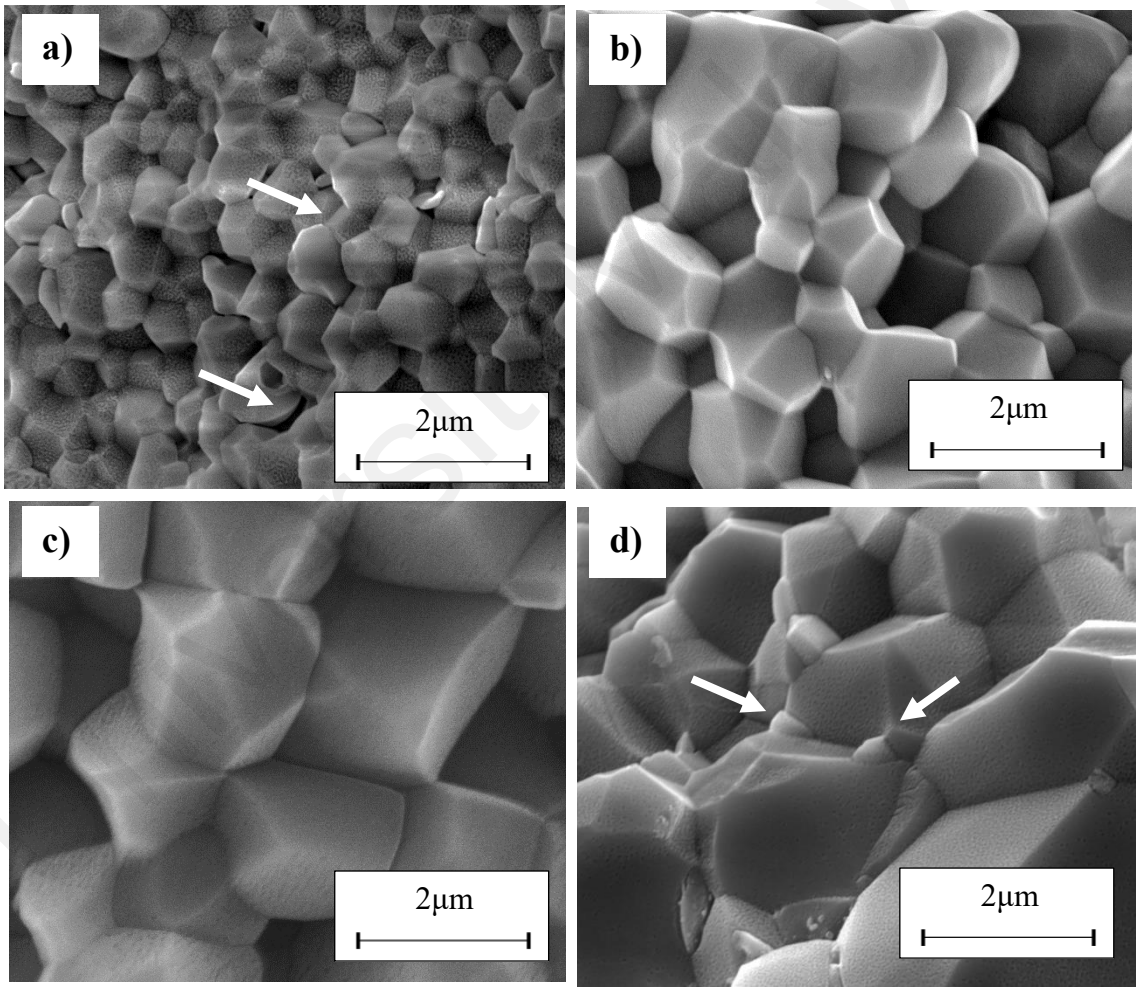

Figure 4.20: FESEM of fractured CHA sintered at a)800 °C, b)900 °C, c)1000 °C and d)1100 °C (Mag: 50KX)

As the sintering temperature was increased to 1000 °C, the porosity of CHA compacts decreased, and grain size increased (Figure 4.20c). Sintering above 1000 °C, resulted in the growth of CaO particles on the surface of grains (marked 'white arrow') (Figure 4.20d). The CaO particles cause loosening of the grain boundaries as a result of a weaker bonding between CHA particles. This result is in consistent with Zyman & Tkachenko (2011) findings.

The grain size of the sintered CHA samples increased from 0.42 ± 0.05 μm (800 °C) to 1.78 ± 0.10 μm (1100 °C) (Table 4.8). As the grain size increases, the porosity of sintered CHA samples decreases and subsequently affect the density and mechanical properties of the CHA samples.

4.3.5 Relative Density, Linear Shrinkage and Grain Size

The relative density (ρ), linear shrinkage (D) and average grain size of the CHA pellets sintered at various temperature in CO_2 atmosphere are depicted in Table 4.8. The relative density was calculated based on the theoretical density of stoichiometric HA (3.156 g/cm^3). It was found that the average density of SCHA1 sample was 83.8%, indicating that the porosity is still present in the sample. Densification continued to occur at higher sintering temperature, resulting in reducing porosity. Additionally, the grain growth upon further sintering as similarly reported by Ring (1996).

The relative density was found to increase to 94.2% at sintering temperature of 1000 °C for SCHA3. Sintering above 1000 °C did not further contribute to the density (Kamalanathan et al., 2014). At 1100 °C the relative density of CHA was drastically decreased (84.7%). This is attributed to the presence of CaO in SCHA4 sample. Similar trend in the reduction of relative density of CHA samples was also reported by Zyman & Tkachenko, (2011).

Table 4.8: Relative density, linear shrinkage and average grain size of sintered CHA pellets

Sample	Temperature °C	Linear shrinkage *D* %	Relative density ρ (g/cm^3) %	Average grain size (μm)
SCHA1	800	12.7 ± 0.3	83.8 ± 1.5	0.42 ± 0.05
SCHA2	900	14.0 ± 0.2	86.2 ± 1.6	0.98 ± 0.10
SCHA3	1000	15.3 ± 0.2	94.2 ± 1.7	1.23± 0.10
SCHA4	1100	13.4 ± 0.3	84.7 ± 1.5	1.78 ± 0.10

Linear shrinkage is widely used as a parameter to control the dimensional variation that may occur during the sintering process. It was found that the linear shrinkage increased from 12.7% of SCHA1 to15.3% of SCHA3 and subsequently decreased to 13.4% for sample SCHA4. The decrease in volume of pellets after sintering indicates the consolidation of the powder phase. The decrease in shrinkage is likely caused by the formation of CaO in the SCHA4 sample.

4.3.6 Microhardness Analysis

The effect of various sintering temperature in CO_2 atmosphere on the Vickers hardness (H_V) and indentation fracture toughness (K_{IC}) of the CHA samples are shown on the Figure 4.21. It was found that the fracture toughness exhibited a similar trend to the Vickers hardness and relative density. As the sintering temperature increased, the average H_V and K_{IC} gradually increased up to 1000 °C. The H_V value increased from 1.79 GPa at 800 °C and reached to a maximum value of 2.08 GPa at 1000 °C (Figure 4.21). Beyond 1000 °C, the Vickers hardness decreased drastically and reached 1.89 GPa at 1100 °C.

The increase in hardness is attributed to the increase of relative density and grain size. It was reported that below a critical grain size the hardness of CHA is determined by density (Muralithran & Ramesh, 2000). On the other hand, the formation of the CaO particles resulting in weakening of the grain boundaries in the CHA sample. This

observation agrees with the weak characteristic CaO peaks observed in the XRD patterns of the samples (Zyman & Tkachenko, 2011). Therefore, it can be inferred that the decrease in hardness and density is attributed to the formation of secondary phase and larger grain size.

For application of CHA as bone graft, higher toughness is desirable. Similarly, the indentation fracture toughness of the CHA samples increased from 0.63 $MPam^{1/2}$ at 800 °C to a maximum value of 1.27 $MPam^{1/2}$ at 1000 °C. Further heating to 1100 °C caused a decrease to 0.68 $MPam^{1/2}$. The low K_{IC} value at low sintering temperature is ascribed to the weak grain boundaries of CHA pellets.

The fracture toughness (K_{IC}) of the sintered CHA samples is improved by the relative density and linear shrinkage. With the increase in density for sample sintered at 1000 °C, the value of K_{IC} increased and gradually decreased with decreasing density and forming CaO as a secondary phase.

Muralithran & Ramesh, (2000) claimed that the decomposition of HA detrimental to density and mechanical properties. Slosarczyk & Białoskórski (1998) reported that with increasing CaO content higher than ≥2 wt.% the value of hardness decreased while K_{IC} increased. It's because of the increasing the porosity of the sintered samples, which limited the crack propagation, and thus increased indentation fracture toughness. However, for CaO ≥1 wt.%, both K_{IC} and H_V decreased.

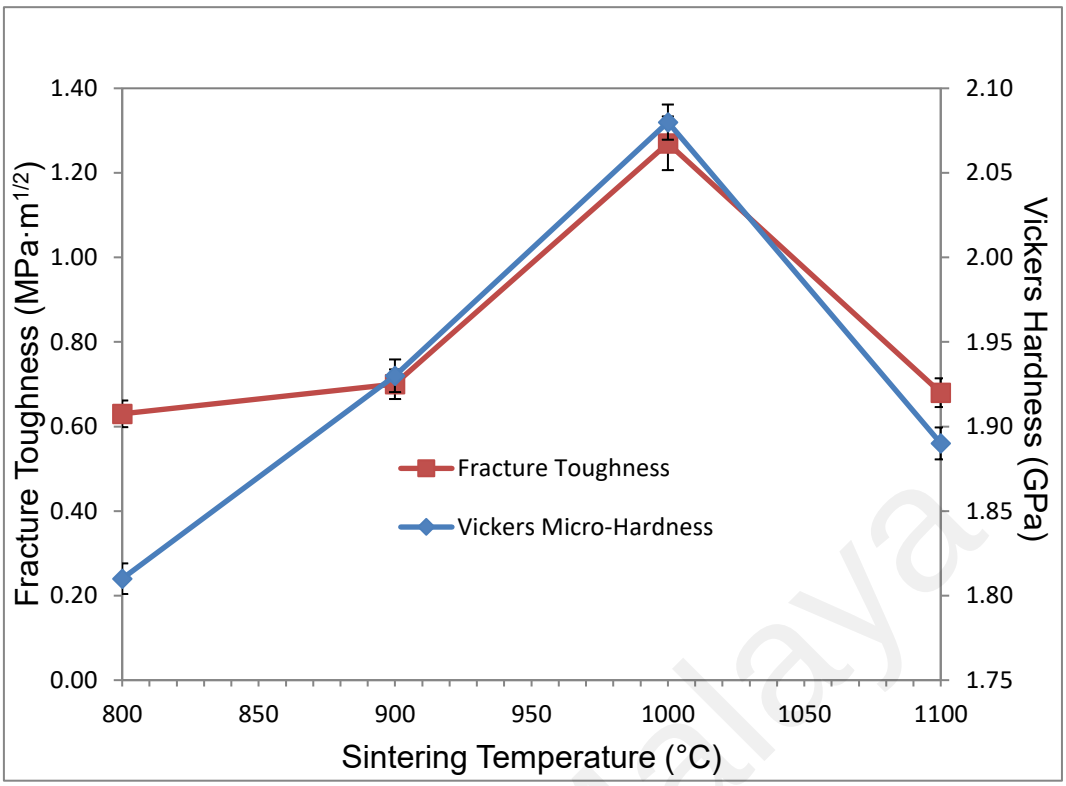

Figure 4.21: Mechanical properties as a function of temperature for B-type CHA pellets

It can be stated that fracture toughness would affected by grain size, where K_{IC} decreases with an increase in grain size. Kamalanathan et al. (2014) reported that smaller grain size decreases inherent flaw sizes resulting in enhancement of the sintered sample's mechanical properties. This concept is related to the theory of Wang and Shaw (2009) and the belief that from 1000 °C to 1100 °C, the formation of intergranular and transgranular fracture, will dictate the fracture toughness. If a crack propagates along the grain-boundary-affected (GBA) zone, intergranular fracture would occur and crack deflection leading to shorter crack lengths and subsequently an increase in K_{IC}. However, if a crack were to grows through the grains rather than at the GBA, transgranular fracture would take place, contributing to a decrease in K_{IC}. Therefore, smaller grain size resulting in intergranular fracture along with crack deflection causes shorter crack lengths and

increasing the toughness. Nevertheless, the probability for a crack to occur at the GBA zone K_{IC} increases as the grain size decreases.

In this part of study, sintering temperature of 900 °C was selected to sinter the CHA pellets. However, the optimum temperature for hardness was 1000 ℃, the carbonate content decreased at elevated temperature.

4.4 Effect of multi-ions doping on the properties of carbonated hydroxyapatite bioceramic

The current research was conducted with the aim of evaluating the effects of incorporating carbonate into the hydroxyapatite structure and co-doping with ions such as Mg^{2+}, SiO_4^{4-}, Zn^{2+} and Cu^{2+} approximated by the general formula of $Ca_{10-a-b-c}Mg_aZn_bCu_c(PO_4)_{6-x-y}(CO_3)_x(SiO4)_y(OH)_{2-y}$ present in the biological apatite. In the present work, four different combination of multi-ions doped CHA powders were prepared and designated as follows: SA1 served (CHA+Mg+Si), SA2 (CHA+Mg+Si+Cu), SA3 (CHA+Mg+Si+Zn) and SA4 (CHA+Mg+Si+Cu+Zn). The as-synthesized dried powders were compacted into disc samples and sintered at 900 °C, in air atmosphere, using a heating and cooling rate of 10 °C/min and holding time of 2h. On cooling from sintering to 200 °C, the samples were taken out from the furnace and placed in a desiccator containing wet carbon dioxide gas, flowing at a constant rate of 0.5 L/min. This is to compensate any loss of carbonate during the sintering process (Wong & Ahmad Fauzi, 2016).

4.4.1 XRD Analysis

XRD results of the as-synthesized multi-ion doped B-type CHA powders with CO_3^{2-}/PO_4^{3-} =1 and substitution of Mg, Si, Zn and Cu ions are shown in Figure 4.22. The International Centre for Diffraction Data (ICDD) PDF number #9–432 for crystallographic planes of HA was used as the reference in XRD analysis to compare

changes in CHA pattern and crystallography. In addition, the reference CHA patterns available do not show if B-, A-, or AB- type CHA is present. The substitution of carbonate into HA structure is less than 10% and also a trace amount of elements may not affect the structural pattern of HA.

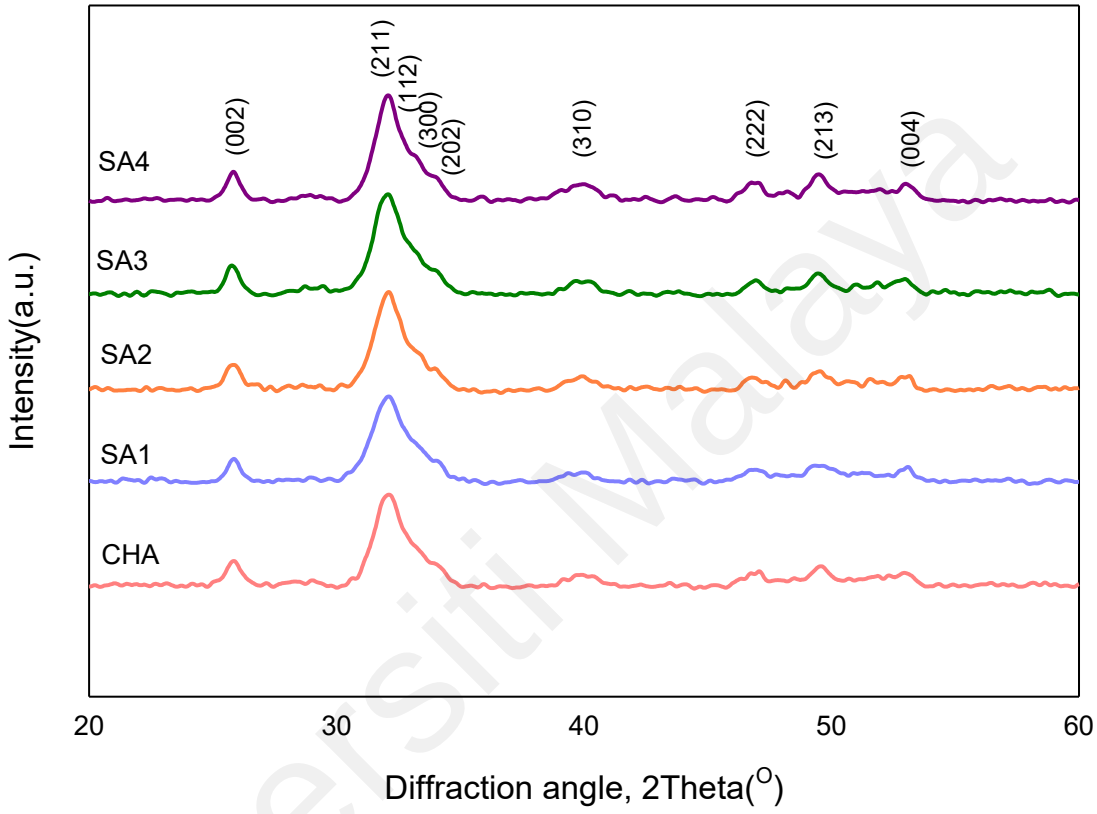

Figure 4.22: XRD diffractograms of as-synthesized multi-ions doped B-typCHA powders

The broad XRD peaks and the absences of secondary phases indicate that the multi-ion doped CHA powders were nanocrystalline as confirmed by Kovaleva et al. (2008) results. The XRD pattern of synthesized multi-ion doped CHA powders shows only single phase carbonated hydroxyapatite (CHA) since no presence of $CaCO_3$ (as aragonite or calcite forms) was found, confirming the complete reaction and washing treatment was sufficient to eliminate any residual compound as indicated by Krajewski et al. (2005).

Nine main peaks with low intensity were detected, i.e. at 2θ=26° indexed (002), four overlapped and broaden peaks of (211), (112), (300) and (202) located at 2θ = 32-34°, one around 40° indexed (310), and peaks at 2θ= 47°, 50° and 53°, respectively indexed (222), (213) and (004).

Apart from that, substitution of Mg^{2+}, SiO_4^{4-}, Zn^{2+} and Cu^{2+} in HA exhibits an evident inhibitory role on the crystal growth due to the presence of lattice defects in the apatite structure (Afshar et al., 2003;Khan et al., 2014), thus reducing the crystallinity of CHA powder and giving smaller crystallite size, leads to the enhance solubility (Landi et al., 2004). The carbonate substitution in HA are known to change the crystal lattice parameter. The results obtained showed in Table 4.9, suggesting the decrease in *a-axis* and increase in *c-axis* for sintered CHA. It has been reported that contraction of *a*- and expansion of *c-axis* indicates the formation of B-type CHA (Landi et al., 2003).

Table 4.9: The lattice properties of multi-ions doped B-type CHA powders

Samples	*a*=*b* (Å) axis	*c* (Å) axis	*c/a* ratio	$FWHM_{(002)}$ (°)	Crystallite size (nm)
HA	9.418	6.884	0.7309	-	-
CHA	9.4129	6.9165	0.7348	1.319	7.9
SA1	9.4120	6.9169	0.7349	1.358	6.0
SA2	9.4117	6.9174	0.7350	1.457	5.6
SA3	9.4113	6.9186	0.7351	1.624	5.0
SA4	9.4111	6.9199	0.7353	1.945	4.2

The XRD analysis of the sintered samples are depicted in Figure 4.23. In the current work, regardless of doping, the XRD patterns for all samples corresponded with ICDD 9-432. However, the peaks of the CHA samples shifted slightly to higher 2θ angles, attributable to the CO_3^{2-} incorporation (Yanny-Marliana & Ahmad-Fauzi, 2011). The minor dopants consisting of Mg, Si, Zn and Cu had not affected the structural integrity of CHA. In addition, the sharp and narrow peaks indicated the relatively high crystalline

structure of the sintered samples. Moreover, $CaCO_3$ (as aragonite or calcite) was not detected in the samples which indicates a complete reaction was achieved in this experiment. The results corresponded well with the findings by Krajewski et al. (2005).

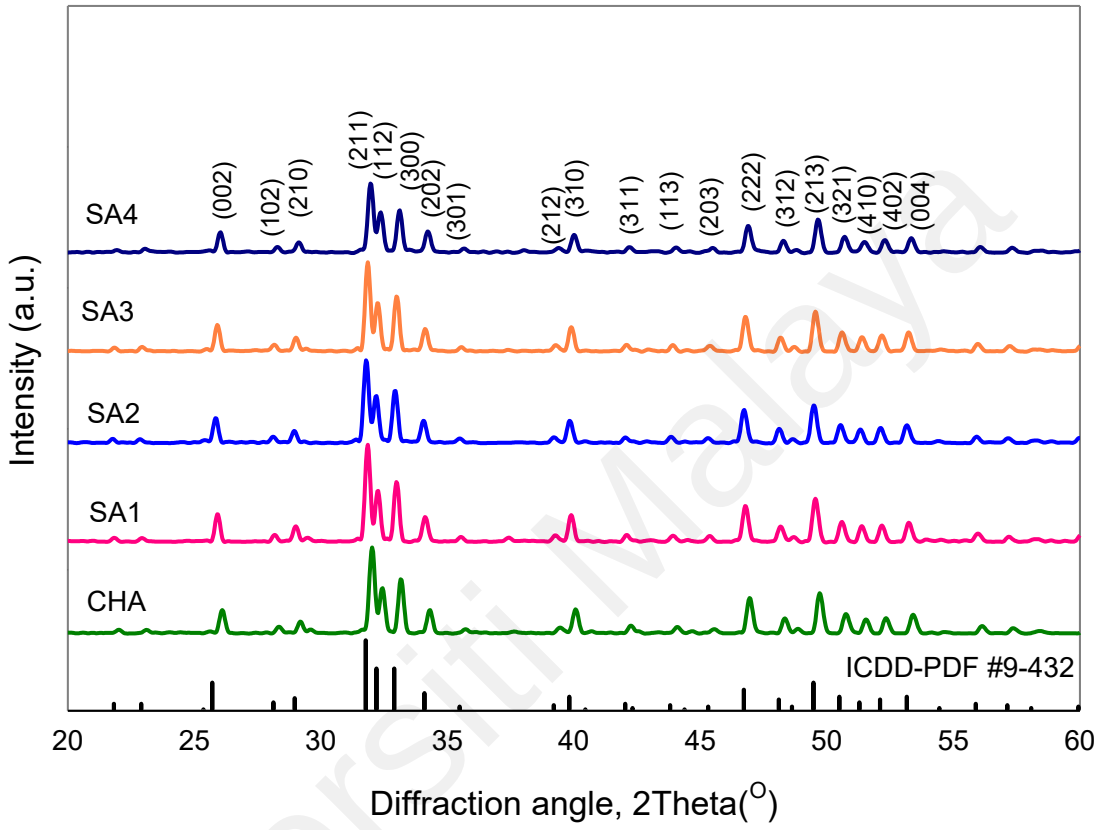

Figure 4.23: XRD diffractograms of sintered multi-ions doped B-type CHA pellets at 900 °C in CO_2

It is known that the substitution of CO_3^{2-} in the apatite structure would modify the lattice parameters (Murugan & Ramakrishna, 2006). Lattice parameters of multi-ions doped CHA powders were determined by Rietveld structure refinement of X-ray diffraction data. As shown in Table 4.10, it was found that the *c/a* ratio increased from 0.731 (HA, ICDD # 9-432) to 0.733 for CHA. Further increase of the *c/a* ratio was observed for multi-ions doped CHA samples, i.e. 0.734 for SA1, SA2, and SA3, and 0.741 for SA4. The rise in *c/a* ratio observed in this study could be attributed to the replacement

of tetrahedral PO_4^{3-} (2.38 Å) by trigonal planar CO_3^{2-} (1.76 Å) (Lee et al., 2007) as well as tetrahedral SiO_4^{4-} (0.42 Å) (Aminian et al., 2011).

In addition, it has been implied that the negative charge of SiO_4^{4-} ion that replaces PO_4^{3-} ion would create a OH^- ion vacancy (Khan et al., 2014). On the other hand, it has been reported in the literatures that the substitution of Ca^{2+} (0.99 Å) with smaller cations of Mg^{2+} (0.69 Å), Zn^{2+} (0.74 Å) and Cu^{2+} (0.73 Å) in the HA lattice could also cause a slight decreased in the *'a'* and *'c'* (shrinkage in unit cell parameters) (Stanić et al., 2010; Lala et al., 2016).

Nevertheless, in the current work, the concentrations of Mg^{2+}, Zn^{2+} and Cu^{2+} were too small to induce significant changes to the CHA cell parameters. The present result of increasing *c/a* ratio for the CHA-doping revealed the presence of B-type CHA (Elena Landi et al., 2004) which is favorable since it is compatible to biological bone (Youness et al., 2017).

Table 4.10: Lattice parameters and crystallite size of multi-ions doped B-type CHA sintered at 900 °C in CO_2

Samples	*a-axis* (Å)	*c-axis* (Å)	*c/a* ratio	$FWHM_{(002)}$ (º)	Crystallite size (nm)
HA (ICDD#9-432)	9.418	6.884	0.7309	-	-
CHA	9.4079	6.8964	0.7330	0.123	59.5
SA1	9.4014	6.8973	0.7336	0.129	57.2
SA2	9.4004	6.8972	0.7337	0.134	55.3
SA3	9.4003	6.8980	0.7338	0.165	51.6
SA4	9.3092	6.8982	0.7410	0.168	50.7

Generally, there were many peaks of HA detected in the XRD pattern as indicated in Figure 4.23. The (002) plane at 2θ =26°, which is the strongest peak without any overlapping in the HA pattern (Kee et al., 2013), was chosen to determine the crystallite size. As shown in Table 4.10, the FWHM (full width at half maximum) parameter

increased for the multi- ions doped CHA samples resulting in a decreased in the calculated crystallite sizes.

4.4.2 FTIR Analysis

The FTIR examination of as-synthesized multi-ion doped CHA powders strongly supported the XRD analysis. As illustrated in Figure 4.24, B-type CHA exhibits characteristic bands of CO_3^{2-} groups at 870–875 cm^{-1} (ν_2 - bending mode), 1410–1430 cm^{-1} (ν_3 - stretching mode) and 1450–1470 cm^{-1} (ν_3 - stretching mode), and this was also reported by other researchers (Rey et al., 1989; Landi et al., 2004; Lafon et al., 2008).

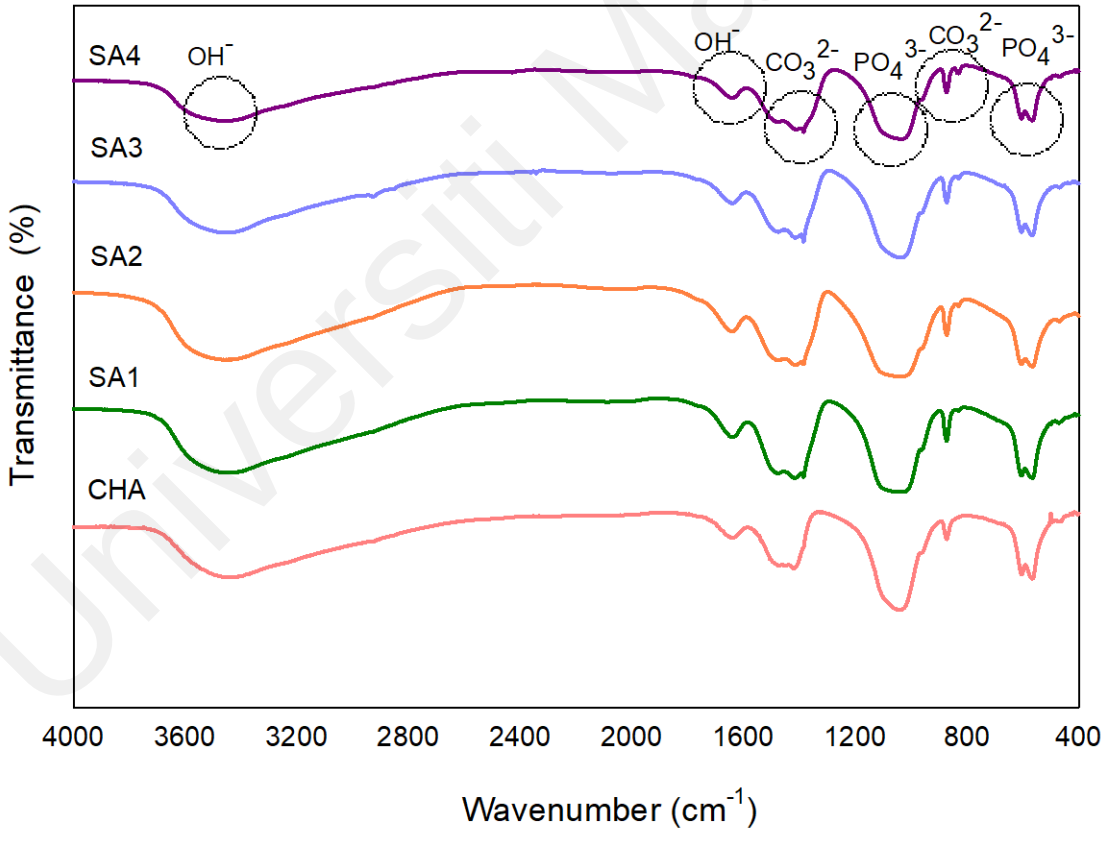

Figure 4.24: FTIR spectra of as-synthesized multi-ions doped B-type CHA powder

The PO_4^{3-}group bands clearly demonstrated at 550–570 cm^{-1}, 600–609 cm^{-1} (ν_4), 960–966 cm^{-1} (ν_1) and 1020–1120 cm^{-1} (ν_3) as detected also by (Krajewski et al., 2005). The broad bands around 1600–1700 cm^{-1} and 3200–3600 cm^{-1} attributed to the adsorbed water (Suchanek et al., 2002).

Moreover, the typical characteristic vibration of A-type CHA which normally appeared at the wavelength of 877–880 cm^{-1}, 1500 cm^{-1} and 1540–1550 cm^{-1}, and the AB-type CHA (at 1515 cm^{-1}) were not observed for all samples. The absence of calcite which typically observed at 712 cm^{-1} is in agreement with the XRD results (Krajewski et al., 2005) and in addition the residual nitrate at the wavelengths of 1380 was not observed (Kovaleva et al., 2009). Marker bands of aragonite around 713 cm^{-1} and 700 cm^{-1} and vaterite at 745 cm^{-1} were not detected in all FTIR spectra (Krajewski et al., 2005).

The FTIR analysis of the sintered samples were in good agreement with that of the XRD analysis. As shown in Figure 4.25, the FTIR spectra was not disrupted with the inclusion of multi dopants. The spectra demonstrated that all samples remained as B-type CHA. These were clearly shown by the typical bands of carbonate group detected at 870–875 cm^{-1} (ν_2 - bending mode) as well as 1410–1430 cm^{-1} (ν_3 - stretching mode) and 1450–1470 cm^{-1} (ν_3 - stretching mode).

These vibrational frequencies signify the substitution of carbonate ions at the phosphate site in the HA structure, thus confirming the B-type CHA (Ślósarczyk et al., 2005). The characteristic vibration of A-type CHA, normally seen at the wavelengths of 877–880 cm^{-1}, 1500 cm^{-1} and 1540–1550 cm^{-1}, and the AB-type CHA (at 1515 cm^{-1}) were not observed for all samples. As for the phosphate groups, the characteristic bands were observed at about 550–570 cm^{-1}, 600–609 cm^{-1} (ν_4), 960–966 cm^{-1} (ν_1) and 1020–1120 cm^{-1} (ν_3) (Krajewski et al., 2005; Kovaleva et al., 2008).

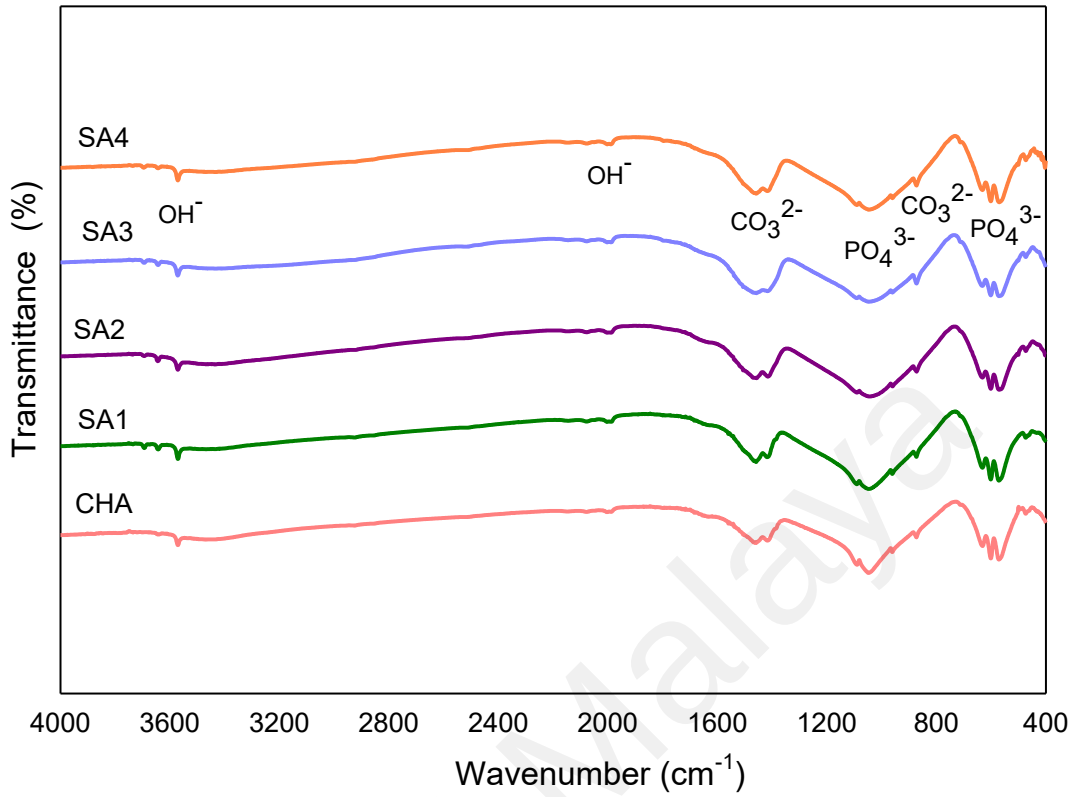

Figure 4.25: FTIR spectra of multi-ions doped B-type CHA sintered at 900 °C in CO_2

The low intensities corresponding to adsorbed water, which were noticed at the wavelengths of 1600–1700 cm^{-1} and 3200–3600 cm^{-1} (Kovaleva et al., 2008) implied the removal of hydroxyls because of the heat treatment. In addition, the stretching vibration of OH^- band which serves as an indicator to show the presence of stoichiometric HA, typically observed at 630 cm^{-1} and 3540 cm^{-1} were absent (Suchanek et al., 2002).

4.4.3 Elemental Analysis (CHN & XRF) and Specific Surface Area

The influence of heat treatment on the carbonate content and Ca/P ratio of the samples are presented in Table 4.11. The amount of carbonate content present in the sintered samples of CHA, SA1, SA2, SA3 and SA4 were 4.70, 4.40, 4.25, 4.30 and 4.15 wt.%,

respectively shows around 45% reduction in carbonate after sintering which were all within the limit of 2–8 wt.% normally found in human bones (Graziani et al., 2017).

The XRF analysis indicated that the Ca/P ratio for all samples were higher (Table 4.11) than the stoichiometric HA of 1.67. This is expected because the substitution of carbonate ions caused a reduction in the phosphate content in the HA matrix, thus resulting in an increased in the Ca/P ratio. The results obtained were in good agreement with other researchers (LeGeros & LeGeros, 2003; Landi et al., 2006; Drouet et al., 2009) who reported that the Ca/P ratio of CHA could range from 1.7 to 2.6.

The specific surface area as obtained by the BET method (S_{BET}) is given in Table 4.11. The result shows that doping of CHA resulted in a higher S_{BET} which coincide with the smaller crystallite sizes of these samples.

Table 4.11: Carbonate content, Ca/P ratio and specific surface area of multi-ion doped CHA samples

Samples	wt.% C	wt.% CO_3^{2-}	Ca/P ratio	S_{BET} (m^2/g)
CHA	0.94	4.70	1.77	67.9
SA1	0.88	4.40	1.74	90.0
SA2	0.85	4.25	1.71	100.6
SA3	0.86	4.30	1.72	107.5
SA4	0.83	4.15	1.70	113.7

4.4.4 FESEM Analysis

Microstructure characteristics of the synthesized multi-ion doped CHA powders characterized by using FESEM with a magnification of 10Kx, is presented in Figure 4.26. All the as-synthesized powders exhibited similar fibrous-like structures with nanometer in size, being less than 100 nm. This means that the powders were agglomerated due to

the high surface energy of nanosized particles. Hence, this makes it difficult to estimate the particle size of multi-ion doped CHA powders.

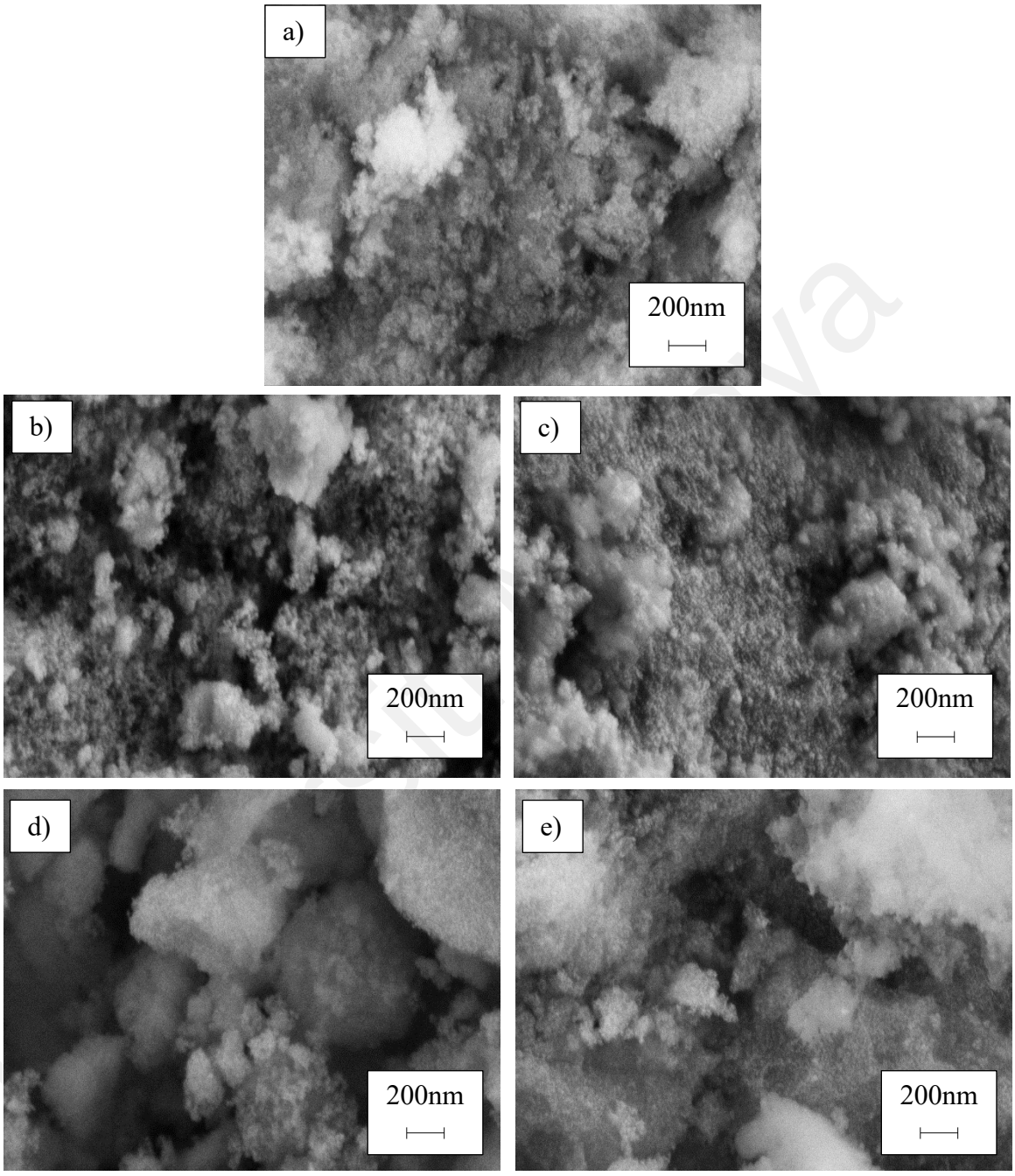

Figure 4.26: FESEM micrographs of as-synthesized powder (a) CHA and multi-ions doped CHA: (b) SA1, (c) SA2, (d) SA3 and (e) SA4 (Mag:20KX)

The microstructure morphology of the sintered samples is presented in Figure 4.27. All the samples exhibited an equiaxed grain structure. The average size of the grains as

calculated from the FESEM micrograph based on the line-intercept analysis (Mendelson, 1969) was found to decreased from 0.53 μm for undoped CHA to 0.49 μm, 0.44 μm, 0.36–0.33 μm for SA1, SA2, SA3 and SA4 samples, respectively. This observation suggested that the multi-ions dopants could have played a role in retarding the grain growth in CHA.

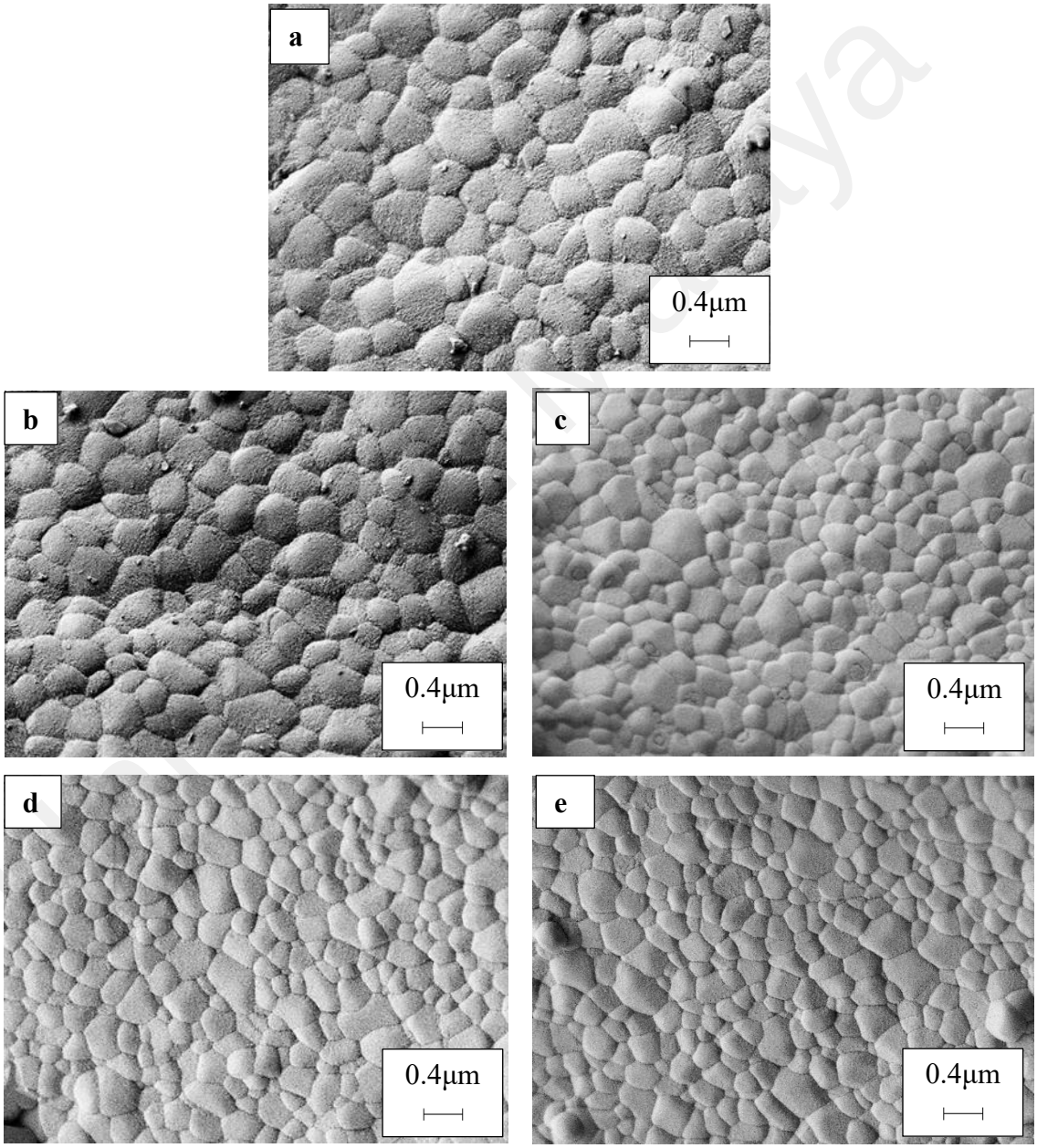

Figure 4.27: FESEM micrographs of sintered (a) CHA and multi-ions doped CHA: (b) SA1, (c) SA2, (d) SA3 and (e) SA4 at 900 °C in CO_2 (Mag:20KX)

4.4.5 Thermal Analysis

The thermal analysis of derived-CHA samples was examined by thermo-gravimetric analysis (TGA) in air, from room temperature RT (25 °C) to 1000 °C, as shown in Figure 4.28. All samples displayed a similar pattern regardless of doping elements. In the initial stage between RT to 600 °C, a significant decrease in the sample weight was observed. This was due to the loss of absorbed H_2O (Zyman & Tkachenko, 2011). The results corresponded well with the low intensity of hydroxyl band discussed earlier in the FTIR results.

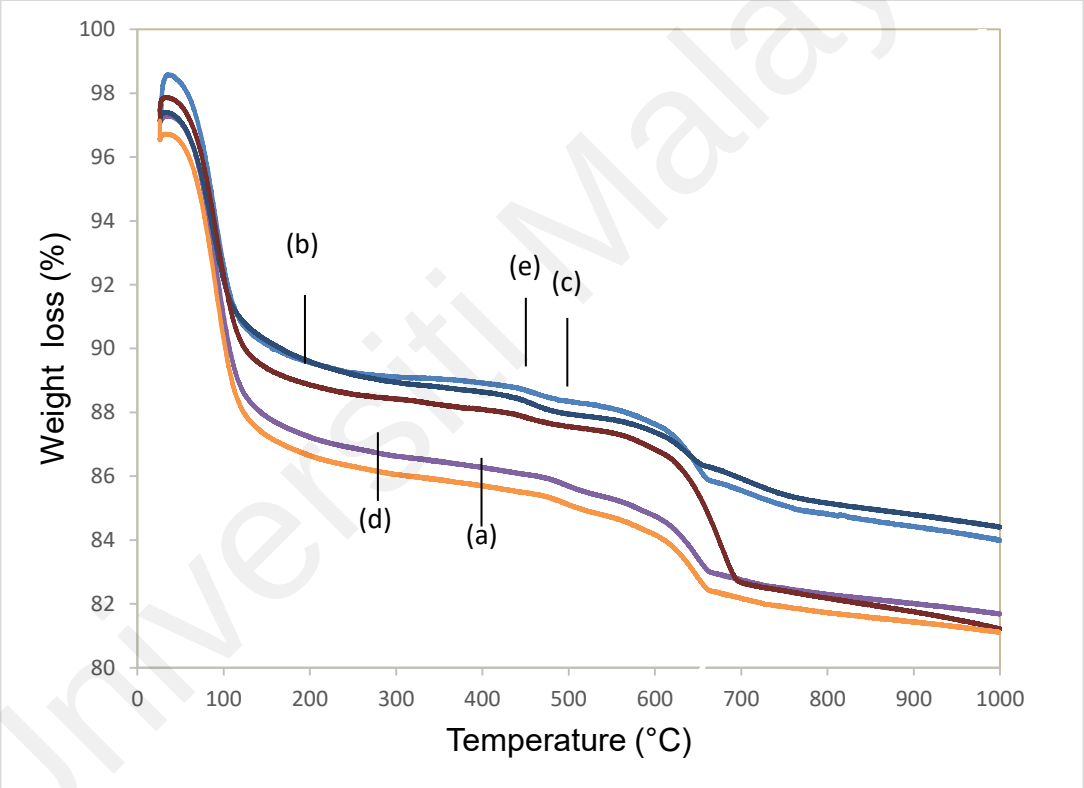

Figure 4.28: Weight loss as a function of temperature for synthesized (a) CHA and multi-ions doped CHA: (b) SA1, (c) SA2, (d) SA3 and (e) SA4

The calculated total weight loss from RT to 600 °C was about 13.3 wt.% which could be attributed to the decomposition of H_2O and dehydration of magnesium nitrate hexahydrate in the samples. The dehydration of $Mg(NO_3)_2 \cdot 6H_2O$ started from 350 °C to 600 °C based on the following equation; $2Mg(NO_3)_2 \xrightarrow{t°C} 2MgO + 4NO_2\uparrow + O_2\uparrow$,

which was accompanied by a weight loss of 0.4 wt.%. In addition to that, the carbonate loss started about ~500 °C and completed at 800–1000 °C, depending on the sample constituents. In the present work, a weight loss of 4.6 wt.% was due to the decomposition of CO_3^{2-}. There was no weight loss detected from 900° to 1000 °C suggesting the completion of CO_3^{2-} breakdown.

CHAPTER 5: CONCLUSIONS AND FURTHER WORKS

5.1 Conclusions

The research explored the effect of multi-ions (Mg^{2+}, SiO_4^{4-}, Zn^{2+} and Cu^{2+}) doping on the properties of CHA via direct pouring wet chemical precipitation method at room temperature and sintered at 900 °C in CO_2 atmosphere. The method of preparation is easily reproducible at room temperature without surfactant and nanoparticle with a narrow size distribution can be achieved. Phase analysis for both as-synthesized powders and sintered pellets revealed that all the samples exhibited a B-type CHA phase regardless of the presences of dopants and this was confirmed through the FTIR analysis. However, the multi-ions dopants were found to increase the *c/a* ratio of the CHA lattice parameter which leads to a concomitant decreased in the Ca/P molar ratio of the sintered samples while Ca/P ratio was higher than the stoichiometric HA of 1.67. The amount of carbonate content in samples was shown around 45% reduction after sintering which were all within the limit of 2–8 wt.% normally found in human bones. The specific surface area (S_{BET}) result revealed a higher S_{BET} with doping of CHA which coincide with the smaller crystallite sizes of these samples. The structural integrity of the CHA lattice was not disrupted by the multi-ions doping, nevertheless the dopants were found to be beneficial in suppressing the grain growth in the carbonated HA. Based on the results obtained, the multi-ions doped CHA demonstrated great potential for use as a graft material in biomedical applications. In order to achieve this goal, the following procedure were carried out;

The B-type CHA was synthesized by variation the CO_3^{2-}/ PO_4^{3-} molar ratios from 0.5 to 5 by using a direct pouring wet chemical method and sintered at 900 °C in CO_2 atmosphere. It was found that with increasing CO_3^{2-}/ PO_4^{3-} ratio from 0.5 to 5, calcium carbonate ($CaCO_3$) formed as a secondary phase at higher ratio of CO_3^{2-}/ PO_4^{3-} ~5. Phase analysis revealed that the phase stability and B-type apatite structure were not disrupted

after sintering. Nevertheless, increasing the CO_3^{2-}/PO_4^{3-} ratio was found to increase the *c/a* ratio of the CHA and resulted in a concomitant decrease in the grain size of the sintered samples. In addition, the relative density, Vickers hardness and fracture toughness of the sintered CHA were found to decrease with increasing CO_3^{2-}/PO_4^{3-} ratio from 0.5 to 4. In comparison to the stoichiometric HA, the carbonate substitution has generally improved the densification and mechanical properties of the sintered body, thus revealing great potential for use as a synthetic bone graft biomaterial.

The effect of sintering temperature (from 800 to 1100 °C) in dry CO_2 atmosphere on CHA (**CO_3^{2-}/ PO_4^{3-}** =1) pellets were studied. It was revealed that regardless of sintering temperature up to 1000 °C, all samples retained single phase B-type CHA. It is confirmed by increase in *c/a* ratio, however decreased by increasing temperature due to the decrease in lattice disorder. Sintering above 1000 °C was found to be detrimental due to the formation CaO in the apatite structure. Increasing sintering temperature led to a gradual decrease in the carbonate content of the CHA pellets while mechanical properties and density improved gradually up to 1000 °C. Sintering above 1000 °C resulted in decrease in density and mechanical properties due to the formation of CaO particles and weakening the grain boundaries.

In order to optimize the sintered CHA pellets, it was found that the CHA with higher ratio of CO_3^{2-}/ PO_4^{3-} =4 had more solubility but lower mechanical properties. In addition, sintering at higher temperature (below 1100 °C) resulted in higher densification and mechanical properties while retaining lower carbonate. Moreover, sintering at CO_2 atmosphere partially compensated for the carbonate loss. Therefore, the optimum solubility and mechanical properties was shown when CHA with CO_3^{2-}/ PO_4^{3-} =1 was sintered at 900 °C in CO_2 atmosphere.

In the study of bioactivity, the SBF test was conducted on the 0.5-4 CHA pellets. It was found that higher solubility of CHA ceramics could be related to the effects of carbonate ion substitution. The accelerated rates of formation of a bone-like apatite layer could be associated with an increase in the carbonate content. In addition, the formation of the apatite layer was also related to the grain size and was found to increase with decreasing grain size. The presence of carbonate group had a synergic effect in improving the solubility of the apatite CHA pellets compared to stoichiometric HA. The study also revealed that the formation of apatite on 4CHA sample was faster if compared to 0.5CHA.

In conclusion, however mechanical properties of CHA are better than HA, still lower than natural bone (Wang et al., 2019). Thus, its application is restricted to non-load bearing parts of the skeleton due to their inferior mechanical properties. CHA can also be used as scaffold for reconstruction of bone as well as filler in bone or teeth and coating of implants (Jarcho, 1981; Shin et al., 1992; Teraoka et al., 1998; Riman et al., 2002).

5.2 Further work

Based on the obtained results through this research, a number of recommendations for the further investigation were proposed to be done as below:

i. The study could explore the effect of using different heating rates and soaking times on the properties of dense multi-ions doped CHA.
ii. The bioactivity of multi-ions doped CHA versus undoped CHA when implanted in animal could be explored.
iii. To explore the effect of other consolidation methods such as microwave sintering and hot pressing on the mechanical properties and microstructural development of CHA.
iv. The effect of other additives such as fluorine on the mechanical properties of CHA could be investigated.

v. To explore the fabrication of multi-ions doped CHA/polymer biocomposite to improve the mechanical properties.

REFERENCES

Admassu, W., & Breese, T. (1999). Feasibility of using natural fishbone apatite as a substitute for hydroxyapatite in remediating aqueous heavy metals. *Journal of Hazardous Materials*, *69*(2), 187–196.

Afshar, A., Ghorbani, M., Ehsani, N., Saeri, M. R., & Sorrell, C. C. (2003). Some important factors in the wet precipitation process of hydroxyapatite. *Materials & Design*, *24*(3), 197–202.

Ahmad-Fuzi M. N., & Zainudin, H. (2016). Magnesium-silicon substituted carbonate hydroxyapatite (Mg-Si CHA): Factors affecting sintering. *Key Engineering Materials*, *694*, 88–93.

Albee, F. H. (1920). Studies in Bone Growth: Triple calcium phosphate as a stimulus to osteogenesis. *Annals of Surgery*, *71*(1), 32–39.

Aminian, A., Solati-Hashjin, M., Samadikuchaksaraei, A., Bakhshi, F., Gorjipour, F., Farzadi, A., Moztarzadeh, F., Schmücker, M. (2011). Synthesis of silicon-substituted hydroxyapatite by a hydrothermal method with two different phosphorous sources. *Ceramics International*, *37*(4), 1219–1229.

Ana, I. D., Matsuya, S., & Ishikawa, K. (2010). Engineering of Carbonate Apatite Bone Substitute Based on Composition-Transformation of Gypsum and Calcium Hydroxide. *Engineering*, *02*(05), 344–352.

Anselme, K. (2000). Osteoblast adhesion on biomaterials. *Biomaterials*, *21*(7), 667–681.

Arcos, D., & Vallet-Regí, M. (2013). Bioceramics for drug delivery. *Acta Materialia*, *61*(3), 890–911.

Baino, F. (2011). Biomaterials and implants for orbital floor repair. *Acta Biomaterialia*, *7*(9), 3248–3266.

Baino, F., Novajra, G., & Vitale-Brovarone, C. (2015). Bioceramics and Scaffolds: A Winning Combination for Tissue Engineering. *Frontiers in Bioengineering and Biotechnology*, *3*(December), 1–17.

Bang, L. T., Long, B. D., & Othman, R. (2014). Carbonate hydroxyapatite and silicon-substituted carbonate hydroxyapatite: synthesis, mechanical properties, and solubility evaluations. *TheScientificWorldJournal*, *2014*, 1–9.

Bang, L. T., Ramesh, S., Purbolaksono, J., Ching, Y. C., Long, B. D., Chandran, H., Ramesh, S., Othman, R. (2015). Effects of silicate and carbonate substitution on the properties of hydroxyapatite prepared by aqueous co-precipitation method. *Materials & Design*, *87*, 788–796.

Barinov, S. M., Rau, J. V, Cesaro, S. N., Ďurišin, J., Fadeeva, I. V, Ferro, D., Medvecky, L., Trionfetti, G. (2006). Carbonate release from carbonated hydroxyapatite in the wide temperature rage. *Journal of Materials Science: Materials in Medicine*, *17*(7), 597–604.

Barinov, S. M., Rau, J. V, Fadeeva, I. V, Cesaro, S. N., Ferro, D., Trionfetti, G., Komlev, V. S., Bibikov, V. Y. (2005). Carbonate loss from two magnesium-substituted carbonated apatites prepared by different synthesis techniques. *Materials Research Bulletin*, *41*(3), 485–494.

Barralet, J., Best, S., & Bonfield, W. (1998). Carbonate substitution in precipitated hydroxyapatite: An investigation into the effects of reaction temperature and bicarbonate ion concentration. *Journal of Biomedical Materials Research*, *41*(1), 79–86.

Barralet, J. E., Best, S. M., & Bonfield, W. (2000). Effect of sintering parameters on the density and microstructure of carbonate hydroxyapatite. *Journal of Materials Science: Materials in Medicine*, *11*(11), 719–724.

Barralet, J., Knowles, J. C., Best, S., & Bonfield, W. (2002). Thermal decomposition of synthesised carbonate hydroxyapatite. *Journal of Materials Science: Materials in Medicine*, *13*(6), 529–533.

Barsoum, M. W. (1997). *Fundamentals Of Ceramics*. *Technology & Engineering*.

Basu, B., & Ghosh, S. (2017). *Introduction. In: Biomaterials for musculoskeletal regeneration*. Indian Institute of Metals Series. Springer, Singapore.

Basu, B., & Nath, S. (2009). Fundamentals of biomaterials and biocompatibility. In B. Basu, D. S. Katti, & A. Kumar (Eds.), *Advanced biomaterials: fundamentals, processing, and applications*, 1–18.

Ben-Nissan, B. (2003). Natural bioceramics: From coral to bone and beyond. *Current Opinion in Solid State and Materials Science*, *7*(4–5), 283–288.

Bertoni, E., Bigi, A., Cojazzi, G., Gandolfi, M., Panzavolta, S., & Roveri, N. (1998). Nanocrystals of magnesium and fluoride substituted hydroxyapatite. *Journal of Inorganic Biochemistry*, *72*(1–2), 29–35. Retrieved from

Best, S. M., Porter, A. E., Thian, E. S., & Huang, J. (2008). Bioceramics: Past, present and for the future. *Journal of the European Ceramic Society*, *28*(7), 1319–1327.

Bigi, A., Falini, G., Foresti, E., Gazzano, M., Ripmonti, A., & Roveri, N. (1996). Rietveld structure refinements of calcium hydroxylapatite containing magnesium. *Acta Crystallographica Section B Structural Science*, *52*(1), 87–92.

Bigi, A., Foresti, E., Gregorini, R., RipamontiN., A., Roveri, N., & Shah, J. S. (1992). The role of magnesium on the structure of biological apatites. *Calcified Tissue International*, *50*(5), 439–444.

Billotte, W. G. (2003). Ceramic biomaterials. In: Park, J. B., Bronzino, J. D. (Eds), *Biomaterials: Principles and Applications*. CRC Press, Boca Raton, FL, 21-35.

Boanini, E., Gazzano, M., & Bigi, A. (2010). Ionic substitutions in calcium phosphates synthesized at low temperature. *Acta Biomaterialia*, *6*(6), 1882–1894.

Bohner, M. (2010). Resorbable biomaterials as bone graft substitutes. *Materials Today*, *13*(1–2), 24–30.

Boneva, R. S., Folks, T. M., & Chapman, L. E. (2001). Infectious disease issues in xenotransplantation. *Clinical Microbiology Reviews*, *14*(1), 1–14.

Boskey, A., & Pleshko Camacho, N. (2007). FT-IR imaging of native and tissue-engineered bone and cartilage. *Biomaterials*, *28*(15), 2465–2478.

Bostrom, R. D., & Mikos, A. G. (1997). Tissue engineering of bone. In Synthetic biodegradable polymer scaffolds. *Springer*, 215–234.

Bouyer, E., Gitzhofer, F., & Boulos, M. I. (2000). Morphological study of hydroxyapatite nanocrystal suspension. *Journal of Materials Science: Materials in Medicine*, *11*(8), 523–531.

Broitman, E. (2016). Indentation Hardness Measurements at Macro-, Micro-, and Nanoscale: A Critical Overview. *Tribology Letters*, *65*(1), 23.

Brunton, P. A., Davies, R. P. W., Burke, J. L., Smith, A., Aggeli, A., Brookes, S. J., & Kirkham, J. (2013). Treatment of early caries lesions using biomimetic self-assembling peptides–a clinical safety trial. *British Dental Journal*, *215*(4).

Burg, K. J. L., Porter, S., & Kellam, J. F. (2000). Biomaterial developments for bone tissue engineering. *Biomaterials*, *21*(23), 2347–2359.

Celotti, G. C., Landi, E., Sandri, M., & Tampieri, A. (2004). New method to prepare natural-like carbonate apatite for bone replacement. *Key Engineering Materials*, *264*, 2071–2074.

Champion, E. (2013). Sintering of calcium phosphate bioceramics. *Acta Biomaterialia*, *9*(4), 5855–5875.

Chang, Q., Ru, H. Q., Chen, D. L., Yue, X. Y., Yu, L., & Zhang, C. P. (2011). An in-vitro Investigation of Iron-Containing Hydroxyapatite/Titanium Composites. *Journal of Materials Science & Technology*, *27*(6), 546–552.

Chappard, C., André, G., Daudon, M., & Bazin, D. (2016). Analysis of hydroxyapatite crystallites in subchondral bone by Fourier transform infrared spectroscopy and powder neutron diffraction methods. *Comptes Rendus Chimie*, *19*(11), 1625–1630.

Cheng, K., Shen, G., Weng, W., & Han, G. (2001). Synthesis of hydroxyapatite / fluoroapatite solid solution by a sol – gel method, (October), 0–4.

Chung, R. J., Hsieh, M. F., Huang, C. W., Perng, L. H., Wen, H. W., & Chin, T. S. (2006). Antimicrobial effects and human gingival biocompatibility of hydroxyapatite sol-gel coatings. *Journal of Biomedical Materials Research*, *76B*(1), 169–178.

Combes, C., Cazalbou, S., & Rey, C. (2016). Apatite biominerals. *Minerals*, *6*(2), 34.

Cullity, B. D., & Stock, S. R. (2001). *Elements of X-ray Diffraction, Third Edition. New York: Prentice-Hall*.

Cullity, B. D. (1978). Elements of X-ray Diffraction. *Addison-Wesley Publishing Company, Inc*. Dordrecht: Springer Netherlands.

Czitrom, A. A., & Gross, A. E. (1992). *Allografts in orthopaedic practice*. Williams & Wilkins.

Davies, J. E. (1996). In Vitro Modeling of the Bone Implant Interface. *The Anatomical Record*, *245*, 426–445.

Diaz-Rodriguez, P., Sánchez, M., & Landin, M. (2018). Drug-Loaded Biomimetic Ceramics for Tissue Engineering. *Pharmaceutics*, *10*(4), 272.

Dimitriou, R., Jones, E., McGonagle, D., & Giannoudis, P. V. (2011). Bone regeneration: current concepts and future directions. *BMC Medicine*, *9*(1), 66.

Doi, Y., Koda, T., Wakamatsu, N., Goto, T., Kamemizu, H., Moriwaki, Y., Adachi, M., Suwa, Y. (1993). Influence of carbonate on sintering of apatites. *Journal of Dental Research*, *72*(01870084), 1279–1284.

Dorozhkin, S. V. (2010). Bioceramics of calcium orthophosphates. *Biomaterials*, *31*(7), 1465–1485.

Driessens, F. C. M. (1980). The mineral in bone, dentin and tooth enamel. *Bulletin Des Sociétés Chimiques Belges*, *89*(8), 663–689.

Driskell, T. D., Hassler, C. R., Tennery, V. J., McCoy, L. R., & Clarke, W. J. (1973). Calcium phosphate resorbable ceramics: a potential alternative to bone grafting. In *Journal of Dental Research*, 52, 123.

Drouet, C., Bosc, F., Banu, M., Largeot, C., Combes, C., Dechambre, G., … Rey, C. (2009). Nanocrystalline apatites: From powders to biomaterials. *Powder Technology*, *190*(1–2), 118–122.

Du, X., Wang, T., & Chen, S. (2018). Synthesis and in vitro biodegradability of carbonatedhydroxyapatite/chitosan composite spheres. In *IOP Conference Series: Materials Science and Engineering*, 382, 22007.

Duminis, T., Shahid, S., & Hill, R. G. (2017). Apatite Glass-Ceramics: A Review. *Frontiers in Materials*.

Feki, El. H., Savariault, J. M., & Ben Salah, A. (1999). Structure refinements by the Rietveld method of partially substituted hydroxyapatite: $Ca_9Na_{0.5}(PO_4)_{4.5}(CO_3)_{1.5}(OH)_2$. *Journal of Alloys and Compounds*, *287*(1), 114–120.

Yacoubi, El., A., Massit, A., Moutaoikel, El. S., Rezzouk, A., & Chafik, El., I., B. (2017). Rietveld Refinement of the Crystal Structure of Hydroxyapatite Using X-ray Powder Diffraction. *American Journal of Materials Science and Engineering*, *5*(1), 1–5.

Eliaz, N., & Metoki, N. (2017). Calcium Phosphate Bioceramics: A Review of Their History, Structure, Properties, Coating Technologies and Biomedical Applications. *Materials (Basel, Switzerland)*, *10*(4), 334.

Ellies, L. G., Carter, J. M., Natiella, J. R., Featherstone, J. D. B., & Nelson, D. G. A. (1988). Quantitative analysis of early in vivo tissue response to synthetic apatite implants. *Journal of Biomedical Materials Research*, *22*(2), 137–148.

Ellies, L. G., Nelson, D. G. A., & Featherstone, J. D. B. (1988). Crystallographic structure and surface morphology of sintered carbonated apatites. *Journal of Biomedical Materials Research*, *22*(6), 541–553.

Elliott, J. C. (1994). Studies in Inorganic Chemistry 18. In *Structure and Chemistry of the Apatites and Other Calcium Orthophosphates, Elsevier,* 18, 1-389.

Erol, M. M., Mouriño, V., Newby, P., Chatzistavrou, X., Roether, J. A., Hupa, L., & Boccaccini, A. R. (2012). Copper-releasing, boron-containing bioactive glass-based scaffolds coated with alginate for bone tissue engineering. *Acta Biomaterialia*, *8*(2), 792–801.

Ezekiel, I., Kasim, S. R., Ismail, Y. M. B., & Noor, A.-F. M. (2018). Nanoemulsion synthesis of carbonated hydroxyapatite nanopowders: Effect of variant CO_3^{2-}/PO_4^{3-} molar ratios on phase, morphology, and bioactivity. *Ceramics International*, *44*(11), 13082–13089.

Fahami, A., Nasiri-Tabrizi, B., Beall, G. W., & Basirun, W. J. (2017). Structural insights of mechanically induced aluminum-doped hydroxyapatite nanoparticles by Rietveld refinement. *Chinese Journal of Chemical Engineering*, *25*(2), 238–247.

Fahami, A., Nasiri-Tabrizi, B., Beall, G. W., & Pingguan-Murphy, B. (2015). Effect of ion concentration on mechanosynthesis of carbonated chlorapatite nanopowders. *Materials Letters*, 146, 16–19.

Fathi, M. H., Hanifi, A., & Mortazavi, V. (2008). Preparation and bioactivity evaluation of bone-like hydroxyapatite nanopowder. *Journal of Materials Processing Technology*, *202*(1–3), 536–542.

Fernández, R. F., Bucchi, C., Navarro, P., Beltrán, V., & Borie, E. (2015). Bone grafts utilized in dentistry: an analysis of patients' preferences. *BMC Medical Ethics*, *16*(1), 71.

Forgiarini, A., Esquena, J., González, C., & Solans, C. (2001). Formation of Nano-emulsions by Low-Energy Emulsification Methods at Constant Temperature. *Langmuir*, *17*(7), 2076–2083.

Frank-Kamenetskaya, O., Kol'tsov, A., Kuz'mina, M., Zorina, M., & Poritskaya, L. (2011). Ion substitutions and non-stoichiometry of carbonated apatite-(CaOH) synthesised by precipitation and hydrothermal methods. *Journal of Molecular Structure*, *992*(1–3), 9–18.

Gandou, Z., Nounah, A., Belhorma, B., & Yahyaoui, A. (2015). Nanosized calcium-deficient carbonated hydroxyapatite synthesized by microwave activation. *Journal of Materials and Environmental Science*, *6*(4), 983–988.

Garskaite, E., Alinauskas, L., Drienovsky, M., Krajcovic, J., Cicka, R., Palcut, M., Jonusauskas, L., Malinauskas, M., Stankeviciute, Z., Kareiva, A. (2016). Fabrication of a composite of nanocrystalline carbonated hydroxyapatite (cHAP) with polylactic acid (PLA) and its surface topographical structuring with direct laser writing (DLW). *RSC Advances*, *6*(76), 72733–72743.

Gasqueres, G., Bonhomme, C., Maquet, J., Babonneau, F., Hayakawa, S., Kanaya, T., & Osaka, A. (2008). Revisiting silicate substituted hydroxyapatite by solid-state NMR. *Magnetic Resonance in Chemistry*, *46*(4), 342–346.

Gergely, G., Wéber, F., Lukács, I., Tóth, A. L., Horváth, Z. E., Mihály, J., & Balázsi, C. (2010). Preparation and characterization of hydroxyapatite from eggshell. *Ceramics International*, *36*(2), 803–806.

Germaini, M. M., Detsch, R., Grünewald, A., Magnaudeix, A., Lalloue, F., Boccaccini, A. R., & Champion, E. (2017). Osteoblast and osteoclast responses to A/B type carbonate-substituted hydroxyapatite ceramics for bone regeneration. *Biomedical Materials*, *12*(3), 035008.

German, R. M. (2010). Coarsening in sintering: grain shape distribution, grain size distribution, and grain growth kinetics in solid-pore systems. *Critical Reviews in Solid State and Materials Sciences*, *35*(4), 263–305.

Giannoudis, P. V, Dinopoulos, H., & Tsiridis, E. (2005). Bone substitutes: an update. *Injury*, *36*(3), 20–27.

Gibson, I. R., & Bonfield, W. (2002). Novel synthesis and characterization of an AB-type carbonate-substituted hydroxyapatite. *Journal of Biomedical Materials Research*, *59*(4), 697–708.

Gibson, I R., Best, S. M., & Bonfield, W. (1999). Chemical characterization of silicon-substituted hydroxyapatite. *Journal of Biomedical Materials Research*, *44*(4), 422–428.

Gibson, Iain R, & Bonfield, W. (2002). Novel synthesis and characterization of an AB-type carbonate-substituted hydroxyapatite. *Journal of Biomedical Materials Research Part A*, *59*(4), 697–708.

Gibson IR, & Bonfield W. (2002). Preparation and characterization of magnesium/carbonate co-substituted hydroxyapatites. *Journal of Materials Science: Materials in Medicine*, *13*(7), 685–693.

Gopi, D., Nithiya, S., Shinyjoy, E., & Kavitha, L. (2012). Spectroscopic investigation on formation and growth of mineralized nanohydroxyapatite for bone tissue engineering applications. *Spectrochimica Acta - Part A: Molecular and Biomolecular Spectroscopycta.*, *92*, 194–200.

Graziani, G., Bianchi, M., Sassoni, E., Russo, A., & Marcacci, M. (2017). Ion-substituted calcium phosphate coatings deposited by plasma-assisted techniques: A review. *Materials Science and Engineering: C*, *74*, 219–229.

Griciuc, A., Popescu-Negreanu, T., Grecu, R., & Simon, V. (2005). Corem composite matrix behaviour in simulated body fluid. *Journal of Optoelectronics and Advanced Materials*, *7*(6), 2827–2830.

Gross, K. A., & Berndt, C. C. (2002). Biomedical application of apatites. *Reviews in Mineralogy and Geochemistry*, *48*(1), 631–672.

Grumezescu, V., & Grumezescu, A. (2019). *Materials for Biomedical Engineering: Inorganic Micro- and Nanostructures*. Elsevier.

Guo, L., Huang, M., & Zhang, X. (2003). Effects of sintering temperature on structure of hydroxyapatite studied with Rietveld method. *Journal of Materials Science: Materials in Medicine*, *14*(9), 817–822.

Guo, Y. P., Yao, Y. B., Guo, Y. J., & Ning, C. Q. (2012). Hydrothermal fabrication of mesoporous carbonated hydroxyapatite microspheres for a drug delivery system. *Microporous and Mesoporous Materials*, *155*, 245–251.

Guo, Y. J., Wang, Y. Y., Chen, T., Wei, Y. T., Chu, L. F., & Guo, Y. P. (2013). Hollow carbonated hydroxyapatite microspheres with mesoporous structure: Hydrothermal fabrication and drug delivery property. *Materials Science and Engineering C*, *33*(6), 3166–3172.

Haberko, K., Bućko, M. M., Mozgawa, W., Pyda, A., Brzezińska-Miecznik, J., & Carpentier, J. (2009). Behaviour of bone origin hydroxyapatite at elevated temperatures and in O2 and CO2 atmospheres. *Ceramics International*, *35*(6), 2537–2540.

Habibovic, P., & Barralet, J. E. (2011). Bioinorganics and biomaterials: Bone repair. *Acta Biomaterialia*, *7*(8), 3013–3026.

Han, Y., Xu, K., Montay, G., Fu, T., & Lu, J. (2002). Evaluation of nanostructured carbonated hydroxyapatite coatings formed by a hybrid process of plasma spraying and hydrothermal synthesis. *Journal of Biomedical Materials Research*, *60*(4), 511–516.

Hayek, E., Newesely, H., & Rumpel, M. L. (1963). Pentacalcium monohydroxyorthophosphate. *Inorganic Syntheses*, *7*, 63–65.

He, Q. J., Huang, Z. L., Cheng, X. K., & Yu, J. (2008). Thermal stability of porous A-type carbonated hydroxyapatite spheres. *Materials Letters*, *62*(3), 539–542.

Hench, L. L. (1991). Bioceramics: From Concept to Clinic. *Journal of the American Ceramic Society*, *74*(7), 1487–1510.

Hench, L. L. (1998). Bioceramics. *Journal of the American Ceramic Society*, *81*(7), 1705–1728.

Hing, K. a. (2005). Bioceramic bone graft substitutes: Influence of porosity and chemistry. *International Journal of Applied Ceramic Technology*, *2*(3), 184–199.

Horváthová, R., Müller, L., Helebrant, A., Greil, P., & Müller, F. A. (2008). In vitro transformation of OCP into carbonated HA under physiological conditions. *Materials Science and Engineering: C*, 28(8), 1414–1419.

Huang, Y., Zhang, X., Mao, H., Li, T., Zhao, R., Yan, Y., & Pang, X. (2015). Osteoblastic cell responses and antibacterial efficacy of Cu/Zn co-substituted hydroxyapatite coatings on pure titanium using electrodeposition method. *RSC Advances*, *5*(22), 17076–17086.

Huang, Y., Zhang, X., & Zhao, R. (2015). Antibacterial efficacy , corrosion resistance , and cytotoxicity studies of copper-substituted carbonated hydroxyapatite coating on titanium substrate, 1688–1700.

Hughes, J. M. (1996). Structure and Chemistry of the Apatites and Other Calcium Orthophosphates. *Journal of the American Chemical Society*, *118*(12), 3072.

Iafisco, M., Morales, J. G., Hernández-Hernández, M. A., García-Ruiz, J. M., & Roveri, N. (2010). Biomimetic carbonate–hydroxyapatite nanocrystals prepared by vapor diffusion. *Advanced Engineering Materials*, *12*(7), B218–B223.

Ibrahim, D., Mostafa, A. A., & Korowash, S. (2011). Chemical characterization of some substituted hydroxyapatites. *Chemistry Central Journal*, *5*(1), 74–86.

Ion, R. M., Iancu, L., Vasilievici, G., Grigore, M. E., Andrei, R. E., Radu, G.-I., Grigorescu, R.-M., Teodorescu, S., Bucurica, I-A., Ion, M.-L. (2019). Ion-substituted carbonated hydroxyapatite coatings for model stone samples. *Coatings*, *9*(4), 231.

Ishikawa, k., Matsuya, S., Miyamoto, Y., & Kawate, K. (2003). Bioceramics. In *Comprehensive Structural Integrity. New York, Elsevier Science*, 9, 169–214.

Ivanova, T. I., Frank-Kamenetskaya, O. V, Kol'tsov, A. B., & Ugolkov, V. L. (2001). Crystal Structure of Calcium-Deficient Carbonated Hydroxyapatite. Thermal Decomposition. *Journal of Solid State Chemistry*, *160*(2), 340–349.

Jaiswal, S., McHale, P., & Duffy, B. (2012). Preparation and rapid analysis of antibacterial silver, copper and zinc doped sol-gel surfaces. *Colloids and Surfaces. B, Biointerfaces*, *94*, 170–176.

Jamuna-Thevi, K., Daud, N. M., Abdul Kadir, M. R., & Hermawan, H. (2014). The influence of new wet synthesis route on the morphology, crystallinity and thermal stability of multiple ions doped nanoapatite. *Ceramics International*, *40*(1, Part A), 1001–1012.

Jamuna-Thevi, K., Suleiman, M. J., & Sabri, S. N. (2017). The in Vitro Degradation of PLGA/Nanoapatite/Lauric Acid Composite Membrane: A Comparative Study in Phosphate Buffer Saline and Simulated Body Fluid. In *Macromolecular Symposia*, 371, 101–106.

Jarcho, M. (1976). Hydroxylapatite synthesis and characterization in dense polycrystalline form. *J. Mater. Sci.*, *11*, 2027–2035.

Jarcho, M. (1981). Calcium phosphate ceramics as hard tissue prosthetics. *Clin Orthop*, *157*, 259–278.

Pasteris, J. D., Wopenkaa, B., Freemana, J. J., Rogers, K., Valsami-Jonesc, E., Van der Houwen, J. A. M., Silva, M. J. (2004). Lack of OH in nanocrystalline apatite as a function of degree of atomic order: implications for bone and biomaterial. *Biomaterials*, *25*, 229–238.

Jong, W. F. De. (1926). La Substance Minérale Dans les Os. *Recueil Des Travaux Chimiques Des Pays-Bas*, *45*(6), 445–448.

Joschek, S., Nies, B., Krotz, R., & Göpferich, A. (2000). Chemical and physicochemical characterization of porous hydroxyapatite ceramics made of natural bone. *Biomaterials*, *21*(16), 1645–1658.

Kaewsichan, L., Riyapana, D., Prommajana, P., & Kaewsrichan, J. (2011). Effects of sintering temperatures on micro-morphology, mechanical properties, and bioactivity of bone scaffolds containing calcium silicate. *Sci Asia*, *37*, 240–246.

Kamalanathan, P., Ramesh, S., Bang, L. T., Niakan, A., Tan, C. Y., Purbolaksono, J., Chandran, H., Teng, W. D. (2014). Synthesis and sintering of hydroxyapatite derived from eggshells as a calcium precursor. *Ceramics International*, *40*(PB), 16349–16359.

Kang, S. J. L. (2005). Sintering: Densification, Grain Growth and Microstructure. *Elsevier*, 280.

Karch, J., Birringer, R., & Gleiter, H. (1987). Ceramics ductile at low temperature. Nature, 330(6148).

Karunakaran, G., Kumar, G. S., Cho, E.-B., Sunwoo, Y., Kolesnikov, E., & Kuznetsov, D. (2019). Microwave-assisted hydrothermal synthesis of mesoporous carbonated hydroxyapatite with tunable nanoscale characteristics for biomedical applications. *Ceramics International*, *45*(1), 970–977.

Kay, M. I., Young, R. A., & Posner, A. S. (1964). Crystal structure of hydroxyapatite. *Nature*, *204*, 1050—1052.

Kee, C. C., Ismail, H., & Mohd Noor, A. F. (2013). Effect of synthesis technique and carbonate content on the crystallinity and morphology of carbonated hydroxyapatite. *Journal of Materials Science and Technology*, *29*(8), 761–764.

Khan, A. F., Saleem, M., Afzal, A., Ali, A., Khan, A., & Khan, A. R. (2014). Bioactive behavior of silicon substituted calcium phosphate based bioceramics for bone regeneration. *Materials Science and Engineering: C*, *35*, 245–252.

Khang, G., Kim, S. H., Kim, M. S., & Lee, H. B. (2008). Hybrid, composite, and complex biomaterials for scaffolds. In *Principles of Regenerative Medicine*, 636–655. *Elsevier.*

Kim, I. S., & Kumta, P. N. (2004). Sol–gel synthesis and characterization of nanostructured hydroxyapatite powder. *Materials Science and Engineering: B*, *111*(2), 232–236.

Kokubo, T. (1990). Surface chemistry of bioactive glass-ceramics. *Journal of Non-Crystalline Solids*, *120*(1), 138–151.

Kokubo, T., & Takadama, H. (2006). How useful is SBF in predicting in vivo bone bioactivity? *Biomaterials*, *27*(15), 2907–2915.

Kolmas, J., Groszyk, E., & Kwiatkowska-Różycka, D. (2014). Substituted hydroxyapatites with antibacterial properties. *BioMed Research International*, *2014*, 178123.

Koumoulidis, G. C., Katsoulidis, A. P., Ladavos, A. K., Pomonis, P. J., Trapalis, C. C., Sdoukos, A. T., & Vaimakis, T. C. (2003). Preparation of hydroxyapatite via microemulsion route. *Journal of Colloid and Interface Science*, *259*(2), 254–260.

Kovaleva, E S, Shabanov, M. P., Putlayev, V. I., Filippov, Y. Y., Tretyakov, Y. D., & Ivanov, V. K. (2008). Carbonated hydroxyapatite nanopowders for preparation of bioresorbable materials. *Materialwissenschaft Und Werkstofftechnik*, *39*(11), 822–829.

Kovaleva, Elena S., Shabanov, M. P., Putlyaev, V. I., Tretyakov, Y. D., Ivanov, V. K., & Silkin, N. I. (2009). Bioresorbable carbonated hydroxyapatite $Ca_{10-x}Na_x(PO_4)_{6-x}(CO_3)_x(OH)_2$ powders for bioactive materials preparation. *Central European Journal of Chemistry,* 7(2), 168–174.

Krajewski, A., Mazzocchi, M., Buldini, P. L., Ravaglioli, A., Tinti, A., Taddei, P., & Fagnano, C. (2005). Synthesis of carbonated hydroxyapatites: Efficiency of the substitution and critical evaluation of analytical methods. *Journal of Molecular Structure*, *744–747*, 221–228.

Kumar, G. S., Thamizhavel, A., Yokogawa, Y., Kalkura, S. N., & Girija, E. K. (2012). Synthesis, characterization and in vitro studies of zinc and carbonate co-substituted nano-hydroxyapatite for biomedical applications. *Materials Chemistry and Physics*, *134*(2–3), 1127–1135.

Kumar, T. S. S., Manjubala, I., & Gunasekaran, J. (2000). Synthesis of carbonated calcium phosphate ceramics using microwave irradiation. *Biomaterials*, *21*(16), 1623–1629.

Kumar, V., Dasgupta, N., & Ranjan, S. (Eds.). (2018). *Environmental Toxicity of Nanomaterials*. CRC Press.

Kumta, P. N., Sfeir, C., Lee, D. H., Olton, D., & Choi, D. (2005). Nanostructured calcium phosphates for biomedical applications: novel synthesis and characterization. *Acta Biomaterialia*, *1*(1), 65–83.

Lafon, J. P., Champion, E., & Bernache-Assollant, D. (2008). Processing of AB-type carbonated hydroxyapatite $Ca_{10-x}(PO_4)_{6-x}(CO_3)_x(OH)_{2-x-2y}(CO_3)_y$ ceramics with controlled composition. *Journal of the European Ceramic Society*, *28*(1), 139–147.

Lafon, J. P., Champion, E., Bernache-Assollant, D., Gibert, R., & Danna, A. M. (2003). Termal decomposition of carbonated calcium phosphate apatites. *Journal of Thermal Analysis and Calorimetry*, *72*(3), 1127–1134.

Lala, S., Ghosh, M., Das, P. K., Das, D., Kar, T., & Pradhan, S. K. (2016). Magnesium substitution in carbonated hydroxyapatite: Structural and microstructural characterization by Rietveld's refinement. *Materials Chemistry and Physics*, *170*, 319–329.

Landi, E., Celotti, G., Logroscino, G., & Tampieri, A. (2003). Carbonated hydroxyapatite as bone substitute. *Journal of the European Ceramic Society*, *23*(15), 2931–2937.

Landi, E., Tampieri, A., Celotti, G., & Sprio, S. (2000). Densification behaviour and mechanisms of synthetic hydroxyapatites. *Journal of the European Ceramic Society*, *20*(14), 2377–2387.

Landi, E., Sprio, S., Sandri, M., Celotti, G., & Tampieri, A. (2008). Development of Sr and CO_3 co-substituted hydroxyapatites for biomedical applications. *Acta Biomaterialia*, *4*(3), 656–663.

Landi, E., Tampieri, A., Celotti, G., Vichi, L., & Sandri, M. (2004). Influence of synthesis and sintering parameters on the characteristics of carbonate apatite. *Biomaterials*, *25*(10), 1763–1770.

Landi, E., Tampieri, A., Mattioli-Belmonte, M., Celotti, G., Sandri, M., Gigante, A., Fava, P., Biagini, G. (2006). Biomimetic Mg- and Mg, CO_3-substituted hydroxyapatites: synthesis characterization and in vitro behaviour. *Journal of the European Ceramic Society*, *26*(13), 2593–2601.

Larson, P. R., Madden, A. S., & Tas, A. C. (2013). Non-stirred synthesis of Na- and Mg-doped, carbonated apatitic calcium phosphate. *Ceramics International*, *39*(2), 1485–1493.

Laurencin, D., Almora-Barrios, N., de Leeuw, N. H., Gervais, C., Bonhomme, C., Mauri, F., Chrzanowski, W., Knowles, J. C., Newport, R. J., Wong, A., Gan, Z., Smith, M. E. (2011). Magnesium incorporation into hydroxyapatite. *Biomaterials*, *32*(7), 1826–1837.

Layrolle, P., Ito, A., & Tateishi, T. (1998). Sol-Gel Synthesis of Amorphous Calcium Phosphate and Sintering into Microporous Hydroxyapatite Bioceramics. *Journal of the American Ceramic Society*, *81*(6), 1421–1428.

Lee, Y., Hahm, Y. M., Matsuya, S., Nakagawa, M., & Ishikawa, K. (2007). Characterization of macroporous carbonate-substituted hydroxyapatite bodies prepared in different phosphate solutions. *Journal of Materials Science*, *42*(18), 7843–7849.

Legeros, R Z. (1965). Effect of Carbon on the Lattice Parameter of Apatite. *Nature*, *206*, 403–404.

LeGeros, R Z., Daculsi, G., & LeGeros, J. (2008). Bioactive Bioceramics. In W. Pietrzak (Ed.), *Musculoskeletal Tissue Regeneration.* Humana Press, 153–181.

Legeros, R Z., Ito, A., Ishikawa, K., Sakae, T., & Legeros, J. P. (2009). Fundamentals of hydroxyapatite and related calcium phosphates. In: Basu, B., Katti, D. S., & Kumar, A. (Eds.) *Advanced Biomaterials: Fundamentals, Processing, and Applications*. Wiley, 19–52.

LeGeros, R Z. (1991). Calcium phosphates in oral biology and medicine. *Monographs in Oral Science*, *15*, 1–201.

LeGeros, R Z. (2002). Properties of osteoconductive biomaterials: Calcium phosphates. *Clinical Orthopaedics and Related Research*, 395, 81–98.

LeGeros, R Z, Trautz, O. R., Klein, E., & LeGeros, J. P. (1969). Two types of carbonate substitution in the apatite structure. *Experientia*, *25*(1), 5–7.

LeGeros, R Z., & LeGeros, J. P. (2003). Calcium Phosphate Bioceramics: Past, Present and Future. *Key Engineering Materials*, *240–242*, 3–10.

LeGeros, R Z., Kijkowska, R., Bautista, C., & Legeros, J. P. (1995). Synergistic effects of magnesium and carbonate on properties of biological and synthetic apatites. *Connective Tissue Research*, *33*(1–3), 203–209.

LeGeros, R Z., & LeGeros, J. P. (1993). Dense hydroxyapatite. In Hench L. L. & Wilson J. (Eds.), *An Introduction to Bioceramics.* World Scientific Publishing, 1, 139–180.

LeGeros, R Z., Trautz, O. R., LeGeros, J. P., Klein, E., & Shirra, W. P. (1967). Apatite Crystallites: Effects of Carbonate on Morphology. *Science*, *155*(3768), 1409–1411.

LeGeros, R Z. (1965). Effect of Carbonate on the Lattice Parameters of Apatite. *Nature*, *206*(4982), 403–404.

Li, M., Xiao, X., Rongfang, L., Cuiyu, C., & Lizhong, H. (2008). Structural characterization of zinc-substituted hydroxyapatite prepared by hydrothermal method. *Journal of Materials Science: Materials in Medicine*, *19*(2), 797–803.

Liao, S., Watari, F., Xu, G., Ngiam, M., Ramakrishna, S., & Chan, C. K. (2007). Morphological effects of variant carbonates in biomimetic hydroxyapatite. *Materials Letters*, *61*(17), 3624–3628.

Lim, G. K., Wang, J., Ng, S. C., & Gan, L. M. (1999). Nanosized hydroxyapatite powders from microemulsions and emulsions stabilized by a biodegradable surfactant. *Journal of Materials Chemistry*, *9*(7), 1635–1639.

Lin, K., Zhou, Y., Zhou, Y., Qu, H., Chen, F., Zhu, Y., & Chang, J. (2011). Biomimetic hydroxyapatite porous microspheres with co-substituted essential trace elements: Surfactant-free hydrothermal synthesis, enhanced degradation and drug release. *Journal of Materials Chemistry*, *21*(41), 16558–16565.

Liu, D. M., Troczynski, T., & Tseng, W. J. (2001). Water-based sol–gel synthesis of hydroxyapatite: process development. *Biomaterials*, *22*(13), 1721–1730.

Liu, D. M., Yang, Q., Troczynski, T., & Tseng, W. J. (2002). Structural evolution of sol–gel-derived hydroxyapatite. *Biomaterials*, *23*(7), 1679–1687.

Liu, Q. (1962). Hydroxyapatite / polymer composites for bone replacement. Thesis

Liu, R., Xu, X., Cai, Y., Cai, A., Pan, H., Tang, R., & Cho, K. (2009). Preparation of calcite and aragonite complex layer materials inspired from biomineralization. *Crystal Growth and Design*, *9*(7), 3095–3099.

Lysenko, O., Dubok, O., Borysenko, A., & Shinkaruk, O. (2015). The biological properties of the silver- and copper-doped ceramic biomaterial. *Journal of Nanoparticle Research*, *17*(4), 178.

Ma, Q. Y., Logan, T. J., Traina, S. J., & Ryan, J. A. (1994). Effects of NO_3^-, Cl^-, F^-, SO_4^{2-}, and CO_3^{2-} on Pb^{2+} Immobilization by Hydroxyapatite. *Environmental Science and Technology*, *28*(3), 408–418.

Madupalli, H., Pavan, B., & Tecklenburg, M. M. J. (2017). Carbonate substitution in the mineral component of bone: Discriminating the structural changes, simultaneously imposed by carbonate in A and B sites of apatite. *Journal of Solid State Chemistry*, *255*, 27–35.

Maeyer, E. A. P. De, Verbeeck, R. M. H., & Naessens, D. E. (1994). Effect of heating on the constitution of Na^+ -and CO_3^{2-} -containing apatites obtained by the hydrolysis of monetite. *Inorganic Chemistry*, 33(26), 5999–6006.

Mata, A., Boehm, C., Fleischman, A. J., Muschler, G., & Roy, S. (2002). Growth of connective tissue progenitor cells on microtextured polydimethylsiloxane surfaces. *Journal of Biomedical Materials Research*, *62*(4), 499–506.

Matsunaga, K., Murata, H., Mizoguchi, T., & Nakahira, A. (2010). Mechanism of incorporation of zinc into hydroxyapatite. *Acta Biomaterialia*, *6*(6), 2289–2293.

Mayer, I., Apfelbaum, F., & Featherstone, J. D. B. (1994). Zinc ions in synthetic carbonated hydroxyapatites. *Archives of Oral Biology*, *39*(1), 87–90.

Mendelson, M. e l i. (1969). Average Grain Size in Polycrystalline Ceramics. *Journal of the American Ceramic Society*, *52*(8), 443–446.

Merry, J. C., Gibson, I. R., Best, S. M., & Bonfield, W. (1998). Synthesis and characterization of carbonate hydroxyapatite. *Journal of Materials Science: Materials in Medicine*, *9*(12), 779–783.

Mirhadi, B., Mehdikhani, B., & Askari, N. (2011). Synthesis of nano-sized β-tricalcium phosphate via wet precipitation. *Processing and Application of Ceramics*, *5*(4), 193–198.

Miyaji, F., Kono, Y., & Suyama, Y. (2005). Formation and structure of zinc-substituted calcium hydroxyapatite. *Materials Research Bulletin*, *40*(2), 209–220.

Mohammad, N. F., Othman, R., Abdullah, N. A., & Yeoh, F. Y. (2016). In vitro Evaluation of Mesoporous Carbonated Hydroxyapatite in MC3T3-E1 Osteoblast Cells. *Procedia Chemistry*, *19*, 259–266.

Morales-Nieto, V., Navarro, C. H., Moreno, K. J., Arizmendi-Morquecho, A., Chávez-Valdez, A., García-Miranda, S., & Louvier-Hernández, J. F. (2013). Poly(methyl methacrylate)/carbonated hydroxyapatite composite applied as coating on ultra high molecular weight polyethylene. *Progress in Organic Coatings*, *76*(1), 204–208.

Mostafa, N. Y., Hassan, H. M., & Abd Elkader, O. H. (2011). Preparation and Characterization of Na^{+}, SiO_4^{4-}, and CO_3^{2-} Co-Substituted Hydroxyapatite. *Journal of the American Ceramic Society*, *94*(5), 1584–1590.

Muralithran, G., & Ramesh, S. (2000). The effects of sintering temperature on the properties of hydroxyapatite. *Ceramics International*, *26*(2), 221–230.

Murugan, R., & Ramakrishna, S. (2006). Production of ultra-fine bioresorbable carbonated hydroxyapatite. *Acta Biomaterialia*, *2*(2), 201–206.

Naceur, H., Megriche, A., & El Maaoui, M. (2014). Effect of sintering temperature on microstructure and electrical properties of $Sr_{1-x}(Na_{0.5}Bi_{0.5})xBi_2Nb_2O_9$ solid solutions. *Journal of Advanced Ceramics*, *3*(1), 17–30.

Narayan, R., Colombo, P. (2009). Advances in Bioceramics and Porous Ceramics II: Ceramic Engineering and Science Proceedings. *The Amercian Ceramic Society*, 30.

Nagai, H., & Nishimura, Y. (1982). Hydroxyapatite, ceramic material and process for preparing thereof.

Niihara, K. (1985). Indentation microfracture of ceramics-Its application and problems. *Bull. Cer. Soc. Jpn.*, *20*, 12–18.

Nilsson, M., Wang, J.-S., Wielanek, L., Tanner, K. E., & Lidgren, L. (2004). Biodegradation and biocompatability of a calcium sulphate-hydroxyapatite bone substitute. *The Journal of Bone and Joint Surgery. British Volume*, *86-B*(1), 120–125.

Othman, R., Mustafa, Z., Loon, C., & Noor, A. (2016). Effect of Calcium Precursors and pH on the Precipitation of Carbonated Hydroxyapatite. *Procedia Chemistry*, *19*, 539–545.

Padmanabhan, S. K., Balakrishnan, A., Chu, M. C., Lee, Y. J., Kim, T. N., & Cho, S. J. (2009). Sol-gel synthesis and characterization of hydroxyapatite nanorods. *Particuology*, *7*(6), 466–470.

Palard, M., Champion, E., & Foucaud, S. (2008). Synthesis of silicated hydroxyapatite $Ca_{10}(PO_4)_{6-x}(SiO_4)_x(OH)_{2-x}$. *Journal of Solid State Chemistry*, *181*(8), 1950–1960.

Pan, H., Zhao, X., Darvell, B. W., & Lu, W. W. (2010). Apatite-formation ability – Predictor of "bioactivity"? *Acta Biomaterialia*, *6*(11), 4181–4188.

Panda, R. N., Hsieh, M. F., Chung, R. J., & Chin, T. S. (2003). FTIR, XRD, SEM and solid state NMR investigations of carbonate-containing hydroxyapatite nano-particles synthesized by hydroxide-gel technique. *Journal of Physics and Chemistry of Solids*, *64*(2), 193–199.

Park, J. B., & Bronzino, J. D. (2003). Biomaterials principles and applications.

Park, J., & Lakes, R. S. (2007). Biomaterials: an introduction. *Springer*.

Percival, M. (1999). Bone health & osteoporosis. *Appl Nutr Sci Rep*, *5*(4), 1–5.

Pietak, A. M., Reid, J. W., Stott, M. J., & Sayer, M. (2007). Silicon substitution in the calcium phosphate bioceramics. *Biomaterials*, *28*(28), 4023–4032.

Pieters, I. Y., Van den Vreken, N. M. F., Declercq, H. A., Cornelissen, M. J., & Verbeeck, R. M. H. (2010). Carbonated apatites obtained by the hydrolysis of monetite: Influence of carbonate content on adhesion and proliferation of MC3T3-E1 osteoblastic cells. *Acta Biomaterialia*, *6*(4), 1561–1568.

Platt, J. L., Vercellotti, G. M., Dalmasso, A. P., Matas, A. J., Bolman, R. M., Najarian, J. S., & Bach, F. H. (1990). Transplantation of discordant xenografts: a review of progress. *Immunology Today*, *11*(0), 450–456.

Porter, A., Patel, N., Brooks, R., Best, S., Rushton, N., & Bonfield, W. (2005). Effect of carbonate substitution on the ultrastructural characteristics of hydroxyapatite implants. *Journal of Materials Science: Materials in Medicine*, *16*(10), 899–907.

Posner, A. S. (1969). Crystal chemistry of bone mineral. *Physiological Reviews*, *49*(4), 760–792.

Posner, A. S., Perloff, A., & Diorio, A. F. (1958). Refinement of the hydroxyapatite structure. *Acta Crystallographica*, *11*(4), 308–309.

Prekajski, M., Mirković, M., Todorović, B., Matković, A., Marinović-Cincović, M., Luković, J., & Matović, B. (2016). Ouzo effect—New simple nanoemulsion method for synthesis of strontium hydroxyapatite nanospheres. *Journal of the European Ceramic Society*, 36(5), 1293–1298.

Radovanović, Ž., Jokić, B., Veljović, D., Dimitrijević, S., Kojić, V., Petrović, R., & Janaćković, D. (2014). Antimicrobial activity and biocompatibility of Ag^{+}- and Cu^{2+}-doped biphasic hydroxyapatite/α-tricalcium phosphate obtained from hydrothermally synthesized Ag^{+}- and Cu^{2+}-doped hydroxyapatite. *Applied Surface Science*, 307, 513-519.

Rahaman, M. N. (2007). Sintering of ceramics. *CRC Press, Taylor & Francis Group*. *Boca Raton*, 388.

Rajabi-Zamani, A. H., Behnamghader, A., & Kazemzadeh, A. (2008). Synthesis of nanocrystalline carbonated hydroxyapatite powder via nonalkoxide sol–gel method. *Materials Science and Engineering: C*, *28*(8), 1326–1329.

Rajesh, R., Hariharasubramanian, A., & Ravichandran, Y. D. (2012). Chicken bone as a bioresource for the bioceramic (Hydroxyapatite). *Phosphorus, Sulfur, and Silicon and the Related Elements*, *187*(8), 914–925.

Ramacharyulu, P. V. R. K., Abbas, S. J., & Shyue-Chu, K. (2017). How charge separation and photoactivity are enhanced in heterostructured g-C_3N_4: A synergistic interaction in environmental friendly CaO/g-C_3N_4. *Catal. Sci. Technol,* 7(21), 4940–4943.

Rau, J. V., Cesaro, S. N., Ferro, D., Barinov, S. M., & Fadeeva, I. V. (2004). FTIR study of carbonate loss from carbonated apatites in the wide temperature range. *Journal of Biomedical Materials Research - Part B Applied Biomaterials*, *71*(2), 441–447.

Ray, R. D., Degge, J., Gloyd, P., & Mooney, G. (1952). Bone regeneration. *J Bone Joint Surg Am*, *34*(3), 638–647.

Refaat, A., Youness, R. A., Taha, M. A., & Ibrahim, M. (2017). Effect of zinc oxide on the electronic properties of carbonated hydroxyapatite. *Journal of Molecular Structure*, *1147*, 148–154.

Reisman, D. J. (1998). Acetone: first draft. Geneva. *World Health Organization*.

Ren, F., Leng, Y., Xin, R., & Ge, X. (2010). Synthesis, characterization and ab initio simulation of magnesium-substituted hydroxyapatite. *Acta Biomaterialia*, *6*(7), 2787–2796.

Ren, F. Z., & Leng, Y. (2011). Carbonated Apatite, Type-A or Type-B? *Key Engineering Materials*, *493–494*, 293–297.

Rey, C., Collins, B., Goehl, T., Dickson, I. R., & Glimcher, M. J. (1989). The carbonate environment in bone mineral: A resolution-enhanced fourier transform infrared spectroscopy study. *Calcified Tissue International*, *45*(3), 157–164.

Rey, C., Renugopalakrishman, V., Collins, B., & Glimcher, M. J. (1991). Fourier transform infrared spectroscopic study of the carbonate ions in bone mineral during aging. *Calcified Tissue International*, *49*(4), 251–258.

Riman, R. E., Suchanek, W. L., Byrappa, K., Chen, C.-W., Shuk, P., & Oakes, C. S. (2002). Solution synthesis of hydroxyapatite designer particulates. *Solid State Ionics*, *151*(1–4), 393–402.

Ring, T. A. (1996). *Fundamentals of Ceramic Powder Processing and Synthesis*.

Rodan, G. A. (1992). Introduction to bone biology. *Bone*, *13*, *Supple*(0), S3–S6.

Rogers, K. D., & Daniels, P. (2002). An X-ray diffraction study of the effects of heat treatment on bone mineral microstructure. *Biomaterials*, *23*(12), 2577–2585.

Roveri, N., & Iafisco, M. (2010). Evolving application of biomimetic nanostructured hydroxyapatite. *Nanotechnology, Science and Applications*, *3*, 107–125.

Roy, D. M., Eysel, W., & Dinger, D. (1974). Hydrothermal synthesis of various carbonate containing calcium hydroxyapatites. *Materials Research Bulletin*, *9*(1), 35–39.

Ruys, A., J. (2013). Biomimetic biomaterials : structure and applications. *Oxford: Woodhead*, 344.

Saber-Samandari, S., Saber-Samandari, S., Ghonjizade-Samani, F., Aghazadeh, J., & Sadeghi, A. (2016). Bioactivity evaluation of novel nanocomposite scaffolds for bone tissue engineering: The impact of hydroxyapatite. *Ceramics International*, *42*(9), 11055–11062.

Sadat-Shojai, M., Khorasani, M. T., Dinpanah-Khoshdargi, E., & Jamshidi, A. (2013). Synthesis methods for nanosized hydroxyapatite with diverse structures. *Acta Biomaterialia*, *9*(8), 7591–7621.

Salgado, A. J., Coutinho, O. P., & Reis, R. L. (2004). Bone Tissue Engineering: State of the Art and Future Trends. *Macromolecular Bioscience*, *4*(8), 743–765.

Sarkar, A., & Kannan, S. (2014). In situ synthesis, fabrication and Rietveld refinement of the hydroxyapatite/titania composite coatings on 316 L SS. *Ceramics International*, *40*(5), 6453–6463.

Siddiqi, S. A., Azhar, U., Manzoor, F., Jamal, A., Tariq, M., Saleem, M., Chaudhry, A. A., Rehman, I. U. (2018). Fabrication of biocompatible nano-carbonated hydroxyapatite/polymer spongy scaffolds. *Digest Journal of Nanomaterials & Biostructures (DJNB)*, 13(2), 439–450.

Siddiqi, S. A., & Azhar, U. (2020). 6 - Carbonate substituted hydroxyapatite. In Khan, A. S., & Chaudhry, A. A., (Eds.) Handbook of Ionic Substituted Hydroxyapatites (1st Edition), *Woodhead Publishing Series in Biomaterials,* 149–173.

Shanmugam, S., & Gopal, B. (2014). Copper substituted hydroxyapatite and fluorapatite: Synthesis, characterization and antimicrobial properties. *Ceramics International*, *40*(10), 15655–15662.

Shatokha, V. (2012). Sintering: Methods and Products. *InTech, US.*

Shepherd, J. H., Shepherd, D. V, & Best, S. M. (2012). Substituted hydroxyapatites for bone repair. *Journal of Materials Science. Materials in Medicine*, *23*(10), 2335–2347.

Shin, Y., Aoki, H., Yoshiyama, N., Akao, M., & Higashikata, M. (1992). Surface properties of hydroxyapatite ceramic as new percutaneous material in skin tissue. *Journal of Materials Science: Materials in Medicine*, *3*(3), 219–221.

Krishna, D. S. R., Siddharthan, A., Seshadri, S. K., & Kumar, T. S. S. (2007). A novel route for synthesis of nanocrystalline hydroxyapatite from eggshell waste. *Journal of Materials Science: Materials in Medicine*, *18*(9), 1735–1743.

Slosarczyk, A., & Białoskórski, J. (1998). Hardness and fracture toughness of dense calcium–phosphate-based materials. *Journal of Materials Science: Materials in Medicine*, *9*(2), 103–108.

Ślósarczyk, A., Paszkiewicz, Z., & Paluszkiewicz, C. (2005). FTIR and XRD evaluation of carbonated hydroxyapatite powders synthesized by wet methods. *Journal of Molecular Structure*, *744–747*, 657–661.

Ślósarczyk, A., Paszkiewicz, Z., & Zima, A. (2010). The effect of phosphate source on the sintering of carbonate substituted hydroxyapatite. *Ceramics International*, *36*(2), 577–582.

Sobczak-Kupiec, A., & Wzorek, Z. (2012). The influence of calcination parameters on free calcium oxide content in natural hydroxyapatite. *Ceramics International*, *38*(1), 641–647.

Solans, C., Izquierdo, P., Nolla, J., Azemar, N., & Garciacelma, M. (2005). Nano-emulsions. *Current Opinion in Colloid & Interface Science*, *10*(3–4), 102–110.

Sommerfeldt, D., & Rubin, C. (2001). Biology of bone and how it orchestrates the form and function of the skeleton. *European Spine Journal*, *10*(2), S86–S95.

Sprio, S., Pezzotti, G., Celotti, G., Landi, E., & Tampieri, A. (2005). Raman and cathodoluminescence spectroscopies of magnesium-substituted hydroxyapatite powders. *Journal of Materials Research*, *20*(4), 1009–1016.

Sprio, S., Tampieri, A., Landi, E., Sandri, M., Martorana, S., Celotti, G., & Logroscino, G. (2008). Physico-chemical properties and solubility behaviour of multi-substituted hydroxyapatite powders containing silicon. *Materials Science and Engineering: C*, *28*, 179–187.

Stanić, V., Dimitrijević, S., Antić-Stanković, J., Mitrić, M., Jokić, B., Plećaš, I. B., & Raičević, S. (2010). Synthesis, characterization and antimicrobial activity of copper and zinc-doped hydroxyapatite nanopowders. *Applied Surface Science*, *256*(20), 6083–6089.

Stanislavov, A. S., Sukhodub, L. F., Sukhodub, L. B., Kuznetsov, V. N., Bychkov, K. L., & Kravchenko, M. I. (2018). Structural features of hydroxyapatite and carbonated apatite formed under the influence of ultrasound and microwave radiation and their effect on the bioactivity of the nanomaterials. *Ultrasonics Sonochemistry*, *42*, 84–96.

Stevens, M. M., & George, J. H. (2005). Exploring and engineering the cell surface interface. *Science*, *310*(5751), 1135–1138.

Suchanek, W. L., Shuk, P., Byrappa, K., Riman, R. E., TenHuisen, K. S., & Janas, V. F. (2002). Mechanochemical-hydrothermal synthesis of carbonated apatite powders at room temperature. *Biomaterials*, *23*(3), 699–710.

Šupová, M. (2015). Substituted hydroxyapatites for biomedical applications: A review. *Ceramics International*, *41*(8), 9203–9231.

Sutherland, D., & Bostrom, M. (2005). Grafts and bone graft substitutes. In J. Lieberman & G. Friedlaender (Eds.), *Bone Regeneration and Repair*. Humana Press, 133–156.

Tadic, D., Peters, F., & Epple, M. (2002). Continuous synthesis of amorphous carbonated apatites. *Biomaterials*, *23*(12), 2553–2559.

Tampieri, A., Celotti, G. C., Landi, E., & Sandri, M. (2004). Magnesium doped hydroxyapatite: synthesis and characterization. In *Key Engineering Materials*, 264, 2051–2054.

Taylor, D. (2018). Measuring fracture toughness in biological materials. *Journal of the Mechanical Behavior of Biomedical Materials*, *77*, 776–782.

Teraoka, K., Ito, A., Maekawa, K., Onuma, K., Tateishi, T., & Tsutsumi, S. (1998). Mechanical properties of hydroxyapatite and OH-carbonated hydroxyapatite single crystals. *Journal of Dental Research*, *77*(7), 1560–1568.

Thamaraiselvi, T. V, & Rajeswari, S. (2004). Biological Evaluation of Bioceramic Materials -A Review. *Trends Biomater. Artif. Organs*, *18*(1), 9–17.

Tkachenko, M. V, & Zyman, Z. Z. (2008). Effect of sintering conditions on physical properties of carbonated hydroxyapatite ceramics. *Functional Materials*, *15*(4), 575.

Tonsuaadu, K., Peld, M., Leskelä, T., Mannonen, R., Niinistö, L., & Veiderma, M. (1995). A thermoanalytical study of synthetic carbonate-containing apatites. *Thermochimica Acta*, *256*(1), 55–65.

Uysal, I., Severcan, F., & Evis, Z. (2013). Characterization by Fourier transform infrared spectroscopy of hydroxyapatite co-doped with zinc and fluoride. *Ceramics International*, *39* (7), 7727–7733.

Uskoković, V. (2020). Ion-doped hydroxyapatite: An impasse or the road to follow? *Ceramics International*, *46*(8, Part B), 11443–11465.

Vagaska, B., Bacakova, L., Filová, E., & Balik, K. (2010). Osteogenic cells on bio-inspired materials for bone tissue engineering. *Physiol Res*, *59*(3), 309–322.

Vallet-Regí, M. (2014). *Bio-Ceramics with Clinical Applications*. *John Wiley & Sons*.

Vallet-Regí, M, & Rámila, A. (2000). New Bioactive Glass and Changes in Porosity during the Growth of a Carbonate Hydroxyapatite Layer on Glass Surfaces. *Chemistry of Materials*, *12*(4), 961–965.

Vallet-Regí, María, & Arcos, D. (2005). Silicon substituted hydroxyapatites. A method to upgrade calcium phosphate based implants. *Journal of Materials Chemistry*, *15*(15), 1509–1516.

Vallet-Regí, María, & González-Calbet, J. M. (2004). Calcium phosphates as substitution of bone tissues. *Progress in Solid State Chemistry*, *32*(1–2), 1–31.

Venkatesan, J., Anil, S., & Kim, S.-K. (2017). *Seaweed Polysaccharides: Isolation, Biological and Biomedical Applications*. Elsevier.

Venkatesan, J., Qian, Z. J., Ryu, B., Thomas, N. V., & Kim, S. K. (2011). A comparative study of thermal calcination and an alkaline hydrolysis method in the isolation of hydroxyapatite from *Thunnus obesus* bone. *Biomedical Materials*, *6*(3), 035003.

Vignoles, M., Bonel, G., Holcomb, D. W., & Young, R. a. (1988). Influence of preparation conditions on the composition of type B carbonated hydroxyapatite and on the localization of the carbonate ions. *Calcified Tissue International*, *43*(1), 33–40.

Wang, J., Yin, B., Liu, G., Li, S., Zhang, X., Hu, Z., Wu, W., Zhang, Y. (2019). Microhardness distribution of the tibial diaphysis and test site selection for reference point indentation technique. *Medicine*, *98*(29), e16523–e16523.

Wang, J., & Shaw, L. L. (2009). Nanocrystalline hydroxyapatite with simultaneous enhancements in hardness and toughness. *Biomaterials*, *30*(34), 6565–6572.

Wang, L., & Nancollas, G. H. (2008). Calcium Orthophosphates: Crystallization and Dissolution. *Chemical Reviews*, *108*(11), 4628–4669.

Wati, R., & Yusuf, Y. (2019). Effect of sintering temperature on carbonated hydroxyapatite derived from common cockle shells (cerastodermaedule): composition and crystal characteristics. *Key Engineering Materials*, 818, 37–43.

Webster, T. J., Ergun, C., Doremus, R. H., Siegel, R. W., & Bizios, R. (2001). Enhanced osteoclast-like cell functions on nanophase ceramics. *Biomaterials*, *22*(11), 1327–1333.

Webster, T. J. (2001). Nanophase ceramics: The future orthopedic and dental implant material. *Advances in Chemical Engineering*, 27, 125–166.

Wong, J. Y., Bronzino, J. D., & Peterson, D. R. (2012). *Biomaterials: Principles and practices*. CRC Press.

Wong, W. Y., & Noor, A.-F. M. (2016). Synthesis and Sintering-wet Carbonation of Nano-sized Carbonated Hydroxyapatite. *Procedia Chemistry*, *19*, 98–105.

Wopenka, B., & Pasteris, J. D. (2005). A mineralogical perspective on the apatite in bone. *Materials Science and Engineering: C*, *25*(2), 131–143.

Wurst, J. C., & Nelson, J. A. (1972). Lineal intercept technique for measuring grain size in two-phase polycrystalline ceramics. *Journal of the American Ceramic Society*, *55*(2), 109.

Xu, G., Aksay, I. A., & Groves, J. T. (2001). Continuous crystalline carbonate apatite thin films. A biomimetic approach. *Journal of the American Chemical Society*, *123*(10), 2196–2203.

Xu, R., Junguo, R., Li, Z., Lin, X., Yang, L., Baohui, S., Jiyong, C., Jiaomin, L., Xindong, Z. (2007). Sonochemical Synthesis of Nanosized Carbonated Hydroxyapatite. *Rare Metal Materials and Engineering*, *36*, 46.

Xue, C., Chen, Y., Huang, Y., & Zhu, P. (2015). Hydrothermal synthesis and biocompatibility study of highly crystalline carbonated hydroxyapatite nanorods. *Nanoscale Research Letters*, *10*(1), 1018.

Yacoubi, A., Massit, A., Moutaoikel, S., Rezzouk, A., & Idrissi, B. (2017). Rietveld refinement of the crystal structure of hydroxyapatite using x-ray powder diffraction. *American Journal of Materials Science and Engineering*, *5*, 1–5.

Yanny-Marliana, B. I., & Ahmad Fauzi, M. N. (2011). Effect of a Novel Approach of Sintering on Physical Properties of Carbonated Hydroxyapatite. *Journal of Materials Science and Engineering B*, *1*(2), 157–163.

Yasukawa, A., Ouchi, S., Kandori, K., & Ishikawa, T. (1996). Preparation and characterization of magnesium–calcium hydroxyapatites. *Journal of Materials Chemistry*, *6*(8), 1401–1405.

Yasumoto, I. (1984). Adsorption of water, ammonia, and carbon dioxide on zinc oxide at elevated temperatures. *The Journal of Physical Chemistry*, *41*(44), 4041–4044.

Yoshikawa, H., & Myoui, A. (2005). Bone tissue engineering with porous hydroxyapatite ceramics. *Journal of Artificial Organs*, *8*(3), 131–136.

Youness, R. A., Taha, M. A., Elhaes, H., & Ibrahim, M. (2017). Molecular modeling, FTIR spectral characterization and mechanical properties of carbonated-hydroxyapatite prepared by mechanochemical synthesis. *Materials Chemistry and Physics*, *190*, 209–218.

Zakaria, F. A., Marsad, N. H., Manaf, A. Y. A., Villamil, M., Montes, T., Carretero, C., & Mikan, J. (2009). Characterisation of carbonated apatite for possible application in biomedical implants. *Materials Research Innovations*, *13*(3), 309–312.

Zhou, J., Zhang, X., Chen, J., Zeng, S., & De Groot, K. (1993). High temperature characteristics of synthetic hydroxyapatite. *Journal of Materials Science: Materials in Medicine*, *4*(1), 83–85.

Zhou, W. Y., Wang, M., Cheung, W. L., Guo, B. C., & Jia, D. M. (2008). Synthesis of carbonated hydroxyapatite nanospheres through nanoemulsion. *Journal of Materials Science: Materials in Medicine*, *19*(1), 103–110.

Zhu, Q. X., Jiang, W. H., Shao, C., & Bao, Y. (2012). Thermophysical and Mechanical Properties of Carbonated Hydroxyapatite. *Key Engineering Materials*, 512, 989–993.

Zhu, Q. X., Li, Y. M., & Han, D. (2015). Co-substitution of carbonate and fluoride in hydroxyapatite: Effect on substitution type and content. *Frontiers of Materials Science*, *9*(2), 192–198.

Zou, Z., Lin, K., Chen, L., & Chang, J. (2012). Ultrafast synthesis and characterization of carbonated hydroxyapatite nanopowders via sonochemistry-assisted microwave process. *Ultrasonics Sonochemistry*, *19*(6), 1174–1179.

Zyman, Z., & Tkachenko, M. (2011). CO_2 gas-activated sintering of carbonated hydroxyapatites. *Journal of the European Ceramic Society*, *31*(3), 241–248.

LIST OF PUBLICATIONS AND PAPERS PRESENTED

PUBLICATIONS

Safarzadeh, M., Ramesh, S., Tan, C. Y., Chandran, H., Ching, Y.C., Ahmad Fauzi, M.N., Krishnasamy, S.,Teng. W.D. (2020). Sintering behaviour of carbonated hydroxyapatite prepared at different carbonate and phosphate ratios. *Boletín de la Sociedad Española de Cerámica y Vidrio,* 59(2), 73-80.

Safarzadeh, M., Ramesh, S., Tan, C. Y., Chandran, H., Ahmad Fauzi, M.N., Krishnasamy, S., Johnson Alengaramf,U., Ramesh, S. (2019). Effect of multi-ions doping on the properties of carbonated hydroxyapatite bioceramic. *Ceramics International*, 45(3), 3473–3477.

Vakili, A. H., Selamat, M. R., Aziz, H. B. A., Mojiri, A., **Safarzadeh, M.** (2017). Treatment of dispersive clay soil by ZELIAC. *Geoderma*, *285*, 270–279.

Safarzadeh, M., Ahmad Fauzi, M.N., Uday, M.B. (2016). Effect of friction speed on the properties of friction welded Alumina-Mullite Composite to 6061 Aluminum alloy. *Journal of the Australian Ceramic Society Volume*, *52*(2), 134–142.

Rewards

Silver Medal on 29th International Invention, Innovation & Technology Exhibition (2017); Kuala Lumpur, Malaysia, for "Calcium Phosphate Engineered from Natural Waste Materials for Biomedical Application".